Title
Mechanistic and Reactivity Studies of Cationic Cyclizations Catalyzed by Supramolecular Encapsulation

Permalink
https://escholarship.org/uc/item/7v25w64c

Author
Hastings, Courtney James

Publication Date
2010

Peer reviewed|Thesis/dissertation

Mechanistic and Reactivity Studies of Cationic Cyclizations Catalyzed by

Supramolecular Encapsulation

by

Courtney James Hastings

A dissertation submitted in partial satisfaction of the

requirements for the degree of

Doctor of Philosophy

in

Chemistry

in the

GRADUATE DIVISION

of the

UNIVERSITY OF CALIFORNIA, BERKELEY

Committee in charge:

Professor Robert G. Bergman, Co-chair
Professor Kenneth N. Raymond, Co-Chair
Professor Alexander Katz

Fall 2010

Abstract

Mechanistic and Reactivity Studies of Cationic Cyclizations Catalyzed by Supramolecular Encapsulation

by
Courtney James Hastings
Doctor of Philosophy in Chemistry
University of California, Berkeley
Professor Robert G. Bergman, Co-Chair
Professor Kenneth N. Raymond, Co-Chair

Chapter 1. A literature review of supramolecular reaction control and the efforts made towards developing supramolecular catalysts is presented. Representative examples of the fundamental ways in which supramolecular encapsulation can promote reactivity are given, with emphasis placed on catalytic reactions involving self-assembled hosts. The $[Ga_4L_6]^{12-}$ supramolecular assembly developed by the Raymond group is introduced, and previous work on its ability to enhance the reactivity of its encapsulated guests is reviewed.

Chapter 2. The tetrahedral $[Ga_4L_6]^{12-}$ assembly encapsulates propargyl enammonium cations capable of undergoing the aza Cope rearrangement. For propargyl enammonium substrates that are encapsulated in the $[Ga_4L_6]^{12-}$ assembly, rate accelerations of up to 184 are observed when compared to the background reaction. After rearrangement, the product iminium ion is released into solution and hydrolyzed allowing for catalytic turnover. The activation parameters for the catalyzed and uncatalyzed reaction were determined, revealing that a lowered entropy of activation is responsible for the observed rate enhancements. The catalyzed reaction exhibits saturation kinetics; the rate data obey the Michaelis-Menten model of enzyme kinetics, and competitive inhibition using a non-reactive guest has been demonstrated.

Chapter 3. The tetrahedral $[Ga_4L_6]^{12-}$ assembly catalyzes the Nazarov Cyclization of 1,3-pentadienols with extremely high levels of efficiency. The catalyzed reaction proceeds at a rate over a million times faster than that of the background reaction, an increase comparable to those observed in some enzymatic systems. This catalysis operates under aqueous conditions at mild temperature and pH ranges, and the reaction is halted by the addition of an appropriate inhibitor. The product of this reaction, pentamethylcyclopentadiene, is a competitive guest in the host assembly, and the catalysis suffers from product inhibition. This was alleviated by the addition of maleimide, which readily undergoes a Diels-Alder reaction with the product to form a more weakly-encapsulated adduct.

Chapter 4. The kinetically-controlled, regioselective deprotonation of cyclopentenyl cations mediated by encapsulation within the $[Ga_4L_6]^{12-}$ assembly is presented. The regiochemistry of the deprotonation step determines which one of two possible products is formed. Although this deprotonation step occurs at both possible positions outside the host interior, encapsulation renders the process >95% regioselective. Moreover, subtle differences in the stereochemistry of the encapsulated cyclopentenyl cation switch the product selectivity of this process. This reactivity shares several

1

features with the regioselective, enzyme-controlled deprotonation of the geranyl cation involved in the biosynthesis of myrcene and β-ocimene.

Chapter 5. Mechanistic studies of the processes described in the two preceding chapters are presented. A combined experimental and computational approach is used to elucidate the reaction mechanism of both the catalyzed and the uncatalyzed Nazarov cyclization of pentadienols. Kinetic analysis, ^{18}O exchange experiments, and computational studies implicate a mechanism in which encapsulation, protonation and water loss from substrate are reversible, followed by irreversible electrocyclization. While electrocyclization is rate-determining in the uncatalyzed reaction, the barrier for water loss and for electrocyclization are nearly equal in the assembly-catalyzed reaction. Analysis of the proposed energetics of the catalyzed and uncatalyzed reaction revealed that transition state stabilization contributes significantly to the catalytic rate acceleration.

In addition to Dennis, Vince and Vy, senior group members Helen Hoyt, Jamin Krinski, Gojko Lalic, Michael Seitz, Georg Seeber, Amanda Samuel and Rebecca Abergel made me feel welcome in my new groups, and helped me figure out how to be a graduate student. Mitch Anstey was always down for an immature joke or a deep discussion about life, and together with Neil Tomson was the core of our awesome 2007 softball team. Melanie Chiu and Miriam Bowring were excellent chamber music partners – I only wish we could have played more interesting music. Jason Nichols was my go-to guy for research advice, manuscript revision and beer brewing instruction. Elena Arceo-Rebollo taught me lots of useful Spanish, and threw the best parties of anyone in the group.

My co-workers on Team Supramolecular, Dennis Leung, Bryan Tiedemann, Mike Pluth, Akos Kokai, Jeff Mugridge, Casey "C-Lite" Brown, Carmelo Sgarlata, Georg Seeber, Martin Pedersen, Greg Miller and Mikael Backlund, were fun and dynamic group, and I learned a lot from working with each of them. Mike was an invaluable source of wisdom and experimental technique for me, and I was always in awe of his efficiency in the lab and his instincts as a researcher. He is the king, and I am certain that he has bright future as a professor. Jeff, in addition to being a great guy, was a model of responsible scientific conduct; on a project with lots of room for over-interpretation, fudging of numbers, and other bamboozlement, Jeff was always skeptical of his results and conservative in his interpretation. I appreciated Casey's enthusiasm, candor and willingness to mock himself and others – qualities that will serve him well in the future, I'm sure. Mikael deserves credit for tolerating my mentorship for two years, and for making substantial contributions to Chapter 4.

Terry Moore's fun but demanding AP chemistry class during my senior year of high school provided me with a solid foundation in laboratory technique, and convinced me to pursue chemistry in college. The three years that I spent in the lab of Professor Elizabeth Harbron at William and Mary got me completely hooked on laboratory research. Having mentored Mikael, an college sophomore possessing substantially more talent and experience than I had at that point, I have a much greater appreciation for the time and effort that Professor Harbron invested in my training.

The support of my parents and my brother has meant a lot to me throughout graduate school. My mom and dad both went to great lengths to provide me with the best education possible, and have not hassled me once about getting a real job. My brother Alex deserves credit for restraining himself from gloating too much about having more money and free time than me while I've been in graduate school. Finally, I will be forever grateful to my wonderful girlfriend Ann Hagan. She has provided pep talks when I had disappointing results in lab, dinner when I have come home late, and motivation when I was tired of working. Her love and good humor have sustained me during my time in Berkeley, and I am very lucky that she is in my life.

Dedicated to the memory of Terry Moore, the first person who encouraged me to try

chemistry research.

Mechanistic and Reactivity Studies of Cationic Cyclizations Catalyzed by

Supramolecular Encapsulation

Chapter 3.   Catalysis of the Nazarov Cyclization of Pentadienols by a Self-Assembled Supramolecular Assembly

Chapter 4.

Chapter 5.

Chapter 1

Stoichiometric   and   Catalytic   Reactions   Mediated   by   Supramolecular   Encapsulation

Introduction

Chemists have traditionally relied on covalent bond-forming and bond-breaking reactions to control molecular structure, and the past century has seen the development of a vast number of such synthetic methods. In contrast, the field of supramolecular chemistry concerns the design of molecular entities that are defined by reversible, non-covalent interactions. While each supramolecular interaction is quite weak individually, the effect of many such interactions working in concert can produce strongly associated and structurally well-defined molecular species. Such additive effects are responsible for the spectacular structural complexity found in biomacromolecules such as proteins. Efforts to characterize these interactions have provided chemists with a "toolbox" of reliable methods to program the association between two or more molecules to form a single complexed species. Thus, supramolecular chemistry represents a complementary approach towards molecular construction, and one that offers certain advantages over covalent chemistry.[1-3]

Cyclic polyethers, or crown ethers, represent one of the earliest and simplest examples of supramolecular binding. Crown ethers form a cyclic array of oxygen donors that interact with alkali metal cations, forming strongly-associated complexes (Figure 1.1).[4-6] While each oxygen-metal interaction is weak, binding constants on the order of 10^6 have been reported for cation binding.[7-9] Crown ethers, which are able to encircle bound cations, also represent one of the first instances of host-guest chemistry. Like supramolecular interactions, host-guest binding relies on manifold non-covalent interactions, with the added requirement that the host possess an interior cavity that is complementary in size and shape to the guest molecule. Over the past four decades host-guest systems have been devised which exhibit high degrees of selectivity in binding one species over other similar guests, including enantioselective binding.[10-19] It is possible for such synthetic hosts to be used for chemical sensing,[20-23] separations,[24-27] and altering the properties of a bound guest molecule.[28-30]
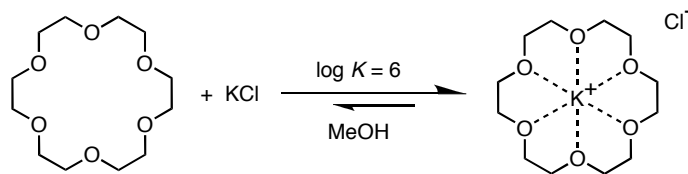
Figure 1.1. Representative crown ether [18]crown-6, which strongly binds the potassium cation.

As target guest molecules have become more complex, the synthetic demands for creating larger and more elaborate hosts have increased as well. Nature has solved this problem by utilizing relatively simple subunits that self-assemble into highly complex and symmetric structures. The self-assembly of such components is directed by noncovalent interactions such as hydrogen-bonding, ion pairing, solvophobic effects, and van der Waals interactions. For example, the MS2 virus capsid assembles from 180 sequence-identical peptide units to form an icosohedral protein shell that is 27 nm across.[31] It is possible to covalently attach small molecules to the interior surface of the MS2 capsid, which can act as a transport agent for biomedical cargo.[32,33]

Synthetic chemists have taken inspiration from such biological structures to design complex molecular hosts that self-assembly from simple subunits. The design of synthetic self-

assembled host molecules requires control over the geometry of the individual components and how the components interact with each other. This control can be achieved through covalent synthesis of the individual components, and by choosing the subunits to interact with each other through known and predictable non-covalent interactions.[34-40] Hydrogen-bonding and metal-ligand interactions are most frequently employed to provide this type of directional binding. This strategy has allowed for the synthesis of a large diversity of self-assembled hosts, formed from as few as two subunits and as many as 36 individual components.[41,42] There is a similarly wide range of guests accommodated by self-assembled hosts. Guests as small as individual metal ions and gas molecules have been reported,[7,43,44] while much larger hosts can accommodate C_{60}, multiple molecules of ferrocene, and even silica nanoparticles containing over 500 SiO_2 units (MW = 3.1 x 10^4).[45-47]

There are strong parallels between host-guest dynamics and ligand-receptor interactions of biomacromolecules, and considerable effort has been made to develop synthetic analogs of important biochemical processes.[48] This analogy is even more apt for self-assembled hosts; as the three-dimensional structure of a protein is dictated by its primary amino acid sequence, the structure of a self-assembled molecule is programmed by the geometrical relationships and functional groups present in each subunit. Enzymes, in particular, have captivated chemists with their ability to catalyze reactions with extremely high levels of selectivity and activity under mild, aqueous conditions, and much effort has gone into emulating their function.[49-59] If synthetic host molecules could be designed to catalyze a desired transformation with high levels of reactivity and selectivity, such catalysts could emerge as a powerful tool for chemical synthesis. Such catalysts rely upon non-covalent interactions to provide the primary associative interaction between catalyst and substrate, a factor that is responsible for the spectacular selectivity and reactivity of enzymes. This mode of reactivity stands in contrast to conventional synthetic catalysts, in which covalent bonding is typically responsible for the association of catalyst and substrate. Supramolecular catalysis is the application of synthetic hosts towards the development of catalysis based on non-covalent interactions, and it is an area of research that has received a considerable amount of attention in the last fifteen years.[60-63]

This chapter is intended to provide an overview of supramolecular reaction control, and the efforts made towards developing highly efficient and selective supramolecular catalysts. Rather than give a comprehensive literature review of supramolecular reactivity, this chapter provides representative examples of the fundamental ways in which supramolecular encapsulation can promote reactivity. This perspective is meant to provide context within which the remaining chapters can be viewed. Emphasis will be placed upon catalytic rather than stoichiometric reactivity, and upon self-assembled rather than covalently-bound host structures. Conceptually related work on encapsulation-mediated reaction control using metal-organic frameworks,[64-68] the inner phase of polymers[69-72] and dendrimers,[73-75] catalytic antibodies[76,77] and other such species is beyond the scope of this chapter, and will be omitted. The end of the chapter will focus on the supramolecular assembly ($[Ga_4L_6]^{12-}$, **1**) developed by Raymond and co-workers, and previous work from our group on its ability to enhance the reactivity of its encapsulated guests.

Supramolecular Catalysis

      Co-encapsulation of Bimolecular Reactants. Rebek and Mecozzi made the observation that host-guest binding is strongest when the ratio of guest volume to host volume (known as the packing coeffiecient) is 0.55, given that shape-complementarity exists between host and guest.[78] This optimal ratio holds true empiricallyregardless of the number of guest molecules that occupy the host, and binding of multiple guest molecules can be quite favorable if their total volume occupies close to 55% of the host interior.[79] The local concentration of multiple guest molecules encapsulated within a molecular host is very high, even if the unencapsulated molecules are dilute in solution.[78] If two co-encapsulated molecules can react in a bimolecular reaction, then supramolecular encapsulation can accelerate the reaction rate by increasing the effective concentration of the reactants in the host interior.

      This mode of reactivity was demonstrated in a pioneering study by Mock and co-workers on the catalysis of a dipolar cycloaddition by encapsulation in cucurbit[6]uril (**2**, Figure 1.2).[80,81] The cucurbituril family of macrocycles contains between five and ten gylcouril units (six in the case of **2**) linked together covalently by methylene groups, and its members are soluble in acidic aqueous solution.[82,83] The rim of the toroidal host is lined by inward-facing carbonyl groups, which interact strongly with cationic molecules, particularly alkylammonium compounds. The alkyl portions of guests such as the propargylammonium cation (**3**) and the azidomethyl ammonium cation (**4**) project into the interior of **2**, while the ammonium portion is bound by the rim of carbonyl groups. When **3** and **4** are both encapsulated by **2**, the alkyne and azido portions of the guests are held within close proximity to one another, and their rate of reaction is substantially accelerated (Figure 1.3a). The thermal reaction between **3** and **4** produces equal amounts of the two regioisomeric cycloaddition products **5** and **6** (Figure 1.3b). Since binding of **3** and **4** orients the amino substituents away from each other, only product **5** is formed in the **2**-catalyzed reaction (Figure 1.3c). In-depth kinetic studies on this reaction indicated that cycloaddition of ternary complex **9 • 10 ⊂ 7** (where ⊂ denotes encapsulation) was approximately 6×10^5 times larger than that of the unencapsulated reaction. However, product release from **2** was rate-limiting, and the rate enhancement for the overall catalytic process was 490.

2
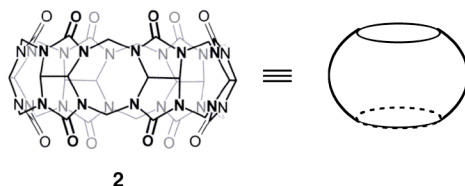
Figure 1.2. Structure of cucurbit[6]uril (**2**), which is depicted by the simple barrel-like cartoon on the right. Figure adapted from reference 84.
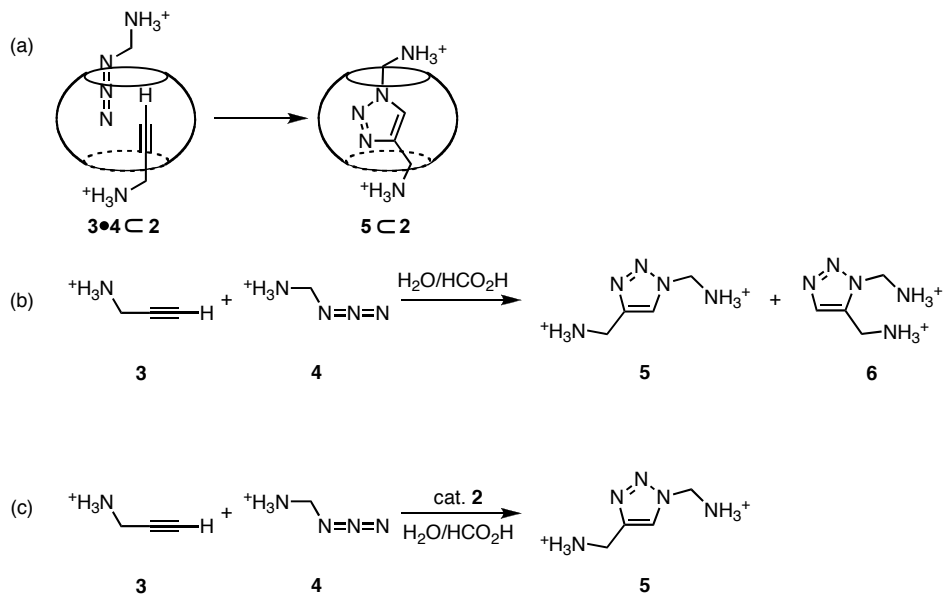
Figure 1.3. Cycloaddition reaction catalyzed by encapsulation within cucurbit[6]uril (**2**). (a) Co-encapsulation of alkyne and azide substrates in **2**. (b) Uncatalyzed reaction of alkyne **3** with azide **4** to form a mixture of two regioisomers. (c) **2**-Catalyzed cycloaddition reaction to form a single cycloaddition regioisomer (**5**).

Rebek and co-workers successfully applied the local concentration strategy to accelerate the Diels-Alder cycloaddition of two molecules co-encapsulated in self-assembled host **7**.[85] Prior to this study it was not clear if reversibly-assembled hosts could enforce close contact between reactants as effectively as covalently-bound hosts. The spherical host **7** assembles via hydrogen bonding from two molecules of the concave precursor **8**, which contains hydrogen bond donors at its two ends, and hydrogen bond acceptors in the middle (Figure 1.4). This and related hosts form stable complexes in aprotic solvents, and are capable of encapsulating small organic molecules.[39]
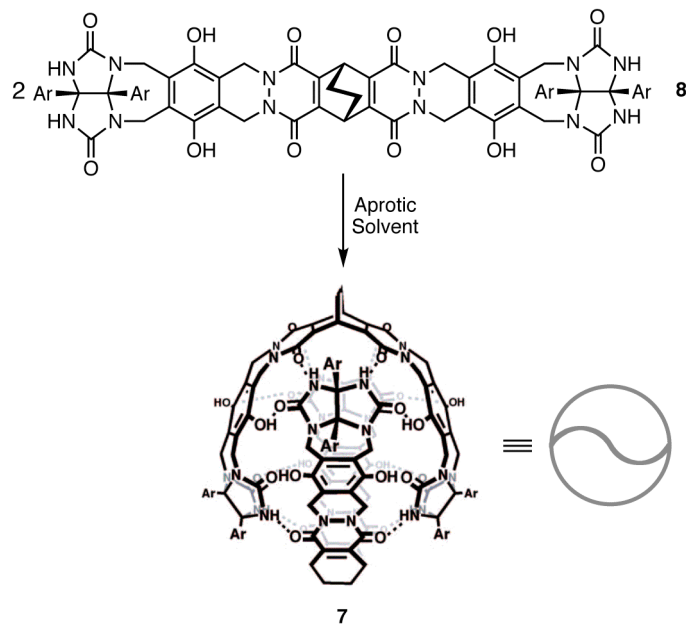
Figure 1.4. Self-assembly of hydrogen-bonded host **7** which is depicted by the simple tennis ball cartoon on the right. Figure adapted from reference 60.

Addition of *p*-benzoquinone (**9**) and cyclohexadiene (**10**) to a solution of **7** in *p*-xylene results in the formation of a host-guest complex containing one molecule of each reactant (**9 • 10** ⊂ **7**,). The Diels-Alder reaction of the encapsulated guests proceeds at a rate 170 times greater than that of the reaction in solution. The Diels-Alder adduct (**11**) of benzoquinone and cyclohexadiene is bound too strongly for additional reactant molecules to enter the cavity of **7**, so catalytic turnover does not occur (Figure 1.5a). Replacing cyclohexadiene with dimethylthiophene dioxide (**12**) yields a Diels-Alder adduct (**13**) that is a poor guest, allowing for further reactant binding and catalytic turnover (Figure 1.5b).[41] Product inhibition, the inability of reactant molecules to displace product from the host interior, is a common feature of many host-catalyzed reactions. Product inhibition can be overcome by discovering reactants that are more strongly bound than the products that they form, or by converting the product into a poor guest. A general solution to the issue of product inhibition remains elusive, and such a solution represents a major goal in supramolecular catalysis research.
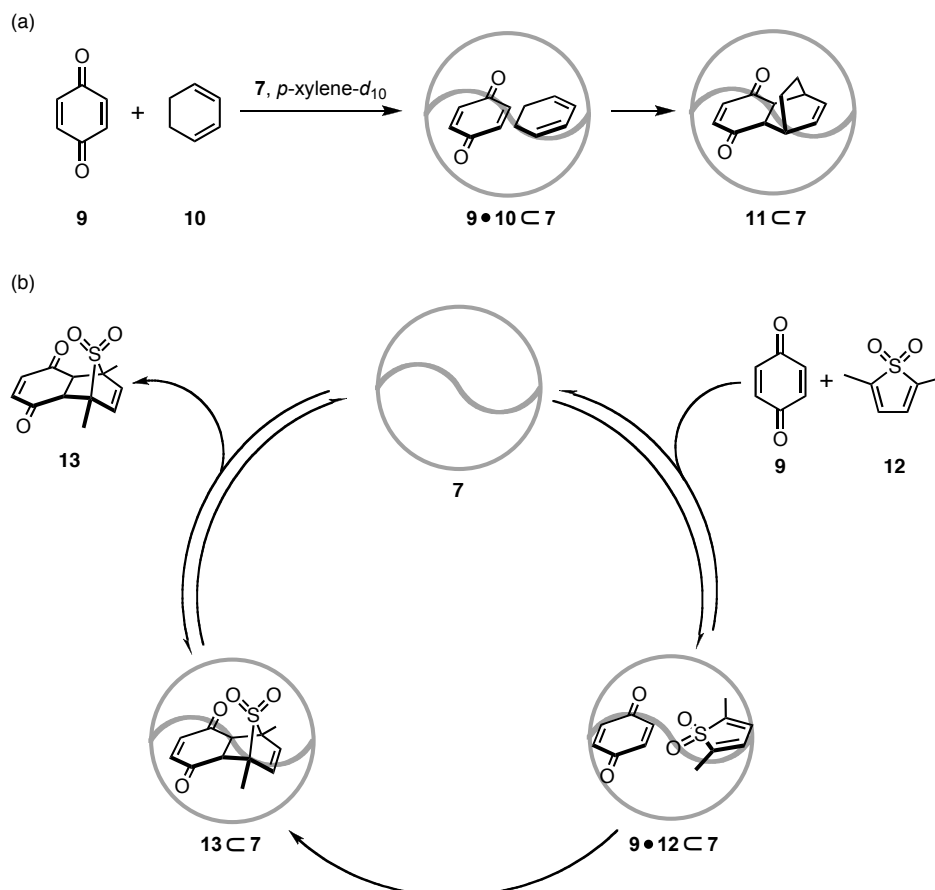
Figure 1.5. Acceleration of the Diels-Alder reaction by co-encapsulation within host **7**. (a) Diels-Alder adduct **11** is bound tightly by **7**, causing product inhibition. (b) Diels-Alder adduct **13** is weakly bound by **7**, allowing catalytic turnover.

Fujita and co-workers have carried out conceptually similar research on cycloaddition reactions using a series of self-assembled metal-ligand cages. Unlike hydrogen bonding, dative metal-ligand interactions are not substantially disrupted by protic solvents, so assemblies based on such interactions can form in aqueous solution. The Fujita cages are based on tripyridyl ligands that coordinate to palladium centers, and can form the octahedral assembly **14** or the trigonal pyramidal assembly **15** (Figure 1.6).[86] Both assemblies have a M_6L_4 stoichiometry, carry a 12+ charge and are soluble in water. The planar, aromatic walls of **14** and **15** are ideally suited for aromatic guest molecules, whose binding is driven by the hydrophobic effect.[87]
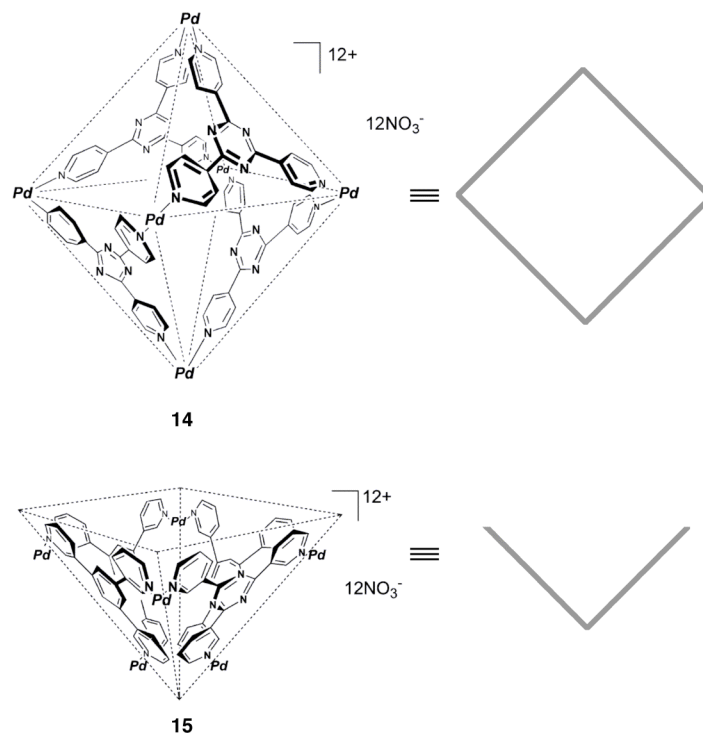
Figure 1.6. Self-assembled cages based on the coordination of tripyridyl ligands with palladium atoms, which are depicted by the simple square and angle cartoons on the right. Figure adapted from reference 62.

Encapsulation within **14** accelerates the rate of the Diels-Alder reaction between benzoquinone (**16**) and isoprene (**17**), again due to the increased local concentration of the bound reactants. The cavity of **14** is quite large, and it is able to accommodate two molecules each of both reactants, which upon heating forms the host-guest complex in which two molecules of product **18** are encapsulated (Figure 1.7a).[86] Although product inhibition occurred for every combination of reactants investigated in the **14**-mediated Diels Alder reaction, the Fujita group was able to achieve catalytic turnover in the reaction of N-cyclohexylmaleimide (**19**) with anthracene derivatives using the bowl-shaped assembly **15**.[88] The catalytic turnover in this system is attributed to the shape of Diels-Alder adduct **21** compared to its anthracene-derived precursor. Attractive π-stacking interactions exist between **15** and the planar anthracene unit of the reactant, while the same interactions are not possible between the host and the bent anthracene framework of the product **21**. Consequently, the host-product complex is destabilized and additional reactant binding occurs.
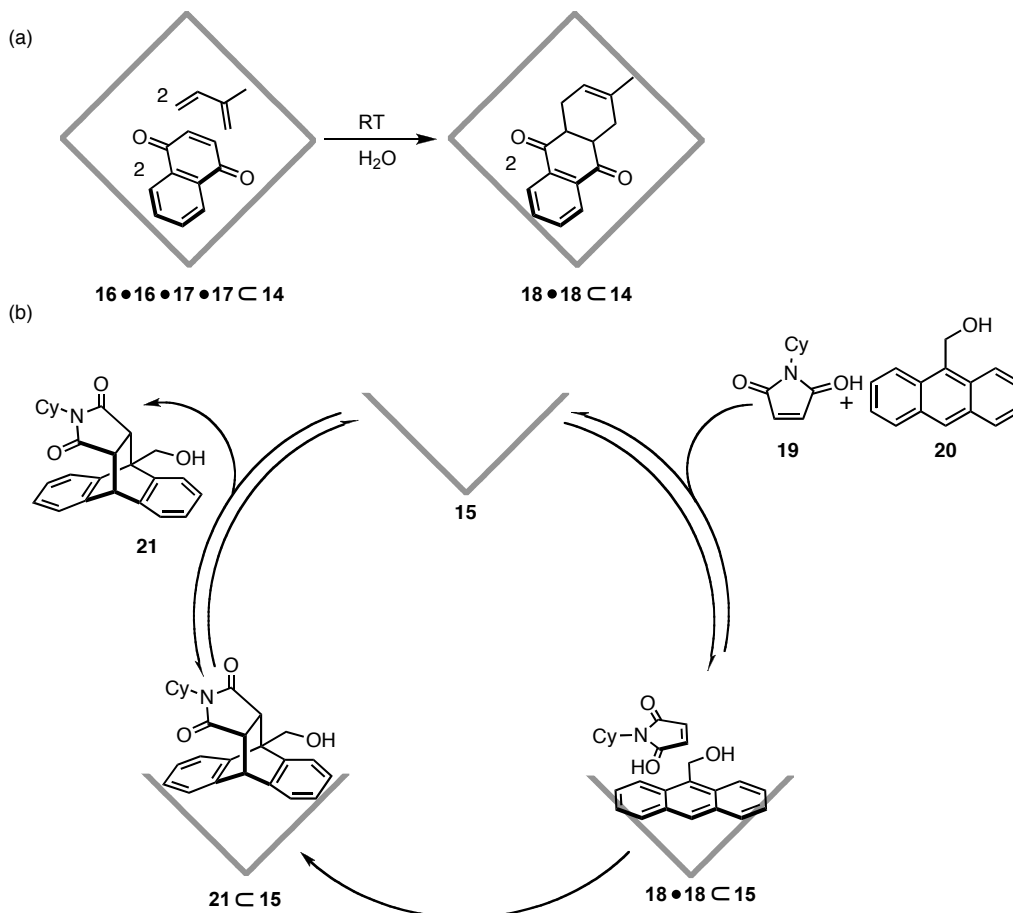
Figure 1.7. Acceleration of the Diels-Alder reaction by co-encapsulation within metal-ligand assemblies. (a) Two molecules of Diels-Alder adduct **18** are bound tightly by **14**, causing product inhibition. (b) Diels-Alder adduct **21** is a poor guest for **15**, allowing for displacement by additional reactant molecules.

Hosts with Catalytic Active Sites. A powerful strategy for achieving supramolecular catalysis is to construct host molecules containing catalytically active functional groups that are positioned to interact with a bound substrate molecule. In such systems, the reactant is recognized by and bound within the host cavity, where it is in intimate contact with the catalytic functional group. As in the case of two co-encapsulated reactants, this molecular preorganization produces a large effective concentration of substrate and catalyst. This motif is especially prevalent in the active sites of many enzymes, in which precisely oriented amino acid residues or cofactors are responsible for spectacularly enhanced reactivity.

Rebek and co-workers have designed a family of open-ended resorcinarene-derived hosts in which a diversity of functional groups are positioned over the host rim, protruding into the cavity.[89] A seam of hydrogen-bonding groups around the rim of the molecule direct these hosts to fold into vase-like structures in aprotic solvent, in which they are capable of binding a variety of guest molecules. Host **22** is functionalized with a carboxylic acid group, which is attached to the host rim and dangles into the binding pocket (Figure 1.8). The intramolecular epoxide ring

opening of 1,5-epoxyalcohol **23** is catalyzed by 5 mol% **22** in mesitylene-d_{12} to form hydroxymethyltetrahydrofuran **24**.[90,91] The host-catalyzed reaction is substantially accelerated when compared to the reaction catalyzed by carboxylic acid **26**, which is electronically similar but lacks any substrate-recognizing cavity. This difference underscores the enhanced reactivity that results from enforcing the close proximity of substrate and a catalytic functional group. Additionally, the **26**-catalyzed reaction produces a mixture of regioisomers, the result of intramolecular nucleophillic attack at both epoxide positions, while the host-catalyzed reaction yields a single regioisomer. Again, this selectivity must be due to the conformation of **23** ⊂ **22**, in which nucleophillic attack is possible at only one of the two positions.
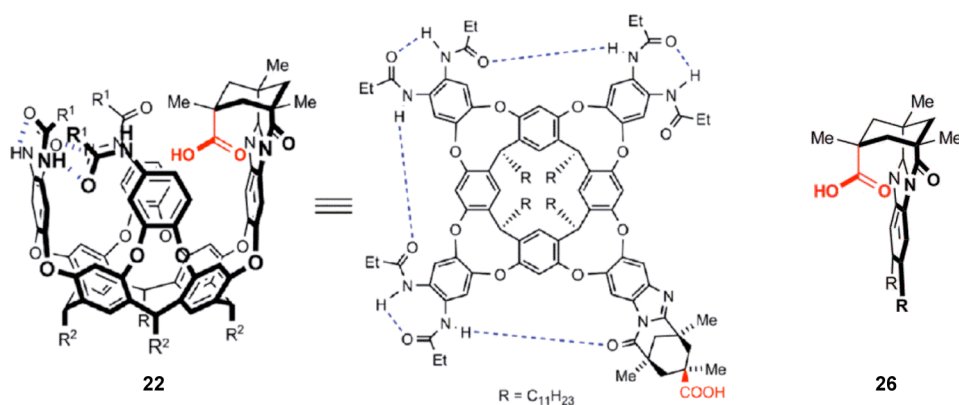
Figure 1.8. Self-folding cavitand **22**, functionalized with an inward-facing carboxylic acid group. Carboxylic acid **26**, which lacks a binding pocket, was used in control experiments. Figure adapted from reference 91.
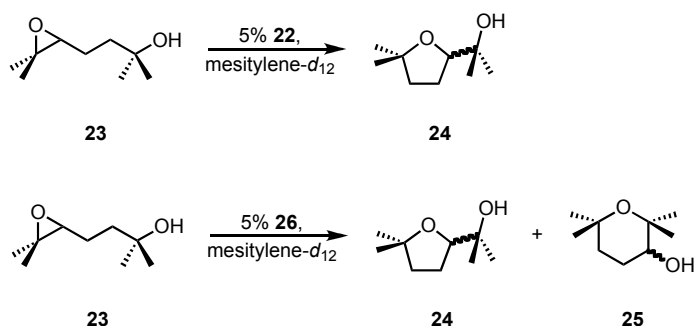
Figure 1.9. Intramolecular ring opening of epoxides, catalyzed by cavitand **22**. The **22**-catalyzed reaction proceeds with 50-fold rate enhancement, and with greater product selectivity.

A related strategy towards supramolecular catalysis is the construction of hosts with appended functional groups that are not catalytically active, but can be converted into a reactive functionality under the appropriate conditions. Cyclodextrin (Figure 1.10a) derivatives have been extensively investigated as catalysts that employ this mode of reactivity. One of the earliest examples of host-mediated reactivity was the chlorination of cyclodextrin-bound anisole. Anisole (**27**) is bound tightly within the cylindrical cavity of α-cyclodextrin (**28**), which exposes

the *para* position of the guest while shielding the *meta* and *ortho* positions. Thus, chlorination occurs at the *para* position exclusively, while the reaction in the absence of cyclodextrin chlorinates both the *ortho* and the *para* position (Figure 1.10b). While hypochlorous acid is the chlorinating reagent in the reaction without cyclodextrin, detailed mechanistic analysis revealed that hypochlorous acid converts one of the cyclodextrin hydroxyl groups into a hypochlorite group, which is the active chlorinating reagent in the cyclodextrin-mediated reaction. Since the *para* position of the bound substrate is held in close proximity to the hypochlorite group, the rate of chlorination is increased.
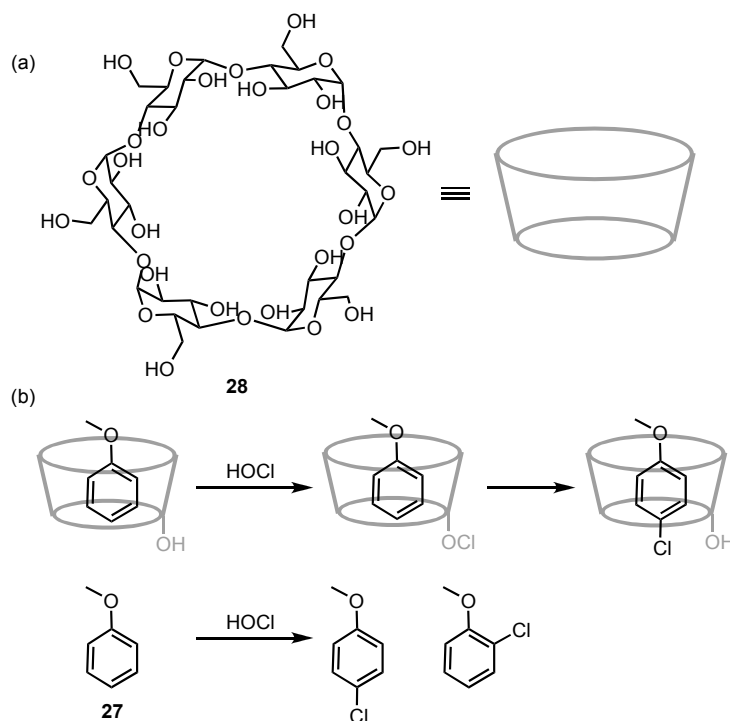
Figure 1.10. (a) The structure of α-cyclodextrin, which is depicted by the simple cylinder cartoon on the right. (b) The chlorination of anisole (**27**) by hypochlorous acid, which is selective for the *para* position when **27** is bound by cyclodextrin. Chlorination occurs at both positions when cyclodextrin is omitted from the reaction.

A similar strategy was employed in oxidation reactions using ketone-bridged cyclodextrin derivatives, such as **29**, as catalysts.[49] In the presence of hydrogen peroxide, the ketone functionality of **29** is converted into the corresponding hydroperoxide adduct, which acts as the active oxidant of alcohols,[92,93] alkenes,[94] and anilines.[95] Significantly, the catalyzed reaction rates are substantially higher using cyclodextrin-derived catalysts compared to ketones such as **30**, which are electronically similar but lack any substrate-binding ability.
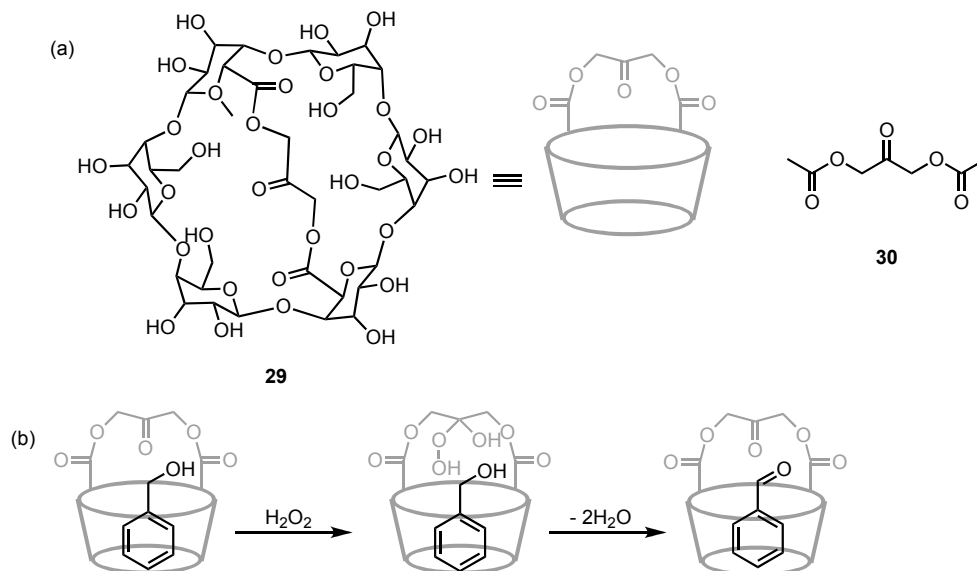
Figure 1.11. (a) Modified cyclodextrin catalyst **29** with bridging ketone group and electronically equivalent ketone **30**. (b) Oxidation catalyst **29**, which oxidizes bound substrates through the intermediacy of a hydroperoxide adduct.

Metallohost Catalysis. One third of all enzymes, including the cytochrome p450 and nitrogenase enzymes, contain catalytically-active metal cofactors that are essential for reactivity.[95] The installation of a catalytically active metal center within a substrate-recognizing host framework provides a strategy for constructing metalloenzyme mimics.[96] This requires some degree of sophistication in the design of the appropriate host, since molecular recognition components for both the metal and for the substrate are required. Although traditional ligands for catalysis are capable of directing the precise interaction of a substrate molecule with the metal center (especially in asymmetric catalysis), these interactions are typically repulsive (via steric interactions) rather than attractive.

Crabtree and co-workers prepared a C-H oxidation catalyst **31** with a catalytic dimanganese core and a ligand that recognizes carboxylic acid substrates.[97] The ligand includes a U-turn motif that terminates in a carboxylic acid, which is capable of binding other carboxylic acids through hydrogen bonding. Significantly, this molecular recognition element positions the bound substrate directly above the manganese center, resulting in improved selectivity in the C-H oxidation of substrates (Figure 1.12). For example, the oxidation of ibuprofen (**32**) using **31** as a catalyst yields ketone **33** almost exclusively, while a catalyst lacking the molecular recognition element (**35**) produces a mixture of products (Figure 1.13). The substrate-recognizing properties of **31** are abolished when excess acetic acid is added as a competitive inhibitor, although the catalytic activity for oxidizing **32** are maintained. These experiments, in conjunction with molecular modeling studies, suggest that molecular recognition of the carboxylate-containing substrates plays a critical role in the selectivity of this process. Similar studies were conducted by Breslow and co-workers using a manganese catalyst with attached cyclodextrin groups for the recognition and selective oxidation of steroids.[98-100] Relatively simple substrate-docking ligands

for rhodium catalysts have been reported, leading to enhanced selectivity and reactivity in hydroformylation reactions.[101,102]
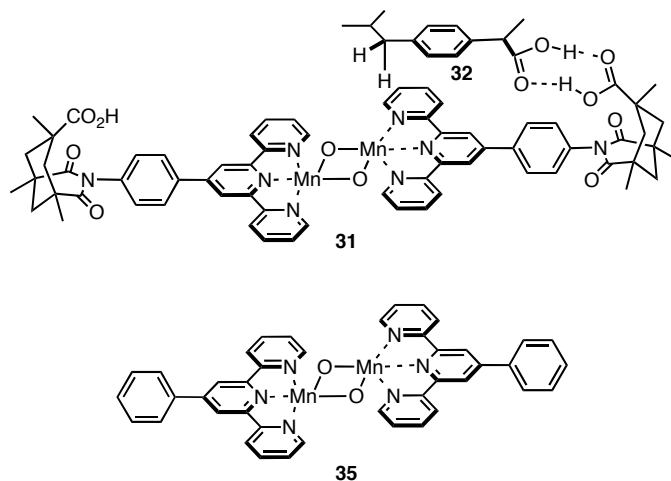
Figure 1.12. Dimanganese C-H oxidation catalyst **31** with substrate-recognizing ligand, shown hydrogen-bonding with substrate **32**. Catalyst **35** lacks the molecular recognition element.
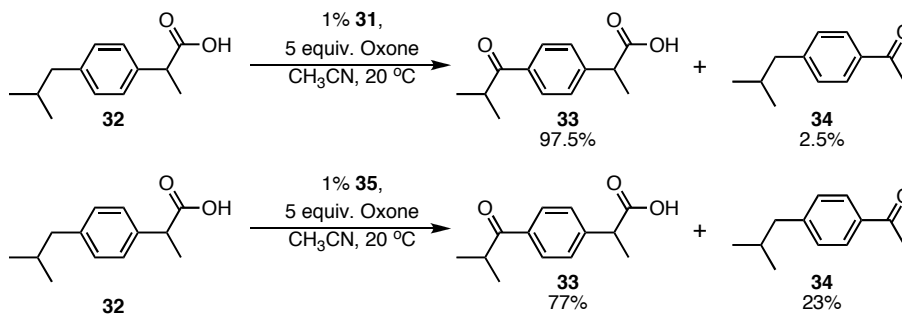
Figure 1.13. The oxidation of ibuprofen (**32**) catalyzed by dimanganese catalysts **31** and **35**.

Placement of a catalytically active metal center within a well-defined binding pocket represents another strategy for metallohost catalysis. Hupp, Nguyen and co-workers have developed a supramolecular metal-ligand box whose interior is paneled by zinc porphyrin units (**36**).[36] This design allows for the installation of a pyridine-substituted manganese porphyrin moiety (**37**), whose pyridine units bind strongly to the zinc porphyrins of the host walls (Figure 1.14). Similar manganese porphyrins are well-known epoxidation catalysts that tend to degrade over time through formation of catalytically-inactive dimers. The encapsulated manganese catalyst (**37** ⊂ **36**) is an effective catalyst for the epoxidation of olefins, and higher turnover numbers are observed relative to unencapsulated catalyst **37**. The authors propose that encapsulation within **32** prevents the formation of catalytically-inactive dimers of **37**, which prolongs catalyst lifetime. Manganese porphyrin **37** only occupies two of the four zinc-binding sites in **36**, and addition of functionalized pyridines allows for additional control over the inner space of the host cavity. This additional modification of the interior of **36** induces selectivity for smaller alkene substrates, which have easier access to the catalytic manganese center. In a

13

related system, tailoring the inner space of self-assembled boxes with chiral pyridine derivatives induces modest enantioselectivity in the oxidation of sulfides.[103]
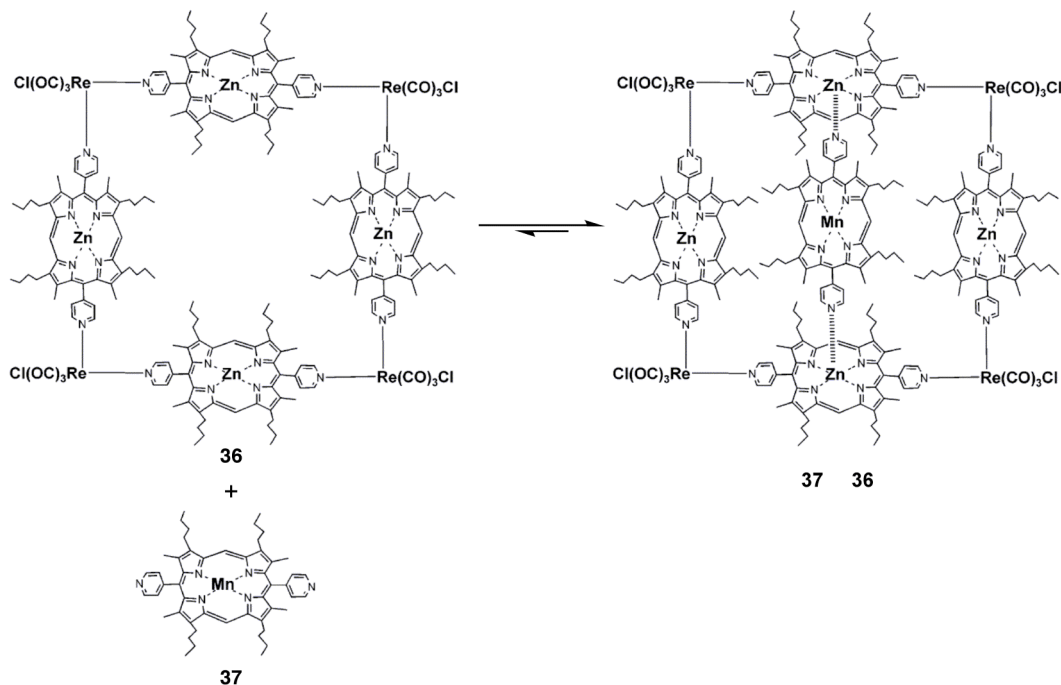
Figure 1.14. Square metal-ligand assembly **36** that binds catalytically active manganese porphyrin **37** in its interior. Figure adapted from reference 62.

     Catalysis With a Self-Assembled $[Ga_4L_6]^{12-}$ Tetrahedron. Raymond and co-workers have developed a series of self-assembled supramolecular metal-ligand assemblies of M_4L_6 stoichiometry (M = Ga^{3+} (**1**), Al^{3+}, Fe^{3+}; L = *N,N'*-bis(2,3-dihydroxybenzoyl)-1,5-diaminonaphthalene).[104-107] The four trivalent metal atoms are located at the vertices of the tetrahedron, while naphthalene-based bis-bidentate catechol ligands span the edges, forming a *T*-symmetric, cavity-containing assembly (Figure 1.15). Strong mechanical coupling between the metal vertices through the ligands enforces self-assembly of a racemic mixture of the homochiral ΔΔΔΔ and ΛΛΛΛ configurations.   The two enantiomers can be resolved and are configurationally stable.[108,109]
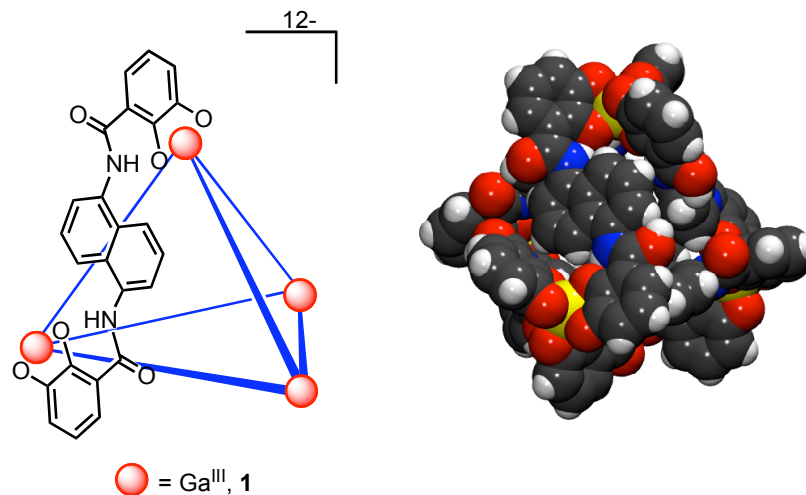
Figure 1.15. (left) Schematic view of **1** in which the bisbidentate ligands are represented by blue lines and the gallium atoms by red circles. (right) Space-filling model of **1**.

A variety of monocationic guests ranging from simple alkylammonium cations to transition metal sandwich complexes, as well as neutral hydrophobic species such as alkanes, are encapsulated in **1**.[110] Molecules that are strongly solvated by water, such as dications and small monocations, are not encapsulated, while anionic molecules suffer from charge-repulsive interactions with the host that prevent their encapsulation. The 12- overall charge of **1** imparts water solubility, while the naphthalene rings of the ligand enclose the interior cavity, providing a hydrophobic environment for guest molecules. These properties allow water-labile cations such as ketone-derived iminium ions,[111] diazonium and tropylium ions,[112] and reactive phosphine-acetone adducts[112,113] to be stabilized by encapsulation. While these cations are unstable, with very short lifetimes in aqueous solution, the polyanionic charge and hydrophobic cavity stabilize these species upon encapsulation.

The properties of **1** that are summarized above have been exploited to develop reactions that occur inside the cavity of **1** with higher degrees of reactivity and/or selectivity than when the reaction is performed in bulk solution. Several encapsulated transition metal complexes can participate in stoichiometric and catalytic organometallic reactions in which **1** imposes strict limits on the size and shape of substrates that will react. For instance, the encapsulation in **1** of a cationic rhodium catalyst for allyl alcohol isomerization dramatically changes the substrate selectivity when compared to the unencapsulated rhodium complex.[114] In bulk solution, $(PMe_3)_2Rh(OD_2)_2^+$ (**38**) quickly converted a variety of allyl alcohols and allyl ethers (**39-43**) into the corresponding carbonyl compounds and enol ethers, respectively. In contrast, the encapsulated species **38** ⊂ **1** was a much more selective catalyst, only converting specific alcohols with the correct size and shape (Figure 1.16). While allyl ether **38** was quantitatively isomerized by **38** ⊂ **1**, isomeric allyl alcohols **36** and **37** were completely unreactive. Encapsulation within **1** controls which substrates interact with the catalytic rhodium center, resulting in a highly selective reaction.

15
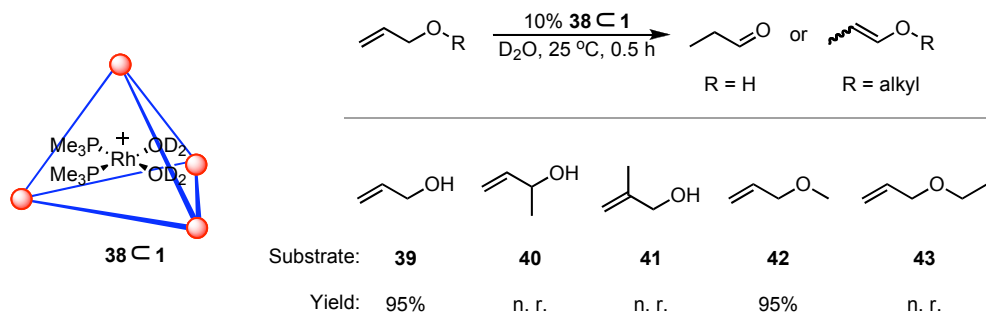
Figure 1.16. Substrate reactivity in the isomerization of allyl alcohols and allyl ethers, catalyzed by encapsulated rhodium catalyst **38 ⊂ 1**. Unencapsulated catalyst **38** converts all substrates (**39-43**) quantitatively into the corresponding products.

Similar substrate selectivity was observed in the stoichiometric C-H activation of aldehydes by cationic half-sandwich iridium species Cp*(PMe₃)Ir(Me)(C₂H₄)⁺ (**40**).[115,116] While unencapsulated **40** reacted with a wide variety of aldehyde substrates, the reaction of host-guest complex **40 ⊂ 1** with aldehyde substrates exhibited both size and shape selectivity. As in the rhodium-catalyzed allyl alcohol isomerization, substrates that were too large or too highly branched were not able to enter the cavity of **1** and react.

Encapsulation in **1** itself can promote reactivity of bound guests, even in the absence of a co-encapsulated transition metal catalyst. Allyl enammonium cations were selected as an attractive class of compounds for investigating this mode of reactivity. Quaternary ammonium compounds are known to be excellent guests in **1**, and appropriately substituted allyl enammonium cations are reactive in the 3-aza Cope rearrangement. In this reaction, the allyl enammonium cation forms a γ,δ-unsaturated iminium cation via [3,3] sigmatropic rearrangement, which is then hydrolyzed to the corresponding aldehyde (Figure 1.17).[117,118] Encapsulation in **1** was found to increase the reaction rate of a variety of allyl enammonium compounds relative to the uncatalyzed reaction rate by up to 854 times (Table 1.1). Rate enhancement was observed in all cases, although the largest rate accelerations were observed for intermediately sized substrates, while smaller rate effects were seen for both large and small substrates. The product aldehydes of this reaction are very poor guests relative to the cationic reactants, and no product inhibition was observed.[119,120]
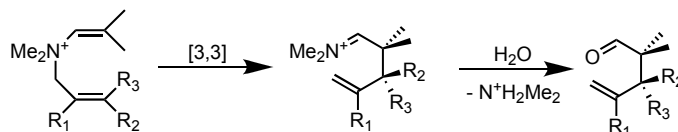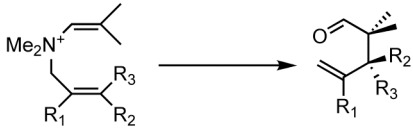
Figure 1.17. General scheme for the 3-aza Cope rearrangement of allyl enammonium cations.

R_1	R_2	R_3	k_{free} $(\times 10^{-5}\,s^{-1})$	k_{encaps} $(\times 10^{-5}\,s^{-1})$	acceleration
H	H	H	3.49	16.3	5
Me	H	H	7.61	198	26
H	Et	H	3.17	446	141
H	H	Et	1.50	135	90
H	n-Pr	H	4.04	604	150
H	H	n-Pr	1.69	74.2	44
H	i-Pr	H	0.37	316	854
H	n-Bu	H	3.97	222	56
H	TMS	H	0.033	1.17	35
H	Me	Me	6.3	331	53

Table 1.1. Rate data for the **1**-catalyzed and uncatalyzed reaction of allyl enammonium substrates. Figure adapted from reference 119.

Mechanistic analysis demonstrated that encapsulation within the constrictive cavity of **1** was responsible for the enhanced reactivity. No reaction occured when a strongly-binding guest (NEt_4^+) was added to prevent substrate binding, and the uncatalyzed reaction rate was insensitive to changes in solvent or ionic strength, implying that the hydrophobic pocket and highly anionic charge of **1** do not accelerate the reaction. The activation parameters for both the free and the assembly-mediated reaction were determined for several substrates, and while the enthalpies of activation were nearly identical, the entropies of activation for reactions of encapsulated guests were less negative compared to those occurring in free solution. This strongly suggests that the major component of the observed rate enhancement is the binding of a single pre-organized substrate conformer that closely resembles the expected transition state of the sigmatropic rearrangement. This hypothesis was confirmed by a NOESY experiment, which showed strong correlations between the two ends of the linear enammonium cation when it is encapsulated, but not when it is free in aqueous solution.[121] This work represents a rare example of a unimolecular rearrangement catalyzed by supramolecular encapsulation in which enhanced reactivity is achieved through conformational selection alone.[122]

Encapsulation in **1** can perturb certain chemical equilibria to favor the formation of species such as iminium ions and labile phosphonium adducts.[111,123,124] This equilibrium shift also applies to a wide range of protonated amines and phosphines that are encapsulated in **1**, even in strongly basic pH.[125,126] Protonation of encapsulated phosphines was proven by ^{31}P NMR spectroscopy in H_2O and D_2O by analysis of the $^1J_{PH}$ and $^1J_{PD}$ coupling constants. Protonation of encapsulated amines was confirmed by the pH dependence of binding strength, and by the observation of encapsulated pro-azaphosphatranes by mass spectrometry. The basicity of protonated guests is enhanced between 2.1 and 4.5 orders of magnitude.

These investigations led to the development of proton-catalyzed hydrolysis reactions inside **1**, in which a protonated transition-state is stabilized in the host interior. These reactions are remarkable in that there are no functional groups in the interior of **1**; the protonation of bound guests is favorable due to the charge of the host assembly and cation-pi interactions with the

17

naphthalene rings of the host walls.[127-132] The stabilization of transient protonated species produces a several thousandfold rate acceleration of orthoformate and acetal hydrolysis under basic conditions. Detailed mechanistic studies of the orthoformate hydrolysis reaction implicate a reaction mechanism in which fast, reversible binding of the neutral substrate is followed by its rate-determining protonation (Figure 1.18). The first hydrolysis step after protonation occurs inside **1**, and the subsequent hydrolysis steps are either acid- or base-catalyzed. A similar mechanism was proposed for the **1**-catalyzed hydrolysis of acetals.
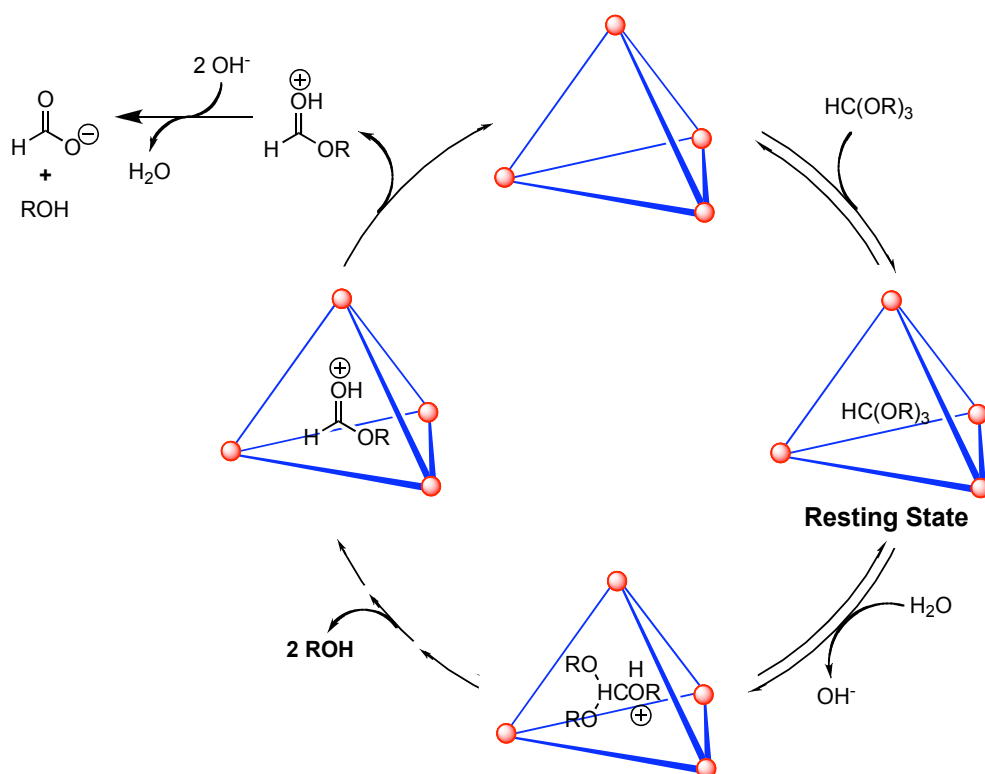
Figure 1.18. Catalytic cycle for the **1**-catalyzed hydrolysis of orthoformates. Figure adapted from reference 129.

Conclusion and Outlook

The examples of reactivity mediated by supramolecular interactions presented in this chapter demonstrate how weak, transient interactions can dramatically affect reactivity. Supramolecular catalysts can bind a reactant molecule in well-defined orientations, enforcing favorable interactions with catalytic functional groups or additional reactant molecules. The structure and geometry of a host catalyst can discriminate between substrates of similar size and shape, producing high levels of selectivity that are difficult to achieve using conventional catalysis. These aspects of supramolecular reaction control have much in common with the action of enzymes. Over the last decade, Raymond, Bergman and co-workers have investigated

the ability of metal-ligand $[Ga_4L_6]^{12-}$ assembly (**1**) to mediate the reactivity of bound guests. The reactivity of cationic transition metal complexes is altered by encapsulation in **1**, greatly increasing the substrate selectivity relative to the unencapsulated catalysts. Encapsulation of reactive allyl enammonium cations in **1** greatly increases the rate of the 3-aza Cope rearrangement by binding a folded conformation of the reactant that resembles the transition state of the reaction. The basicity of **1**-bound guests is greatly enhanced by encapsulation, a property that was exploited in the catalysis of acetal and orthoformate hydrolysis in basic solution.

The research presented in chapters 2 through 5 builds upon previous work using **1** as a catalyst. Among the most important features of **1** are the constrictive interior of its cavity and its highly anionic charge, which favors cationic reaction intermediates. These features make acid-catalyzed cyclization reactions a particularly attractive target for catalysis by encapsulation in **1**. The emulation of enzymatic activity using synthetic, supramolecular catalysis is a particularly attractive goal, and special attention was devoted towards studies that highlight the similarity of **1**-catalyzed reactivity to biological catalysis. In Chapter 2 the **1**-catalyzed aza Cope rearrangement is extended to the less reactive propargyl enammonium substrate class. The **1**-catalyzed reaction obeys the Michaelis-Menten model of enzyme kinetics, and competitive inhibition of this reaction can be observed using NPr_4^+, a non-reactive guest. Chapter 3 describes the development of the **1**-catalyzed Nazarov cyclization of 1,4-pentadien-3-ol substrates. Kinetic studies reveal that the rate of the catalyzed reaction is up to 2,100,000 times larger than that of the uncatalyzed reaction, representing the first instance of supramolecular catalysis that achieves rate enhancements comparable in size to those seen in enzymatic systems. Chapter 4 describes the selective, kinetic deprotonation of a cyclopentenyl carbocation intermediate mediated by supramolecular encapsulation in the **1**. In this system, encapsulation within **1** forces deprotonation to occur at a single position, which is similar to the regioselectivity in enzyme-mediated deprotonations involved in terpene biosynthesis. Chapter 5 presents a detailed mechanistic study of the reactivity described in the preceding two chapters.

References

(1)   Lehn, J. M. *Angew. Chem. Int. Ed.* **1990**, *29*, 1304.

(2)   Cram, D. J. *Angew. Chem. Int. Ed.* **1988**, *27*, 1009.

(3)   Lehn, J. M. *Science* **1985**, *227*, 849.

(4)   Pedersen, C. J. *Angew. Chem. Int. Ed.* **1998**, *27*, 1021.

(5)   Pedersen, C. J. *J. Am. Chem. Soc.* **1967**, *89*, 2495.

(6)   Pedersen, C. J. *J. Am. Chem. Soc.* **1967**, *89*, 7017.

(7)   Bajaj, A. V.; Poonia, N. S. *Coord. Chem. Rev.* **1988**, *87*, 55.

(8)   Izatt, R. M.; Bradshaw, J. S.; Nielsen, S. A.; Lamb, J. D.; Christensen, J. J. *Chem. Rev.* **1985**, *85*, 271.

(9)   Steed, J. W.; Atwood, J. L. *Supramolecular Chemistry*; John Wiley & Sons, Ltd: Chichester, 2000.

(10)   Castellano, R.; Kim, B.; Rebek, J. *J Am Chem Soc* **1997**, *119*, 12671.

(11)   Hastings, C. J.; Pluth, M. D.; Biros, S. M.; Bergman, R. G.; Raymond, K. N. *Tetrahedron* **2008**, *64*, 8362.

(12)   Ikeda, A.; Udzu, H.; Zhong, Z.; Shinkai, S.; Sakamoto, S.; Yamaguchi, K. *J. Am. Chem. Soc.* **2001**, *123*, 3872.

(13)   Palmer, L.; Zhao, Y.; Houk, K.; Rebek *Chem. Commun.* **2005**, 3667.

(14)   Rivera, J. M.; Martin, T.; Rebek, J. *J. Am. Chem. Soc.* **2001**, *123*, 5213.

(15)   Shirakawa, S.; Moriyama, A.; Shimizu, S. *Org Lett* **2007**, *9*, 3117.

(16)   Terpin, A.; Ziegler, M.; Johnson, D.; Raymond, K. *Angew Chem Int Edit* **2001**, *40*, 157.

(17)   Tokunaga, Y.; Rebek, J. *J. Am. Chem. Soc.* **1998**, *120*, 66.

(18)   Yoshizawa, M.; Tamura, M.; Fujita, M. *Angew Chem Int Ed Engl* **2007**, *46*, 3874.

(19)   Ziegler, M.; Davis, A.; Johnson, D.; Raymond, K. *Angew Chem Int Edit* **2003**, *42*, 665.

(20)   Thomas, S. W.; Joly, G. D.; Swager, T. M. *Chem. Rev.* **2007**, *107*, 1339.

(21)   Wright, A. T.; Anslyn, E. V. *Chem. Soc. Rev.* **2006**, *35*, 14.

(22)   Nguyen, B.; Anslyn, E. *Coord. Chem. Rev.* **2006**, *250*, 3118.

(23)   McQuade, D. T.; Pullen, A. E.; Swager, T. M. *Chem. Rev.* **2000**, *100*, 2537.

(24)   Szigethy, G.; Raymond, K. N. *Inorg. Chem.* **2009**, *48*, 11489.

(25)   Tandy, S.; Bossart, K.; Mueller, R.; Ritschel, J.; Hauser, L.; Schulin, R.; Nowack, B. *Environ. Sci. Technol.* **2004**, *38*, 937.

(26)   Gorden, A. E. V.; Xu, J.; Raymond, K. N.; Durbin, P. *Chem. Rev.* **2003**, *103*, 4207.

(27)   Piotrowski, H.; Severin, K. *Proc. Natl. Acad. Sci. USA* **2002**, *99*, 4997.

(28)   Legrand, Y.-M.; van der Lee, A.; Barboiu, M. *Science* **2010**, *329*, 299.

(29)   Mal, P.; Breiner, B.; Rissanen, K.; Nitschke, J. R. *Science* **2009**, *324*, 1697.

(30)   Cram, D. J.; Tanner, M. E.; Thomas, R. *Angew. Chem. Int. Ed.* **1991**, *30*, 1024.

(31)   Valegard, K.; Liljas, L.; Fridborg, K.; Unge, T. *Nature* **1990**, *345*, 36.

(32)   Datta, A.; Hooker, J. M.; Botta, M.; Francis, M. B.; Aime, S.; Raymond, K. N. *J. Am. Chem. Soc.* **2008**, *130*, 2546.

(33)   Hooker, J. M.; Datta, A.; Botta, M.; Raymond, K. N.; Francis, M. B. *Nano. Lett.* **2007**, *7*, 2207.

(34)   Mastalerz, M. *Angew. Chem. Int. Ed.* **2010**, *49*, 5042.

(35)   Northrop, B. H.; Zheng, Y.-R.; Chi, K.-W.; Stang, P. J. *Acc. Chem. Res.* **2009**, *42*, 1554.

(36) Nguyen, S.; Gin, D.; Hupp, J.; Zhang, X. *Proc. Natl. Acad. Sci. USA* **2001**, *98*, 11849.

(37) Caulder, D.; Raymond, K. *Acc. Chem. Res.* **1999**, *32*, 975.

(38) Caulder, D.; Powers, R.; Parac, T.; Raymond, K. *Angew. Chem. Int. Ed.* **1998**, *37*, 1840.

(39) Conn; Rebek, J. *Chem. Rev.* **1997**, *97*, 1647.

(40) Kang, J.; Rebek, J. *Nature* **1996**, *382*, 239.

(41) Kang, J.; Santamaria, J.; Hilmersson, G.; Rebek Jr, J. *J. Am. Chem. Soc* **1998**, *120*, 7389.

(42) Tominaga, M.; Suzuki, K.; Kawano, M.; Kusukawa, T.; Ozeki, T.; Sakamoto, S.; Yamaguchi, K.; Fujita, M. *Angew. Chem. Int. Ed.* **2004**, *43*, 5621.

(43) Chen, B.; Xiang, S.; Qian, G. *Acc. Chem. Res.* **2010**, *43*, 1115.

(44) Rudkevich, D. M. *Angew. Chem. Int. Ed.* **2004**, *43*, 558.

(45) Suzuki, K.; Takao, K.; Sato, S.; Fujita, M. *J. Am. Chem. Soc.* **2010**, *132*, 2544.

(46) Suzuki, K.; Sato, S.; Fujita, M. *Nature Chem.* **2009**, *2*, 25.

(47) Sun, W.-Y.; Kusukawa, T.; Fujita, M. *J. Am. Chem. Soc.* **2002**, *124*, 11570.

(48) Dugas, H. *Bioorganic Chemistry: A Chemical Approach to Enzyme Action*; 3rd ed.; Springer-Verlag: New York, 1999.

(49) Bjerre, J.; Rousseau, C.; Marinescu, L.; Bols, M. *Appl. Microbiol. Biotechnol.* **2008**, *81*, 1.

(50) Ren, X.; Xue, Y.; Liu, J.; Zhang, K.; Zheng, J.; Luo, G.; Guo, C.; Mu, Y.; Shen, J. *Chembiochem* **2002**, *3*, 356.

(51) Breslow, R.; Dong, S. *Chem. Rev.* **1998**, *98*, 1997.

(52) Zhang, B.; Breslow, R. *J. Am. Chem. Soc.* **1997**, *119*, 1676.

(53) Kirby, A. J. *Angew. Chem. Int. Ed.* **1996**, *35*, 708.

(54) Breslow, R. *Acc. Chem. Res.* **1995**, *28*, 146.

(55) Hosseini, M. W.; Lehn, J. M.; Jones, K. C.; Plute, K. E.; Mertes, K. B.; Mertes, M. P. *J. Am. Chem. Soc.* **1989**, *111*, 6330.

(56) Hosseini, M. W.; Lehn, J. M.; Mertes, M. P. *Helv. Chim. Acta.* **1983**, *66*, 2454.

(57) Cram, D. J.; Katz, H. E. *J. Am. Chem. Soc.* **1983**, *105*, 135.

(58) Trainor, G. L.; Breslow, R. *J. Am. Chem. Soc.* **1981**, *103*, 154.

(59) Lehn, J. M.; Sirlin, C. *J. Chem. Soc., Chem. Comm.* **1978**, 949.

(60) Yoshizawa, M.; Klosterman, J. K.; Fujita, M. *Angew. Chem. Int. Ed.* **2009**, *48*, 3418.

(61) Koblenz, T. S.; Wassenaar, J.; Reek, J. N. H. *Chem. Soc. Rev.* **2008**, *37*, 247.

(62) Vriezema, D.; Aragones, M.; Elemans, J.; Cornelissen, J.; Rowan, A.; Nolte, R. *Chem. Rev.* **2005**, *105*, 1445.

(63) Sanders, J. *Chem. Eur. J.* **1998**, *4*, 1378.

(64) Uemura, T.; Yanai, N.; Kitagawa, S. *Chem. Soc. Rev.* **2009**, *38*, 1228.

(65) Ma, L.; Abney, C.; Lin, W. *Chem. Soc. Rev.* **2009**, *38*, 1248.

(66) Lee, J.; Farha, O. K.; Roberts, J.; Scheidt, K. A.; Nguyen, S. T.; Hupp, J. T. *Chem. Soc. Rev.* **2009**, *38*, 1450.

(67) Suslick, K. S.; Bhyrappa, P.; Chou, J.-H.; Kosal, M. E.; Nakagaki, S.; Smithenry, D. W.; Wilson, S. R. *Acc. Chem. Res.* **2005**, *38*, 283.

(68) Kesanli, B.; Lin, W. *Coord. Chem. Rev.* **2003**, *246*, 305.

(69) Lensen, D.; Vriezema, D. M.; van Hest, J. C. M. *Macromol. Biosci.* **2008**, *8*, 991.

(70) Helms, B.; Liang, C. O.; Hawker, C. J.; Frechet, J. M. J. *Macromolecules* **2005**, *38*, 5411.

(71) Liu, L.; Rozenman, M.; Breslow, R. *J. Am. Chem. Soc.* **2002**, *124*, 12660.
(72) Liu, L.; Breslow, R. *J. Am. Chem. Soc.* **2002**, *124*, 4978.
(73) Chi, Y.; Scroggins, S. T.; Fréchet, J. M. J. *J. Am. Chem. Soc.* **2008**, *130*, 6322.
(74) Liu, L.; Breslow, R. *J. Am. Chem. Soc.* **2003**, *125*, 12110.
(75) Diederich, F.; Felber, B. *Proc. Natl. Acad. Sci. USA* **2002**, *99*, 4778.
(76) Jacobs, J. W. *Nat. Biotechnol.* **1991**, *9*, 258.
(77) Xu, Y.; Yamamoto, N.; Janda, K. D. *Bioorg. Med. Chem.* **2004**, *12*, 5247.
(78) Mecozzi, S.; Rebek, J. *Chem. Eur. J.* **1998**, *4*, 1016.
(79) Rebek, J. *Angew. Chem. Int. Ed.* **2005**, *44*, 2068.
(80) Mock, W. L.; Irra, T. A.; Wepsiec, J. P.; Adhya, M. *J. Org. Chem.* **1989**, *54*, 5302.
(81) Mock, W. L.; Irra, T. A.; Wepsiec, J. P.; Manimaran, T. L. *J. Org. Chem.* **1983**, *48*, 3619.
(82) Mock, W. L.; Shih, N. Y. *J. Org. Chem.* **1983**, *48*, 3618.
(83) Mock, W. L.; Shih, N. Y. *J. Org. Chem.* **1986**, *51*, 4440.
(84) Ling, X.; Samuel, E. L.; Patchell, D. L.; Masson, E. *Org. Lett.* **2010**, *12*, 2730.
(85) Kang, J.; Rebek, J. *Nature* **1997**, *385*, 50.
(86) Kusukawa, T.; Nakai, T.; Okano, T.; Fujita, M. *Chem. Lett.* **2003**, *32*, 284.
(87) Yoshizawa, M.; Nakagawa, J.; Kumazawa, K.; Nagao, M.; Kawano, M.; Ozeki, T.; Fujita, M. *Angew. Chem. Int. Ed.* **2005**, *44*, 1810.
(88) Yoshizawa, M.; Tamura, M.; Fujita, M. *Science* **2006**, *312*, 251.
(89) Purse, B. W.; Rebek, J. *Proc. Natl. Acad. Sci. USA* **2005**, *102*, 10777.
(90) Pinacho Crisóstomo, F. R.; Lledó, A.; Shenoy, S. R.; Iwasawa, T.; Rebek, J. *J. Am. Chem. Soc.* **2009**, *131*, 7402.
(91) Shenoy, S. R.; Pinacho Crisóstomo, F. R.; Iwasawa, T.; Rebek, J. *J. Am. Chem. Soc.* **2008**, *130*, 5658.
(92) Marinescu, L. G.; Doyaguez, E. G.; Petrillo, M.; Fernãndez-Mayoralas, A.; Bols, M. *Eur. J. Org. Chem.* **2010**, *2010*, 157.
(93) Marinescu, L. G.; Bols, M. *Angew. Chem. Int. Ed.* **2006**, *45*, 4590.
(94) Rousseau, C.; Christensen, B.; Bols, M. *Eur. J. Org. Chem.* **2005**, 2734.
(95) Marinescu, L.; Molbach, M.; Rousseau, C.; Bols, M. *J. Am. Chem. Soc.* **2005**, *127*, 17578.
(96) Das, S.; Brudvig, G. W.; Crabtree, R. H. *Chem. Commun.* **2008**, 413.
(97) Das, S.; Incarvito, C. D.; Crabtree, R. H.; Brudvig, G. W. *Science* **2006**, *312*, 1941.
(98) Fang, Z.; Breslow, R. *Org. Lett.* **2006**, *8*, 251.
(99) Breslow, R.; Fang, Z. *Tetrahedron Lett.* **2002**, *43*, 5197.
(100) Breslow, R.; Zhang, X.; Huang, Y. *J. Am. Chem. Soc.* **1997**, *119*, 4535.
(101) Lightburn, T. E.; Dombrowski, M. T.; Tan, K. L. *J. Am. Chem. Soc.* **2008**, *130*, 9210.
(102) Smejkal, T.; Breit, B. *Angew. Chem. Int. Ed.* **2007**, *47*, 311.
(103) Lee, S. J.; Cho, S.-H.; Mulfort, K. L.; Tiede, D. M.; Hupp, J. T.; Nguyen, S. T. *J. Am. Chem. Soc.* **2008**, *130*, 16828.
(104) Caulder, D. L.; Bruckner, C.; Powers, R. E.; Konig, S.; Parac, T. N.; Leary, J. A.; Raymond, K. N. *J. Am. Chem. Soc.* **2001**, *123*, 8923.
(105) Caulder, D. L.; Powers, R. E.; Parac, T. N.; Raymond, K. N. *Angew. Chem. Int. Ed.* **1998**, *37*, 1840.

(106) Caulder, D. L.; Raymond, K. N. *J. Chem. Soc., Dalton Trans.* **1999**, 1185.

(107) Caulder, D. L.; Raymond, K. N. *Acc. Chem. Res.* **1999**, *32*, 975.

(108) Terpin, A. J.; Ziegler, M.; Johnson, D. W.; Raymond, K. N. *Angew. Chem. Int. Ed.* **2001**, *40*, 157.

(109) Ziegler, M.; Davis, A. V.; Johnson, D. W.; Raymond, K. N. *Angew. Chem. Int. Ed.* **2003**, *42*, 665.

(110) Biros, S. M.; Bergman, R. G.; Raymond, K. N. *J. Am. Chem Soc.* **2007**, *129*, 12094.

(111) Dong, V. M.; Fiedler, D.; Carl, B.; Bergman, R. G.; Raymond, K. N. *J. Am. Chem. Soc.* **2006**, *128*, 14464.

(112) Fiedler, D.; Pagliero, D.; Brumaghim, J. L.; Bergman, R. G.; Raymond, K. N. *Inorg. Chem.* **2004**, *43*, 846.

(113) Ziegler, M.; Brumaghim, J. L.; Raymond, K. N. *Angew. Chem. Int. Ed.* **2000**, *39*, 4119.

(114) Leung, D. H.; Bergman, R. G.; Raymond, K. N. *J. Am. Chem. Soc.* **2007**, *129*, 2746.

(115) Leung, D. H.; Bergman, R. G.; Raymond, K. N. *J. Am. Chem. Soc.* **2006**, *128*, 9781.

(116) Leung, D.; Fiedler; Bergman; Raymond, K. *Angew. Chem. Int. Ed.* **2004**, *43*, 963.

(117) Elkik, E.; Francesch, C. *Bull. Soc. Chim.* **1968**, *3*, 903.

(118) Opitz, G. *Justus Liebigs Ann. Chem.* **1961**, 122.

(119) Fiedler, D.; Bergman, R. G.; Raymond, K. N. *Angew. Chem. Int. Ed.* **2004**, *43*, 6748.

(120) Fiedler, D.; Halbeek, H. V.; Bergman, R. G.; Raymond, K. N. *J. Am. Chem. Soc.* **2006**, *128*, 10240.

(121) Fiedler, D.; Bergman, R. G.; Raymond, K. N. *Angew. Chem. Int. Ed.* **2004**, *43*, 6748.

(122) Hirst, S. C.; Hamilton, A. D. *J. Am. Chem. Soc.* **1991**, *113*, 382.

(123) Brumaghim, J. L.; Michels, M.; Raymond, K. N. *Eur. J. Org. Chem.* **2004**, *22*, 4552.

(124) Ziegler, M.; Brumaghim, J. L.; Raymond, K. N. *Angew. Chem. Int Ed* **2000**, *39*, 4119.

(125) Pluth, M. D.; Bergman, R. G.; Raymond, K. N. *Science* **2007**, *316*, 85.

(126) Pluth, M. D.; Bergman, R. G.; Raymond, K. N. *J. Am. Chem Soc* **2007**, *129*, 11459.

(127) Pluth, M. D.; Bergman, R. G.; Raymond, K. N. *Angew. Chem. Int. Ed.* **2007**, *46*, 8587.

(128) Pluth, M. D.; Bergman, R. G.; Raymond, K. N. *Science* **2007**, *316*, 85.

(129) Pluth, M. D.; Bergman, R. G.; Raymond, K. N. *J. Am. Chem. Soc.* **2008**, *130*, 11423.

(130) Pluth, M. D.; Bergman, R. G.; Raymond, K. N. *Acc. Chem. Res.* **2009**, *42*, 1650.

(131) Pluth, M. D.; Bergman, R. G.; Raymond, K. N. *J. Org. Chem.* **2009**, *74*, 58.

(132) Ma, J.; Dougherty, D. *Chem. Rev.* **1997**, *97*, 1303.

Chapter 2

Enzyme-like Mechanism of the Propargylic Aza Cope Rearrangement Catalyzed by Supramolecular Encapsulation

Introduction

Pericyclic reactions are attractive targets in supramolecular catalysis because encapsulation can enforce the geometries necessary for enhanced reactivity, even in the absence of accelerating functional groups within the cavity. Diels-Alder reactions, for example, are particularly well suited for this mode of catalysis, since co-encapsulation of the diene and the dienophile in a constrictive environment dramatically increases the local concentration of these reactants. Rebek and co-workers reported the first example of a host-mediated Diels-Alder reaction, and several reports from the Fujita research group have utilized a metal-ligand host to accelerate the Diels-Alder reaction of dienes that are unreactive in the absence of a catalyst.[1-5] In both systems, product inhibition is observed unless the Diels-Alder adduct has a lower affinity for the host interior than the reactants.[2,5] Thus, low levels of discrimination between the reactants and products of host-accelerated reactions are a major limitation of these reactions.

= Ga^{III}, **1**

One strategy that can be used to circumvent this problem is the continuous conversion of product into a species that is not bound by the host. This approach was taken in the catalysis of the sigmatropic rearrangement of allyl enammonium cations using the $[Ga_4L_6]^{12-}$ assembly (**1**, where L = N,N′-bis(2,3-dihydroxybenzoyl)-1,5-diaminonaphthalene).[6,7] The 3-aza Cope rearrangement first converts an allyl enammonium cation to a γ,δ-unsaturated iminium cation via [3,3] sigmatropic rearrangement, which is then hydrolyzed to the corresponding aldehyde (Figure 2.1).[8,9] This reaction is catalyzed by **1**, and rate enhancements of up to 854 times were measured.[6] Although the product iminium ion is encapsulated in **1**, hydrolysis converts this species to a neutral aldehyde which in turn is much more weakly encapsulated, thereby allowing for catalytic turnover. The activation parameters for both the free and the assembly-mediated reaction were determined for several substrates, and while the enthalpies of activation were nearly identical, the entropies of activation for reactions of encapsulated guests were less negative compared to those occurring in free solution. This strongly suggests that a major component of the observed rate enhancement is the pre-organization of the encapsulated substrate into a chair-like conformation that closely resembles the expected transition state of the sigmatropic rearrangement. This hypothesis was confirmed by a NOESY experiment, which showed strong correlations between the two ends of the linear enammonium cation when it is encapsulated, but not when it is free in aqueous solution.[6]
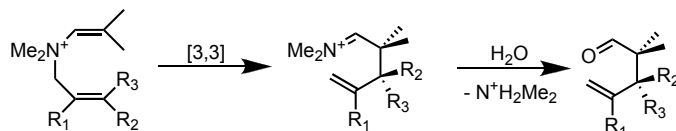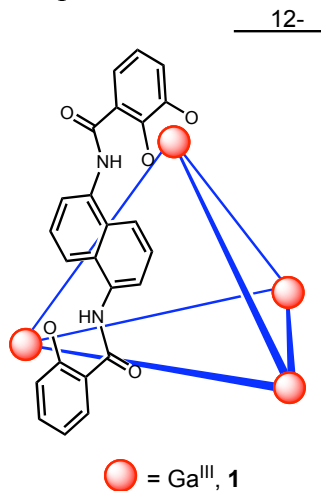
Figure 2.1. General scheme for the aza Cope rearrangement of allyl enammonium cations.

Having investigated the catalysis of the aza Cope rearrangement of allyl enammonium ions using **1**, the scope of this reaction is now expanded to include propargyl-enammonium substrates (Figure 2.2). The uncatalyzed reaction rates of these compounds are slower than those

of the allyl-vinyl substrates, necessitating elevated temperatures to obtain useful rates of reaction. For this reason, it was of interest to determine whether encapsulation within **1** would accelerate this more challenging reaction. Furthermore, having observed that rate enhancements are highly shape-selective in the original studies, the series of propargyl compounds were interesting because they presumably require more energy to adopt the conformations similar to those of their as the vinyl analogues.
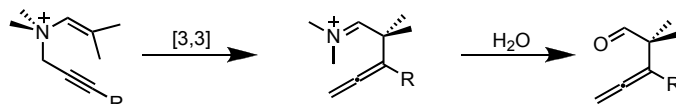
Figure 2.2. General reaction scheme of the 3-aza Cope rearrangement. Starting from a propargyl enammonium cation, [3,3] sigmatropic rearrangement leads to an allenyl iminium cation, which then hydrolyzes to an allenyl aldehyde.

Results and Discussion

  Substrate Synthesis. A range of propargyl enammonium tosylates with varying alkyl substituents at the alkyne terminus was prepared (Figure 2.3). Substrates were synthesized by alkylation of *N,N*-dimethylisobutenylamine with the appropriate propargyl tosylate, which was derived from the corresponding propargyl alcohol. Propargyl alcohols that were not commercially available were prepared by alkylation of the primary acetylide with paraformaldehyde, or by the Corey-Fuchs alkyne synthesis (Figure 2.4).[10] While crude yields were generally 80-90%, low isolated yields for substrates **5**, **6**, **7**, and **10** were a result of inefficient recrystallizations necessary to obtain analytically pure material. The enamine alkylation reaction of 3-butynyl-2-tosylate failed to provide compound **13**, presumably due to the added steric hindrance caused by the additional methyl group at the 2 position.
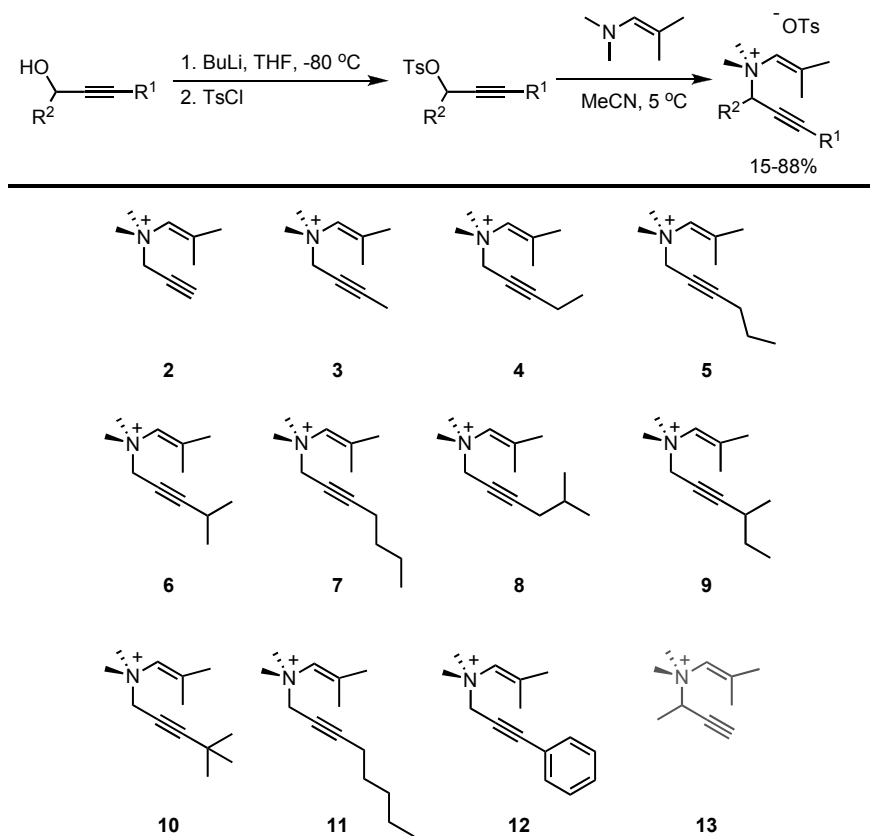
Figure 2.3. Synthesis of the propargyl enammonium substrates. Attempts to prepare **13** were not successful.
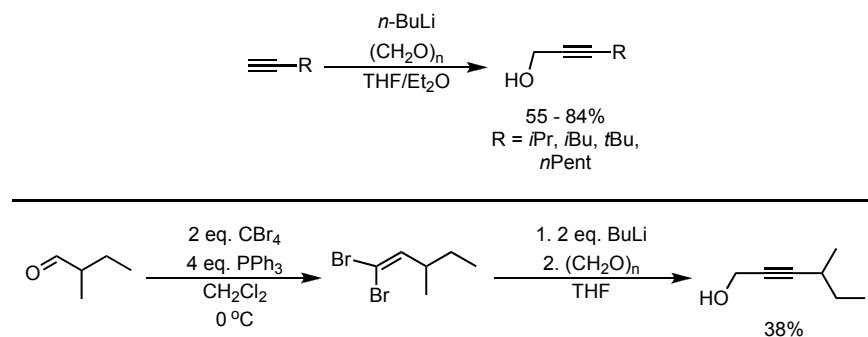
Figure 2.4. Propargyl alcohol synthesis for the preparation of aza Cope substrates.

Encapsulation and Rate Acceleration. Upon encapsulation in **1**, the guest proton NMR resonances are shifted upfield 2-4 ppm relative to the unencapsulated species, due to the anisotropic ring current in the nearby naphthalene walls of **1**. Furthermore, encapsulation into the chiral interior of **1** renders enantiotopic guest protons diastereotopic. This typically affects the protons of a methylene group and the two *N*-methyl groups present in each substrate

27

molecule. Host-guest complexes of compounds **2-9** are formed quantitatively in D_2O and DMSO-d_6, as determined by ^{1}H-NMR spectroscopy. Further evidence for these host-guest complexes was obtained by high-resolution electrospray mass spectrometry. Although conventional mass spectrometry methods cause fragmentation of the metal-ligand assembly during ionization, it is possible to detect the intact assembly using a Quadrupole Time-of-Flight (Q-TOF) instrument equipped with a Z-spray ion source.[11] The host-guest complexes are typically detected with between six and eight associated counterions, corresponding to species with overall charge between -5 and -3. Two to three distinct charge states are typically observed for each host-guest complex. Encapsulation occurs within minutes, and substrates can be ejected from the host interior by the addition of the tetraethylammonium cation, a strongly binding guest. Guests bearing more sterically demanding *tert*-butyl (**10**), *n*-pentyl (**11**), and phenyl (**12**) substituents are not encapsulated, demonstrating that encapsulation of these substrates is highly size-dependent. It is noteworthy that among the four isomers bearing a butyl group at the alkyne terminus (**7-10**), only the *tert*-butyl substituted substrate **10** is excluded from the host interior. These results suggest that butyl-substituted compounds are only encapsulated if they possess a certain degree of conformational flexibility, and reflect the shape-selectivity of **1**.

After demonstrating the scope of encapsulation, the rates of the aza Cope rearrangement/hydrolysis of both the free and encapsulated substrates were measured at 60 ˚C. Reactions were monitored by ^{1}H-NMR spectroscopy, and rates of reaction were measured by following the disappearance of starting material due to the insolubility of the product aldehydes in D_2O (product formation is observed by ^{1}H-NMR when wet DMSO-d_6 is used as the solvent). The reaction rates of encapsulated enammonium cations were measured using a stoichiometric amount of **1**, and the background reaction was monitored in the absence of **1**. Clean first-order disappearance of starting material was observed in both the encapsulated and unencapsulated reactions, and the observed rate constants are shown in Table 2.1. For each substrate that was encapsulated by **1** (compounds **2-9**), encapsulation accelerated the rate of reaction up to two orders of magnitude over that of the free reaction. In the unencapsulated reaction, the substrates with larger groups at the alkyne terminus (**4-8**) react more slowly due to steric repulsion that disfavors the reactive, chair-like conformation required in the transition state. In the reaction of encapsulated substrates, however, the fastest rates were observed for the medium-sized substrates (**3-6**), while the largest and smallest compounds reacted more slowly. This "optimal fit" trend was also observed in earlier work on allyl enammonium guests.[7]

Substrate	R	k_{free} (x 10^{-8} s^{-1})	k_{encaps} (x 10^{-8} s^{-1})	k_{encaps}/k_{free}
2	H	62.4	237	4
3	Me	62.3	6200	100
4	Et	20.0	3670	184
5	*n*-Pr	19.5	1920	98
6	*i*-Pr	6.7	870	129
7	*n*-Bu	15.1	73	5
8	*i*-Bu	17.0	477	28
9	*s*-Bu	50.0	1150	23

Table 2.1. Rate constants for background (k_{free}) and encapsulated (k_{encaps}) reactions (Measured at 60 °C in D_2O) and their rate accelerations.

Catalytic Kinetics. With the exception of **6**, the iminium rearrangement product is rapidly hydrolyzed to the corresponding aldehyde, leaving behind **1** absent any strongly binding guest. Previous studies have shown that the iminium hydrolysis step occurs outside the host cavity.[7] Encouraged by the regeneration of empty **1**, the feasibility of using **1** as a catalyst for this reaction was explored. Due to the relatively slow reaction rates of the reactions catalyzed by **1**, substrate **3**, having the fastest encapsulated rate of reaction (k_{encaps}), was used to study the kinetics of the catalytic system. The addition of over five equivalents of **3** to an aqueous solution of **1** caused significant precipitation, likely due to the strong electrostatic binding of additional substrate molecules to the exterior of the assembly. Addition of NMe_4^+, a cation with a strong exterior binding affinity for **1** that does not cause precipitation when added in superstoichiometric amounts, does not displace **3** or prevent precipitation of **1**. Solutions of **1** and **3** in DMSO-d$_6$ or D_2O/DMSO-d$_6$ are homogeneous even at high ratios of **3** to **1**. A minimum of 20% DMSO-d$_6$ (by volume) in D_2O is necessary to ensure homogeneity; those conditions were used for the all catalytic kinetic studies. Interestingly, the rate of the **1**-catalyzed reaction of **3** in nearly-anhydrous DMSO-d$_6$ is substantially slower than when water has been added. Under these reaction conditions a new encapsulated species is observed by ^{1}H-NMR, which is presumably the product iminium ion, and the resonance corresponding to residual H_2O is consumed. This implies that under anhydrous conditions, the iminium hydrolysis step following rearrangement slows to the point of being rate-limiting, while it is rapid when higher concentrations of water are present.

Kinetic analysis of the catalytic reaction of substrate **3** showed that when over 3 equivalents of substrate are present, the overall reaction is zeroth order in substrate (Figure 2.5). This suggests that the encapsulated starting material is the resting state of the catalyst and the rate-limiting step of the reaction is the sigmatropic rearrangement of the bound substrate, followed by rapid product release and binding an additional substrate molecule (Figure 2.6). Thus, the rate of reaction is dependent on the concentration of host-bound substrate, rather than the total concentration of substrate, leading to the equation: rate = k_2[**3** ⊂ **1**] (where ⊂ denotes

encapsulation). Consistent with this rate law, under zeroth order conditions, the observed concentration of [**3** ⊂ **1**] is invariant (Figure 2.5), confirming that host-bound starting material [**3** ⊂ **1**] is the catalyst resting state. Using the experimentally determined concentration of [**3** ⊂ **1**] and the observed rate of reaction, it is possible to determine the rate constant k_2 for this rate law. This first order rate constant is identical to the rate constant determined from the first order plot of the stoichiometric reaction of [**3** ⊂ **1**]. Thus, the proposed rate law describes both the stoichiometric and the catalytic reaction. Throughout these experiments, the only encapsulated species present is host-bound starting material [**3** ⊂ **1**]; the encapsulation of the iminium rearrangement product is never observed. Taken together with the kinetic profile of this reaction, one can conclude that **1** is a true catalyst in this reaction and does not suffer from product inhibition.
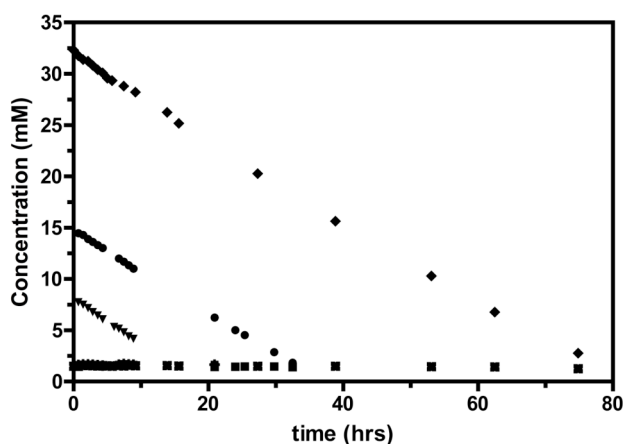
Figure 2.5. Concentration vs. time plots of the catalytic aza Cope rearrangement of **3**. Unbound starting material concentration: ◆, 19 equivalents of **3** with respect to **1**; ●, 9 equivalents of **3**; ▲, 4.5 equivalents of **3**. Concentration of host-bound substrate [**3** ⊂ **1**]: ×, ✳ and ■; 19, 9, and 4.5 equivalents of **3** with respect to **1**, respectively. The concentration of [**3** ⊂ **1**] is constant regardless of [**3**], and the points from different experiments are overlapping.
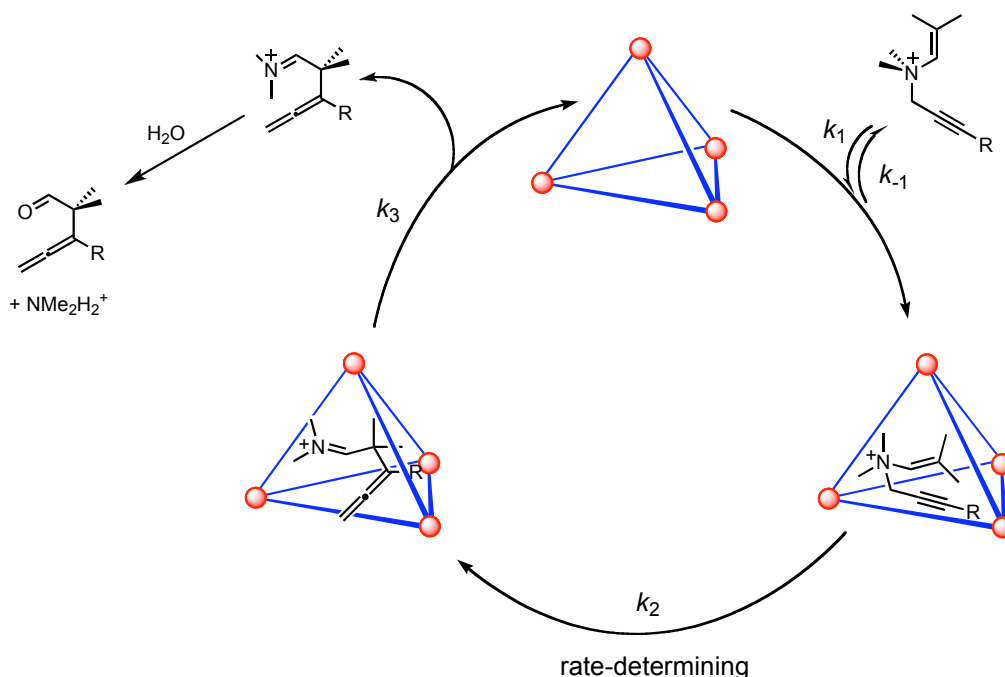
Figure 2.6. Proposed catalytic cycle for the propargyl 3-aza Cope rearrangement. The rearrangement of the encapsulated substrate (k_2) is rate determining.

Michaelis-Menten Analysis. In enzymatic catalysis, a substrate and enzyme are typically in a reversible equilibrium with an enzyme-substrate complex, and the conversion of enzyme-bound substrate into enzyme-bound product is rate determining. A consequence of this scenario is the observation of rate saturation at high substrate concentration, when the enzyme-substrate complex is quantitatively formed. The Michaelis-Menten kinetic model is most frequently used to understand this type of enzymatic pathway.[12] The kinetic parameters of the catalyzed rearrangement for this model were determined from an Eadie-Hofstee plot of the substrate saturation curve of **3** (V_{max} = 1.2 x 10^{-4} mM s^{-1}, K_m = 0.67 mM, and k_{cat} = 7.0 x 10^{-5} s^{-1} where V_{max} is the maximum velocity of the reaction, K_m is the Michaelis constant, and k_{cat} is the turnover rate of the bound substrate).[13,14] The calculated V_{max} is identical to the maximum measured velocity of the reaction under saturation conditions and the calculated k_{cat} is equal to the rate constant for the rearrangement of the encapsulated guest measured under stoichiometric conditions. In systems such as this, where a fast pre-equilibrium is established prior to the catalytic step (k_1 and k_{-1} are much larger than k_2), the Michaelis constant K_m is essentially a dissociation constant. The K_m for **3** is larger than the K_d for NEt_4^+ (5.1 x 10^{-2} mM), but smaller than the K_d of NMe_4^+ (9.0 mM), which is consistent with competitive binding experiments in which **3** displaces [$NMe_4^+ \subset$ **1**], and NEt_4^+ displaces [**3** $\subset$ **1**].

A characteristic aspect of enzymatic catalysis is the inhibition of the enzyme active site with a suitable, non-reactive molecule whose binding is competitive with that of the substrate.[12] A bound inhibitor will exclude substrate from the active site thereby inhibiting the activity of the enzyme. If the binding of the substrate and the inhibitor is truly competitive, the inhibitor can be completely displaced if the substrate concentration is sufficiently high, and at infinite substrate

concentration, the maximum reaction velocity (V_{max}) will be equal to that of the uninhibited reaction. To perform these experiments using **1**, several non-reactive alkylammonium guests were considered as competitive inhibitors. In previous work, it was determined that ionic strength has no effect on the rate of reaction, so there was no concern about any salt effects from added alkylammonium species.[7] The resonances of encapsulated NMe_4^+ overlap with those of encapsulated **3**, and the displacement of strongly bound NEt_4^+ requires a large excess of **3**. Thus, both NMe_4^+ and NEt_4^+ are not suitable inhibitors for these experiments. The ^{1}H-NMR resonances of encapsulated NPr_4^+ are easily resolved from those of encapsulated **3** (Figure 2.7), and their binding constants are the same order of magnitude, making NPr_4^+ an ideal inhibitor for these experiments.
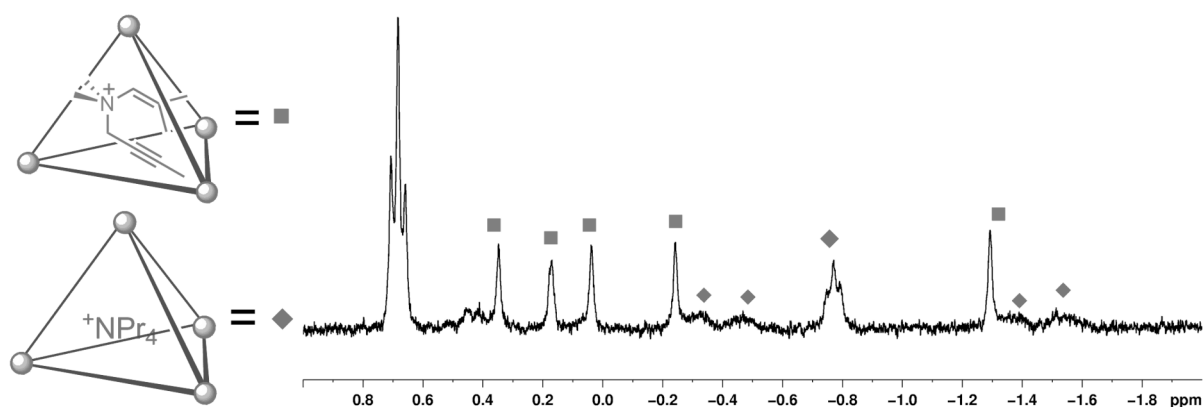
Figure 2.7. ^{1}H-NMR spectrum of a sample containing 1 equivalent each of **1** (■), substrate **3** (◆), and NPr_4Br. Encapsulation is observed for both species.

Rate data under saturation conditions were collected in the presence of 4 and 10 equivalents of NPr_4^+ with respect to **1**. These data, together with the saturation data obtained in the absence of inhibitor, are shown in an Eadie-Hofstee plot (Figure 2.8), from which the relevant Michaelis-Menten parameters were determined. [13,14] As expected, a larger excess of substrate is required to reach the maximum reaction velocity in the presence of inhibitor, but the same V_{max} is eventually achieved. These experiments clearly demonstrate that NPr_4^+ acts as a competitive inhibitor in this system, and show that the kinetic behavior of this system is comparable to that observed in earlier studies of assembly-catalyzed orthoformate and acetal hydrolysis, as well as to the mode of action of enzymes.[15]
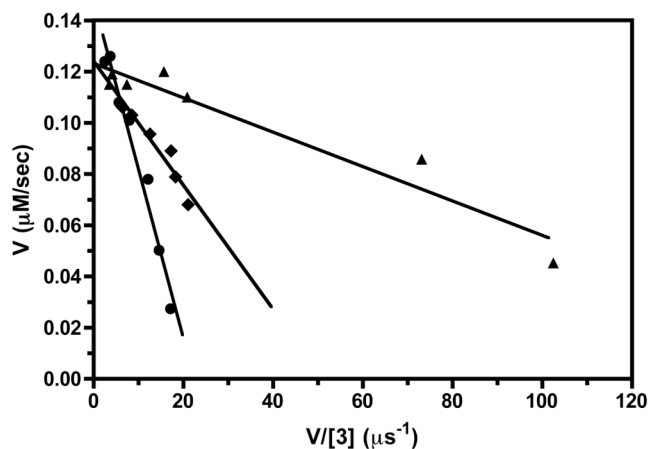
Figure 2.8. Eadie-Hofstee plot of inhibition data for the catalytic 3-aza Cope rearrangement of [**3** $\subset$ Ga$_4$L$_6$]$^{11-}$, using NPr$_4^+$ inhibitor. $\blacktriangle$, no inhibitor added; $\blacklozenge$, 4 equivalents NPr$_4^+$; $\bullet$, 10 equivalents NPr$_4^+$.

Activation Parameters of the Catalytic Reaction. Previous studies on the **1**-catalyzed aza Cope rearrangement revealed that lowered entropy of activation is responsible for rate enhancements over the background reaction. It was of interest to determine whether rate accelerations originated from similar entropic considerations in this system. Variable temperature kinetics of the catalyzed and uncatalyzed reaction of **3** were measured, and Eyring analysis of the resulting data provided activation parameters for both reactions. The activation parameters of the uncatalyzed rearrangement of **3** are $\Delta H^{\ddagger} = 23(3)$ kcal/mol and $\Delta S^{\ddagger} = -19(4)$ e.u. (Figure 2.9). The highly negative $\Delta S^{\ddagger}$ is a common feature of [3,3] sigmatropic rearrangements, and it reflects the organized transition state that the molecule must adopt in this reaction. The $\Delta S^{\ddagger}$ for this reaction is more negative than that measured for analogous allyl enammonium species, which accounts for the lower reactivity of the propargyl systems in the aza Cope rearrangement.[6] In general, however, the $\Delta S^{\ddagger}$ of the [3,3] sigmatropic rearrangement of 1,5-eneynes is not more negative than the $\Delta S^{\ddagger}$ of corresponding 1,5 dienes, and no clear trend in the activation parameters between these two classes of compounds has been identified.[16]
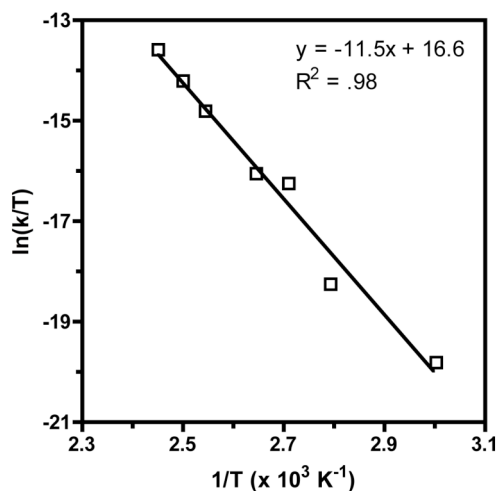
Figure 2.9. Eyring plot used to determine activation parameters for the uncatalyzed aza Cope rearrangement of **3**.

The activation parameters for the catalyzed rearrangement of **3** are $\Delta H^{\ddagger} = 26(5)$ kcal/mol and $\Delta S^{\ddagger} = +2.8(9)$ e.u. (Figure 2.10). The $\Delta S^{\ddagger}$ differs by more than 20 e.u. from that of the background rearrangement, a dramatic change that strongly suggests that **1** selectively binds a pre-organized, reactive conformation of the substrate. The bound substrate has fewer degrees of freedom in the confines of the assembly, and cannot adopt the conformation that would be lowest in energy for the unencapsulated molecule. The enthalpies of activation of the two reactions are equal within error, so it is clear that the entropic component of this reaction determines the observed rate enhancements.
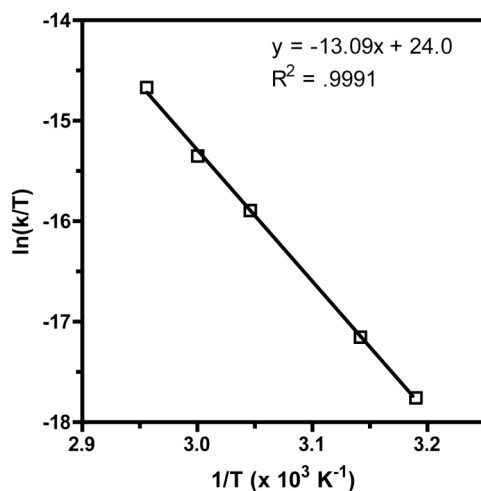
Figure 2.10. Eyring plot used to determine activation parameters for the **1**-catalyzed aza Cope rearrangement of **3**.

Conclusion

In summary, a supramolecular metal-ligand assembly can catalyze the aza Cope rearrangement of propargyl enammonium cations. While classical catalysis of such sigmatropic rearrangements typically requires Lewis or Brønsted acid, substrate encapsulation within the confined host interior enforces a reactive conformation that accelerates the rates of rearrangement by up to 184 times. Consistent with this explanation, the determination of the activation parameters for the host-catalyzed and uncatalyzed reactions reveals that rate enhancements are due to a more positive $\Delta S^{\ddagger}$ for rearrangement in the catalytic reaction. The catalytic reaction obeys the Michaelis-Menten model of enzyme kinetics, and competitive inhibition of this reaction can be observed using NPr_4^+, a non-reactive guest. These studies demonstrate how supramolecular hosts are able to act as enzyme mimics in the catalysis of challenging reactions under mild, aqueous conditions.

Experimental Section

  General Considerations. Unless otherwise noted, reactions and manipulations were performed using standard Schlenk and high-vacuum techniques, and conducted at room temperature. Glassware was dried in an oven at 150 °C overnight or flame-dried under vacuum prior to use. NMR spectra were obtained on Bruker Avance AV 300, AV 400, DRX 500, or AV-500 spectrometers. Chemical shifts are reported as δ in parts per million (ppm) relative to residual protonated solvent resonances. For NMR spectra run in D_2O, ^{13}C shifts were referenced to an internal standard of CD_3OD.[17] Coupling constants are reported in Hz. IR spectra were measured on neat samples using a Nicolet Avatar 370 FT-IR instrument with a zinc selenide attenuated total reflective (ATR) accessory. Peak intensities are reported as (b) broad, (w) weak, (m) medium, or (s) strong. Only peaks in the functional group region (4000-1300 cm^{-1}) are reported.

  Elemental analyses, low resolution fast atom bombardment, high resolution fast atom bombardment, and high resolution electrospray time of flight (TOF-ESMS) mass spectrometry were performed at the University of California, Berkeley, Microanalytical Facility. Elemental analyses were performed on a Perkin-Elmer Series II CHNO/S analyzer. Reliable combustion analyses for the host-guest compounds were not possible due to varying amounts of solvent bound to the exterior of the assembly. Fast atom bombardment mass spectra were recorded on a Micromass ZAV2-EQ (magnetic sector) instrument. High resolution TOF ESMS of the host-guest complexes were recorded on a Waters QTOF API mass spectrometer equipped with a Z-spray source.

  Unless otherwise noted, reagents were obtained from commercial suppliers and used without further purification. Anhydrous solvents were dried over activated alumina under nitrogen pressure and sparged with nitrogen before use.[18] $K_{12}Ga_4L_6$ (K_{12}**1**),[19] *N,N*-dimethylisobutenylamine,[20] 4-methyl-2-hexynol,[21] and 5-methyl-2-hexynol[22] were prepared according to published procedures.

  General Procedure for Tosylation Reactions. Tosylates were prepared by analogy to a published procedure.[6] Typical procedure: in a 500mL Schlenk flask, 15.0 mmol of the appropriate propargyl alcohol was combined with 80 mL of THF and the solution was cooled to –78 °C. To this solution was added *n*-butyllithium (6.5 mL, 15.0 mmol, 2.3 M in hexanes). *p*-Toluenesulfonyl (tosyl) chloride (2.86 g, 15.0 mmol) was then added in a single portion and the resulting homogeneous solution was put in the freezer at –80 °C for 2 days. The reaction was worked up by diluting the reaction mixture with 150 mL of petroleum ether. The organic phase was washed with 50% saturated aqueous $NaHCO_3$ (2 x 50 mL) and saturated aqueous $NaHCO_3$ (1x 50 mL). The aqueous layers were combined and extracted with 50 mL of petroleum ether and the combined organic layers were dried over $MgSO_4$. After filtration, the volatile materials were removed by rotary evaporation, affording the propargyl tosylates. The tosylates decompose rapidly, and were therefore characterized by ^1H only and immediately used without further purification.

Data for Propargyl Tosylates, Prepared As Described Above.

2-Propynyl tosylate. The reaction was carried out using 2-propynol (1.121 g, 20.0 mmol) with an equimolar amount of *n*-butyllithium (3.2 mL, 20.0 mmol, 2.45 M) and tosyl chloride (3.813 g, 20.0 mmol). The title compound was obtained as a yellow oil in 77% yield (3.272 g, 15.4 mmol), and exhibited spectroscopic properties consistent with those reported in the literature.[23]

2-Butynyl tosylate. The reaction was carried out using 2-butynol (1.816 g, 40.0 mmol) with an equimolar amount of *n*-butyllithium (16.4 mL, 40.0 mmol, 2.45 M) and tosyl chloride (7.619 g, 40.0 mmol). The title compound was obtained as an orange oil in 63% yield (5.65 g, 25.2 mmol), and exhibited spectroscopic properties consistent with those reported in the literature.[24]

2-Pentynyl tosylate. The reaction was carried out using 2-pentynol (3.370 g, 40.0 mmol) with an equimolar amount of *n*-butyllithium (16.4 mL, 40.0 mmol, 2.45 M) and tosyl chloride (7.61 g, 40.0 mmol). The title compound was obtained as an orange oil in 51% yield (4.88 g, 20.5 mmol), and exhibited spectroscopic properties consistent with those reported in the literature.[24]

2-Hexynyl tosylate. The reaction was carried out using 2-hexynol (1.472 g, 15.0 mmol) with an equimolar amount of *n*-butyllithium (6.0 mL, 15.0 mmol, 2.5 M) and tosyl chloride (2.864 g, 15.0 mmol). The title compound was obtained as a pale yellow oil in 93% yield (3.52 g, 14.1 mmol), and exhibited spectroscopic properties consistent with those reported in the literature.[25]

4-Methyl-2-pentynyl tosylate. The reaction was carried out using 4-methyl-2-pentynol (464 mg, 4.7 mmol) with an equimolar amount of *n*-butyllithium (1.9 mL, 4.7 mmol, 2.5 M) and tosyl chloride (906 mg, 4.7 mmol). The title compound was obtained as a pale yellow oil in 41% yield (487 mg, 1.9 mmol). **^{1}H NMR** (300 MHz, CDCl$_3$): δ 7.77 (d, ^3J = 8.1 Hz, 2H, Ar-*H*), 7.31 (d, ^3J = 8.1 Hz, 2H, Ar-*H*), 4.67 (s, 2H, OC*H*$_2$), 2.3-2.5 (m, 4H, Ar-C*H*$_3$, C=C-*H*), 0.99 (d, ^3J = 6.9 Hz, 6H, CH(C*H*$_3$)$_2$) ppm.

2-Heptynyl tosylate. The reaction was carried out using 2-heptynol (1.690 g, 15.0 mmol) with an equimolar amount of *n*-butyllithium (6.0 mL, 15.0 mmol, 2.5 M) and tosyl chloride (2.853 g, 15.0 mmol). The title compound was obtained as a yellow oil in 88% yield (3.13 g, 13.2 mmol). **^{1}H NMR** (300 MHz, CDCl$_3$): δ 7.76 (d, ^3J = 8.1 Hz, 2H, Ar-*H*), 7.30 (d, ^3J = 8.4 Hz, 2H, Ar-*H*), 4.65 (s, 2H, OC*H*$_2$), 2.40 (s, 3H, Ar-C*H*$_3$), 2.01 (t, ^3J = 4.5 Hz, 2H, C≡C-C*H*$_2$), 1.28 (m, 4H, C*H*$_2$- C*H*$_2$-CH$_3$), 0.82 (t, ^3J = 6.9 Hz, 3H, C*H*$_3$) ppm.

5-Methyl-2-hexynyl tosylate. The reaction was carried out using 5-methyl-2-hexynol (2.332 g, 20.8 mmol) with an equimolar amount of *n*-butyllithium (8.3 mL, 20.8 mmol, 2.5 M) and tosyl chloride (3.969 g, 20.8 mmol). The title compound was obtained as a colorless oil in 97% yield (5.3832 g, 20.2 mmol). **^{1}H NMR** (300 MHz, CDCl$_3$): δ 7.79 (d, ^3J = 8.3 Hz, 2H, Ar-*H*), 7.32 (d, ^3J = 8.3 Hz, 2H, Ar-*H*), 4.69 (t, ^4J = 2.2 Hz, 2H, OC*H*$_2$), 2.42 (s, 3H, Ar-C*H*$_3$), 1.95

(dt, ^3J = 6.6 Hz, ^4J = 2.2 Hz, C≡C-CH_2), 1.66 (m, 1H, CH(CH$_3$)$_2$), 0.86 (d, , ^3J = 6.6 Hz, 6H, CH(CH_3)$_2$) ppm.

4-Methyl-2-hexynyl tosylate. The reaction was carried out using 4-methyl-2-hexynol (2.378 g, 21.2 mmol) with an equimolar amount of *n*-butyllithium (9.9 mL, 21.2 mmol, 2.15 M) and tosyl chloride (4.04 g, 20.8 mmol). The title compound was obtained as a colorless oil in 97% yield (3.470 g, 13.0 mmol). **^{1}H NMR** (300 MHz, CDCl$_3$): δ 7.80 (d, ^3J = 8.1 Hz, 2H, Ar-H), 7.33 (d, ^3J = 8.0 Hz , 2H, Ar-H), 4.71 (d, ^3J = 2.0 Hz 2H, OCH_2), 2.43 (s, 3H, Ar-CH_3), 2.23 (m, 1H, C≡C-CH), 1.31 (m, 2H, C≡C-CH-CH_2) 1.0 (d, ^3J = 6.9 Hz, 3H, C≡C-CH-CH_3), 0.8 (t, ^3J = 7.4 Hz, 3H, C≡C-CH-CH$_2$-CH_3) ppm.

4,4-Dimethyl-2-pentynyl tosylate. The reaction was carried out using 4,4-dimethyl-2-pentynol (1.03 g, 9.2 mmol) with an equimolar amount of *n*-butyllithium (3.7 mL, 9.2 mmol, 2.5 M) and tosyl chloride (1.75 g, 9.2 mmol). The title compound was obtained as a pale yellow oil in 43% yield (1.07 g, 4.0 mmol). **^{1}H NMR** (300 MHz, CDCl$_3$): δ 7.77 (d, ^3J = 8.4 Hz, 2H, Ar-H), 7.30 (d, ^3J = 8.1Hz, 2H, Ar-H), 4.97 (s, 2H, OCH_2), 2.40 (s, 3H, Ar-CH_3), 1.03 (s, 9H, (CH_3)$_3$) ppm.

2-Octynyl Tosylate. The reaction was carried out using 2-octynol (1.52 g, 10.7 mmol) with an equimolar amount of *n*-butyllithium (4.3 mL, 10.7 mmol, 2.5 M) and tosyl chloride (1.83 g, 9.6 mmol). The title compound was obtained as a pale yellow oil in 54% yield (1.56 g, 5.2 mmol) and exhibited spectroscopic properties consistent with those reported in the literature.[26]

3-Phenyl-2-propynyl tosylate. The reaction was carried out using 4-methyl-2-pentynol (464 mg, 4.7 mmol) with an equimolar amount of *n*-butyllithium (1.9 mL, 4.7 mmol, 2.5 M) and tosyl chloride (906 mg, 4.7 mmol). The title compound was obtained as a yellow oil in 84% yield (3.61 g, 12.6 mmol).   **^{1}H NMR** (300 MHz, CHCl$_3$): δ 7.86 (d, ^3J = 8.4 Hz, 2H, Ar-H), 7.34-7.24 (m, 7 H, Ar-H + Ph-H + CHCl$_3$), 4.96 (s, 2H, OCH_2), 2.40 (s, 3H, Ar-CH_3) ppm.

3-Butynyl-2-tosylate. The reaction was carried out using 3-butyn-2-ol (980 mg, 13.8 mmol) with stoichiometric amounts of *n*-butyllithium (5.5 mL, 13.8 mmol, 2.5 M) and TsCl (2.86 g, 15.0 mmol). The product was obtained as a pale yellow oil in 67% yield (2.09 g, 9.3 mmol). **^{1}H NMR** (300 MHz, CDCl$_3$): δ 7.76 (d, ^3J = 8.4 Hz, 2H, Ar-H), 7.29 (d, ^3J = 8.4 Hz, 2H, Ar-H), 5.11 (qd, ^3J = 6.6 Hz, ^4J = 2.1, 1H, OCH), 2.40 (s, 4H, CH + Ar-CH_3), 1.51 (d, ^3J = 6.6, 3H, CH_3) ppm.

General Procedure for Alkylation Reactions. Propargyl enammonium tosylates **2-12** were prepared by analogy to a literature procedure.[6] Typical procedure: under positive N$_2$ pressure, a cooled solution (0 °C) of N,N-dimethylisobutenylamine (382 mg, 3.9 mmol) in 5 mL of acetonitrile was added by syringe to a cooled solution (0 °C) of the appropriate propargyl tosylate (4.3 mmol) in 5 mL acetonitrile. The resulting mixture was stirred at 5 °C for 48 h. All volatile materials were removed under reduced pressure, giving oily residues. The residues were washed with 5 x 20 mL dry Et$_2$O, yielding crude material as either an off-white powder or a

yellow oil. For all propargyl enammonium tosylates, the parent ion of the enammonium cation was detected by mass spectrometry.

Data for Enammonium Salts, Prepared As Described Above.
　　　　[NMe₂(2-propynyl)(CH=C(CH₃)₂)][OTs] (2). This reaction was carried out using 382 mg enamine (3.9 mmol) and 904 mg tosylate (4.3 mmol). The analytically pure product was isolated in 89% yield (1.18 g, 3.35 mmol) as an off-white sticky residue which solidified upon cooling to -30 °C. **¹H NMR** (500 MHz, D₂O): δ 7.69 (d, ^3J = 8.1 Hz, 2H, Ar-*H*), 7.36 (d, ^3J = 8.4 Hz, 2H, Ar-*H*) 5.97 (br, 1H, C=C*H*), 4.38 (d, ^3J = 2.5 Hz, 2H, N-C*H₂*), 3.36 (s, 6H, N(C*H₃*)₂), 2.70 (s, 1H, C≡C-*H*), 2.38 (s, 3H, Ar-C*H₃*), 1.98 (s, 3H, C=C-C*H₃*), 1.79 (s, 3H, C=C-C*H₃*) ppm. **¹³C{¹H} NMR** (125.8 MHz, CDCl₃): δ 143.8, 139.3, 135.4, 129.0, 128.7, 125.8, 80.9, 72.4, 58.0, 54.0, 25.4, 21.3, 18.8 ppm. **IR**: 3209 (m), 3034 (w), 3966 (w), 2127 (m), 1597 (w), 1474 (m), 1418 (w), 1373 (w). **HRFAB-MS** for C₉H₁₆N. Calc'd: 138.1283; Found: 138.1281.

　　　　[NMe₂(2-butynyl)(CH=C(CH₃)₂)][OTs] (3). This reaction was carried out using 3.047 g enamine (30.0 mmol) and 5.929 g tosylate (25.0 mmol). Triturating the crude product with THF afforded pure **3** in 83% yield (6.75 g, 20.9 mmol) as an off white powder. **¹H NMR** (500 MHz, D₂O): δ 7.68 (d, ^3J = 8.1 Hz, 2H, Ar-*H*), 7.37 (d, ^3J = 8.4 Hz, 2H, Ar-*H*), 5.97 (br, 1H, C=C*H*), 4.31 (2H, N-C*H₂*), 3.35 (s, 6H, N(C*H₃*)₂), 2.39 (s, 3H, Ar-C*H₃*), 2.00 (s, 3H, C*H₃*), 1.90 (s, 3H, C*H₃*), 1.81 (s, 3H, C*H₃*) ppm. **¹³C{¹H} NMR** (125.8 MHz, CDCl₃): δ 144.1, 138.8, 134.8, 128.8, 128.3, 125.6, 88.25, 67.7, 58.6, 53.3, 25.2, 21.1, 18.6, 3.6 ppm. **IR**: 3033 (w), 2975 (w), 2244 (w), 1599 (w), 1495 (w), 1479 (w). **Anal. Calc'd. for C₁₇H₂₅NO₃S**: C, 63.13; H, 7.79; N, 4.33. Found: C, 62.80; H, 7.99; N, 4.40.

　　　　[NMe₂(2-pentynyl)(CH=C(CH₃)₂)][OTs] (4). This reaction was carried out using 1.049 g enamine (10.6 mmol) and 3.044 g tosylate (10.3 mmol). Recrystallization of the crude material from CH₂Cl₂/Et₂O yielded the analytically pure product as a white powder in 46% yield (1.60 g, 4.7 mmol). **¹H NMR** (500 MHz, CDCl₃): δ 7.68 (d, ^3J = 8.1 Hz, 2H, Ar-*H*), 7.36 (d, ^3J = 8.4 Hz, 2H, Ar-*H*) 5.96 (br, 1H, C=C*H*), 4.31 (s, 2H, N-C*H₂*), 3.35 (s, 6H, N(C*H₃*)₂), 2.39 (s, 3H, Ar-C*H₃*), 2.28 (m, 2H, C≡C-C*H₂*), 1.98 (s, 3H, C=C-C*H₃*), 1.80 (s, C=C-C*H₃*) 1.11 (t, ^3J = 7.5 Hz, 3H, CH₂C*H₃*) ppm. **¹³C{¹H} NMR** (125.8 MHz, CDCl₃): 143.86, 139.15, 135.19, 129.00, 128.59, 125.87, 94.12, 68.03, 58.95, 53.71, 25.40, 21.27, 18.83, 13.21, 12.44 δ ppm. **IR**: 3034 (w), 2975 (m), 2963 (m), 2940 (w), 2918 (w), 1599 (w), 1494 (w), 1480 (w), 1455 (m), 1432 (w), 1420 (w), 1373 (m), 1317 (w). **HRFAB-MS** for C₁₁H₂₀N. Calc'd: 166.1596; Found: 166.1592.

　　　　[NMe₂(2-hexynyl)(CH=C(CH₃)₂)][OTs] (5). This reaction was carried out using 1.64 g enamine (16.3 mmol) and 4.107 g tosylate (16.5 mmol). Recrystallization of the crude material from CH₂Cl₂/Et₂O yielded the analytically pure product as an off-white hygroscopic powder in 22% yield (1.216 g, 3.6 mmol). **¹H NMR** (300 MHz, D₂O): δ 7.68 (d, ^3J = 8.1 Hz, 2H, Ar-*H*), 7.36 (d, ^3J = 8.4 Hz, 2H, Ar-*H*), 5.93 (br, 1H, C=C*H*), 4.30 (t, ^3J = 2.1 Hz, 2H, N-C*H₂*), 3.32 (s, 6H, N(C*H₃*)₂), 2.38 (s, 3H, Ar-C*H₃*), 2.26 (m, 2H, C≡C-C*H₂*), 1.96 (d, ^4J = 1.5 Hz, 3H, C=C-C*H₃*), 1.79 (d, ^4J = 1.2, 3H, C=C-C*H₃*), 1.53 (m, 2H, -CH₂C*H₂*CH₃), 0.96 (t, ^3J = 7.2 Hz, 3H, -

CH$_2$CH$_2$CH_3) ppm. ^{13}C{^{1}H} NMR (75.5 MHz, D$_2$O): δ 142.6, 139.9, 137.1, 129.7, 128.3, 125.6, 93.9, 68.4, 58.8, 53.6, 24.6, 21.2, 20.8, 20.2, 18.3, 13.0 ppm. **IR**: 3024 (w), 2966 (m), 2926 (m), 2871 (w), 2237 (m), 1596 (w), 1476 (m), 1451 (m), 1413 (w), 1367 (m), 1338 (w), 1325 (w). **HRFAB-MS** for C$_{12}$H$_{22}$N. Calc'd: 180.1752; Found: 180.1757. **Anal. Calcd. for C$_{19}$H$_{29}$NO$_3$S**: C, 64.92; H, 8.32; N, 3.98. Found: C, 64.09; H, 8.64; N, 3.96.

[NMe$_2$(4-methyl-2-pentynyl)(CH=C(CH$_3$)$_2$)][OTs] (6). This reaction was carried out using 192 mg enamine (1.93 mmol) and 487 mg tosylate (1.93 mmol). Recrystallization of the crude material from CH$_2$Cl$_2$/Et$_2$O yielded the analytically pure product as a white hygroscopic powder in 36% yield (245 mg, 0.70 mmol). ^{1}**H NMR** (500 MHz, D$_2$O): δ 7.67 (d, ^3J = 8.0 Hz, 2H, Ar-H), 7.35 (d, ^3J = 7.5 Hz, 2H, Ar-H), 5.91 (s, br, 1H C=CH), 4.27 (s, 2H, N-CH_2), 3.32 (s, 6H, N(CH_3)$_2$), 2.64 (m, 1H, C≡C-CH(CH$_3$)$_2$), 2.38 (s, 3H, Ar-CH_3), 1.95 (s, 3H, C=C-CH_3), 1.79 (s, 3H, C=C-CH_3), 1.16 (d, ^3J = 2.0 Hz, 6H, CH(CH_3)$_2$) ppm. ^{13}C{^{1}H} NMR (125.8 MHz, D$_2$O): δ 142.3, 139.5, 136.8, 129.3, 127.9, 125.3, 98.8, 67.2, 58.4, 53.2, 24.2, 21.4, 20.4, 20.0, 17.9 ppm. **IR**: 3028 (w), 2963 (m), 2922 (w), 2868 (w), 2234 (w), 1596 (w), 1474 (m), 1450 (m), 1410 (w), 1384 (m), 1367 (m), 1319 (w). **LRFAB-MS** (+), *m/z*: 180. **Anal. Calcd. for C$_{19}$H$_{29}$NO$_3$S**: C, 64.92; H, 8.32; N, 3.98; S, 9.12. Found: C, 64.65; H, 8.39; N, 4.09; S, 9.32.

[NMe$_2$(2-heptynyl tosylate)(CH=C(CH$_3$)$_2$)][OTs] (7). The reaction was carried out using 403 mg enamine (4.1 mmol) and 923 mg tosylate (3.9 mmol). Recrystallization of the crude material from CH$_2$Cl$_2$/Et$_2$O yielded the analytically pure product as a white hygroscopic powder in 47% yield (669 mg, 1.83 mmol). ^{1}**H NMR** (500 MHz, D$_2$O): δ 7.69 (d, ^3J = 8.0 Hz, 2H, Ar-H), 7.37 (d, ^3J = 8.0 Hz, 2H, Ar-H), 5.95 (s, br, 1H, C=CH), 4.31 (s, 2H, N-CH_2), 3.34 (s, 6H, N(CH_3)$_2$), 2.39 (s, 3H, Ar-CH_3), 2.30 (t, ^3J = 7.0 Hz, 2H, C≡C-CH_2), 1.98 (s, 3H, C=C-CH_3), 1.81 (s, 3H, C=C-CH_3), 1.51 (m, 2H, CH$_2$-CH_2-CH$_2$-CH$_3$), 1.40 (m, 2H, CH$_2$-CH$_2$-CH_2-CH$_3$), 0.89 (t, ^3J = 2.5 Hz, 3H, CH$_2$-CH$_2$-CH$_2$-CH_3) ppm. ^{13}C{^{1}H} NMR (100.6 MHz, D$_2$O): δ 142.3, 139.6, 136.9, 129.4, 128.0, 125.4, 93.8, 68.0, 58.6, 53.3, 29.3, 24.3, 21.3, 20.5, 18.0, 17.6, 12.8 ppm. **IR**: 3023 (w), 2956 (m), 2871 (m), 2234 (w), 1496 (w), 1481 (m), 1463 (m), 1376 (m). **LRFAB-MS** (+), *m/z*: 194. **Anal. Calcd. for C$_{20}$H$_{31}$NO$_3$S**: C, 65.72; H, 8.85; N, 3.83; S, 8.77. Found: C, 65.43; H, 8.97; N, 3.95; S, 8.62.

[NMe$_2$(5-methyl-2-hexynyl)(CH=C(CH$_3$)$_2$)][OTs] (8). This reaction was carried out using 382 mg enamine (3.9 mmol) and 1.14 g tosylate (4.3 mmol). Recrystallization of the crude material from CH$_2$Cl$_2$/petroleum ether yielded the analytically pure product as a white, hygroscopic solid in 67% yield (955 mg, 2.61 mmol). ^{1}**H NMR** (400 MHz, CDCl$_3$): d 7.77 (d, ^3J = 8.0 Hz, 2H, Ar-H), 7.13 (d, ^3J = 8.0 Hz, 2H, Ar-H), 5.98 (s, 1H, C=CH), 4.64 (s, 2H, N-CH_2), 3.59 (s, 6H, N(CH_3)$_2$), 2.33 (s, 3H, Ar-CH_3), 2.13 (d, ^3J = 6.4 Hz, 2H, -CH_2-CH), 1.98 (s, 3H, C=C-CH_3), 2.7-2.9 (m, 4H, C≡C-CH + C=C-CH_3), 0.96 (d, ^3J = 6.7 Hz CH(CH_3)$_2$) ppm. ^{13}C{^{1}H} NMR (125.8 MHz, CDCl$_3$): δ 144.1, 138.9, 134.9, 128.9, 128.4, 125.7, 91.6, 69.5, 58.7, 53.6, 27.7, 27.5, 25.3, 21.8, 21.2, 18.7 ppm. **LRFAB-MS** (+), *m/z*: 194. **HRFAB-MS** for C$_{13}$H$_{24}$N. Calc'd: 194.190875; Found: 194.190940.

[NMe₂(4-methyl-2-hexynyl)(CH=C(CH₃)₂][OTs] (9). This reaction was carried out using 382 mg enamine (3.9 mmol) and 1.12 mg tosylate (4.3 mmol). The crude material could not be crystallized from a number of different solvent systems. The resulting yellow oil was analytically pure, and was isolated in 61% yield (870 mg, 2.38 mmol). **¹H NMR** (300 MHz, D₂O): d 7.77 (d, ^3J = 8.0 Hz, 2H, Ar-*H*), 7.13 (d, ^3J = 8.0 Hz, 2H, Ar-*H*), 5.98 (s, 1H, C=C*H*), 4.64 (s, 2H, N-C*H₂*), 3.59 (s, 6H, N(C*H₃*)₂), 2.33 (s, 3H, Ar-C*H₃*), 2.15 (m, 1H, C≡C-C*H*), 1.98 (s, 3H, C=C-C*H₃*), 1.79 (s, 3H, C=C-C*H₃*), 1.35-1.65 (m, 2H, C*H₂*), 1.2 (d, 3H, C≡C-CH-C*H₃*), 0.9 (m, 3H, CH₂-C*H₃*) ppm. **HRFAB-MS for C₁₃H₂₄N.** Calc'd: 194.1909; Found: 194.1911.

[NMe₂(4,4-dimethyl-2-pentynyl)(CH=C(CH₃)₂][OTs] (10). The reaction was carried out using 416 mg enamine (4.2 mmol) and 1.077 g tosylate (4.2 mmol). Recrystallization of the crude material from CH₂Cl₂/Et₂O yielded the analytically pure product as a white hygroscopic solid in 31% yield (488 mg, 1.33 mmol). **¹H NMR** (400 MHz, D₂O): δ 7.69 (d, ^3J = 8.0 Hz, 2H, Ar-*H*), 7.37 (d, ^3J = 8.0 Hz, 2H, Ar-*H*), 5.94 (s, br, 1H, C=C*H*), 4.31 (s, 2H, N-C*H₂*), 3.34 (s, 6H, N(C*H₃*)₂), 2.39 (s, 3H, Ar-C*H₃*), 1.97 (s, 3H, C=C-C*H₃*), 1.82 (s, 3H, C=C-C*H₃*), 1.24 (s, 9H, C(C*H₃*)₃) ppm. **¹³C{¹H} NMR** (125.8 MHz, D₂O): δ 143.2, 141.9, 138.3, 130.7, 129.5, 126.9, 102.8, 68.3, 59.9, 54.8, 31.0, 28.8, 25.8, 21.9, 19.4 ppm. **IR:** 3034 (w), 2962 (m), 2242 (w), 1597 (w), 1475 (m), 1410 (w), 1364 (w). **HRFAB-MS** for C₁₃H₂₄N. Calc'd: 194.1909; Found: 194.1906.

[NMe₂(2-octynyl)(CH=C(CH₃)₂][OTs] (11). The reaction was carried out using 1.55 g enamine (5.2 mmol) and 5.24 g tosylate (5.2 mmol). Recrystallization of the crude material from CH₂Cl₂/Et₂O yielded the analytically pure product as white hygroscopic crystals in 88% yield (112 mg, 0.28 mmol). **¹H NMR** (300 MHz, D₂O): δ 7.68 (d, ^3J = 8.1 Hz, 2H, Ar-*H*), 7.36 (d, ^3J = 7.8 Hz, 2H, Ar-*H*), 5.97 (s, br, 1H, C=C*H*), 4.33 (s, 2H, N-C*H₂*), 3.36 (s, 6H, N(C*H₃*)₂), 2.39 (s, 3H, Ar-C*H₃*), 2.30 (t, ^3J = 6.6 Hz, 2H, -C*H₂*-), 1.99 (d, ^4J = 1.2 Hz, 3H, C=C-C*H₃*), 1.81 (d, ^4J = 1.2 Hz, 3H, C=C-C*H₃*), 1.53 (m, 2H, -C*H₂*-), 1.34 (m, 4H, -C*H₂*CH₂CH₃), 0.87 (t, ^3J = 6.9 Hz, 3H, C*H₃*) ppm. **¹³C{¹H} NMR** (125.8 MHz, D₂O): δ 143.5, 141.5, 138.3, 130.8, 129.4, 126.9, 95.1, 69.6, 60.1, 54.9, 31.8, 28.5, 25.9, 23.0, 22.0, 19.5, 19.4, 14.9 ppm. **IR:** 6025 (w), 2976 (w), 2955 (m), 2924 (m), 2860 (w), 2238 (w), 1599 (w), 1494 (w), 1468 (m), 1430 (w), 1423 (m), 1370 (m), 1337 (w). **LRFAB-MS** (+), *m/z*: 208. **Anal. Calcd. for C₂₁H₃₃NO₃S:** C, 66.45; H, 8.76; N, 3.69; S, 8.45. Found: C, 66.12; H, 9.09; N, 3.85; S, 8.68.

[NMe₂(3-phenyl-2-propynyl)(CH=C(CH₃)₂][OTs] (12). This reaction was carried out using 388 mg enamine (3.9 mmol) and 1.154 g tosylate (4.0 mmol). The crude material could not be crystallized from a number of different solvent systems. The resulting yellow oil was pure by NMR analysis, and was isolated in 15% yield. (228 mg, 0.59 mmol). **¹H NMR** (400 MHz, D₂O): δ 7.66 (d, ^3J = 8.4 Hz, 3H, Ar-*H*), 7.55 (d, ^3J = 6.4, 2H, Ar-*H*), 7.50-7.39 (3 H, Ar-*H* + CHCl₃), 7.32 (d, ^3J = 7.6 Hz, 2H, Ar-*H*), 6.01 (s, 1H C=C*H*), 4.58 (s, 2H, N-C*H₂*), 3.41 (s, 6H, N(C*H₃*)₂), 2.35 (s, 3H, Ar-C*H₃*), 2.00 (d, ^4J = 1.6 Hz, 3H, C=C-C*H₃*), 1.81 (d, ^4J = 1.2 Hz, 3H, C=C-C*H₃*) ppm. **¹³C{¹H} NMR** (100.6 MHz, D₂O): δ 142.4, 137.2, 132.0, 130.0, 129.4, 128.7, 128.0, 125.3, 120.3, 90.8, 77.7, 76.8, 58.6, 53.6, 24.34, 20.45, 18.07 ppm. **IR**: 2963 (m),

1490 (m), 1444 (m), 1415 (w), 1372 (m). **HRFAB-MS** for $C_{15}H_{20}N$. Calc'd: 214.1596; Found: 214.1601.

General Procedure for Encapsulation Reactions. The potassium or sodium salt of **1** (3.0 mg, 0.85 μmol) and the enammonium tosylate (0.90 μmol) were combined in a vial and dissolved in 600 μL D_2O. The solution was transferred to an NMR tube and the spectrum was recorded within 20 minutes after dissolution. Samples for mass spectrometry were prepared in an identical fashion, using H_2O instead of D_2O. Samples were flushed with N_2 after mixing and mass spectra were obtained within 12 hours of sample preparation.

Analytical Data for Host-Guest Complexes, Prepared As Described Above.
$K_{11}[2 \subset Ga_6L_6]$. ^1H **NMR** (400 MHz, D_2O): δ 8.01 (d, ^3J = 7.6 Hz, 12H, Ar-H), 7.91 (d, ^3J = 6.8 Hz, 2H, OTs), 7.83 (d, ^3J = 8.4 Hz, 12H, Ar-H), 7.69 (d, , ^3J = 8.4 Hz, 2H, OTs), 7.31 (d, ^3J = 8.4 Hz, 12H, Ar-H), 7.09 (t, ^3J = 8.4 Hz, 12H, Ar-H), 6.77 (d, ^3J = 7.2 Hz, 12H, Ar-H), 6.62 (d, ^3J = 8.0 Hz, 12H, Ar-H), 2.37 (s, 3H, OTs), 2.06 (s, 1H, CH, encaps.), 0.52 (s, 1H, CH, encaps.), 0.48 (s, 1H, CH, encaps.), 0.28 (d, , ^4J = 16.0, 1H, CH, encaps.), -0.06 (s, 3H, CH_3, encaps.), -0.14 (s, 3H, CH_3, encaps.), -0.49 (s, 3H, CH_3, encaps.), -0.89 (s, 3H, CH_3, encaps.) ppm. **TOF MS ES** (-): (♦ denotes the host-guest species $K_{11}[2 \subset Ga_6L_6]$). Calc'd (found) m/z: $Ga_4C_{153}H_{103}N_{13}O_{36}K_8$ (♦ − 3K^+)$^{3-}$ 1096.0198 (1096.0209), $Ga_4C_{153}H_{105}N_{13}O_{36}K_6$ (♦ − 5K^+)$^{4-}$ 802.53 (802.53).

$K_{11}[3 \subset Ga_6L_6]$. ^1H **NMR** (400 MHz, D_2O): δ 8.04 (s, br, 12H, Ar-H), 7.82 (d, ^3J = 7.6 Hz, 12H, Ar-H), 7.69, (d, ^3J = 8.0 Hz, 2H, OTs), 7.35 (d, ^3J = 8.4 Hz, 2H, OTs), 7.30 (d, ^3J = 7.6 Hz, 12H, Ar-H), 7.07 (t, ^3J = 7.6 Hz, 12H, Ar-H), 6.76 (d, ^3J = 6.8 Hz, 12H, Ar-H), 6.61 (t, ^3J = 7.6 Hz, 12H, Ar-H), 2.37 (s, 3H, OTs), 1.95 (s, 1H, CH, encaps.), 0.65 (s, 3H, CH_3, encaps.), 0.57 (d, 1H, CH, encaps.), 0.51 (d, 1H, CH, encaps.), 0.19 (s, 6H, CH_3, encaps.), -0.18 (s, 3H, CH_3, encaps.), -1.10 (s, 3H, CH_3, encaps.) ppm. **TOF MS ES** (-): (♦ denotes the host-guest species $K_{11}[3 \subset Ga_6L_6]$). Calc'd (found) m/z: $Ga_4C_{154}H_{105}N_{13}O_{36}K_8$ (♦ − 3K^+)$^{3-}$ 1100.692 (1100.693), $Ga_4C_{154}H_{106}N_{13}O_{36}K_7$ (♦ − 4K^+)$^{4-}$ 815.776 (815.775).

$K_{11}[4 \subset Ga_6L_6]$. ^1H **NMR** (400 MHz, D_2O): δ 8.04 (d, ^3J = 7.6 Hz, 12H, Ar-H), 7.76 (d, ^3J = 8.8 Hz, 12H, Ar-H), 7.70 (d, ^3J = 7.7 Hz, 2H, OTs), 7.38 (d, ^3J = 8.0 Hz, 2H, OTs), 7.33 (d, ^3J = 8.0 Hz, 12H, Ar-H), 7.03 (t, ^3J = 8.0 Hz, 12H, Ar-H), 6.78 (d, ^3J = 6.8 Hz, 12H, Ar-H), 6.62 (t, ^3J = 8.0 Hz, 12H, Ar-H), 2.40 (s, 3H, OTs), 1.76 (s, 1H, CH, encaps.), 0.94 (d, ^2J = 15.7 Hz, 1H, CH, encaps.), 0.75 (s, 3H, CH_3, encaps.), 0.67 (s, 3H, CH_3, encaps.), 0.40 (s, 3H, CH_3, encaps.), 0.09 (d, ^2J = 15.4 Hz, 1H, CH, encaps.), -0.52 (m, 2H, CH_2, encaps.), -1.02 (s, 3H, CH_3, encaps.), -1.06 (t, ^3J = 7.6 Hz, 3H, CH_3, encaps.) ppm. **TOF MS ES** (-): (♦ denotes the host-guest species $K_{11}[4 \subset Ga_6L_6]$). Calc'd (found) m/z: $Ga_4C_{155}H_{107}N_{13}O_{36}K_8$ (♦ − 3K^+)$^{3-}$ 1105.364 (1105.364), $Ga_4C_{155}H_{108}N_{13}O_{36}K_7$ (♦ − 4K^+)$^{4-}$ 819.280 (819.279).

$K_{11}[5 \subset Ga_6L_6]$. ^1H **NMR** (500 MHz, D_2O): δ 8.06 (d, ^3J = 7.5 Hz, 12H, Ar-H), 7.84 (d, ^3J = 9.0 Hz, 12H, Ar-H), 7.64 (d, ^3J = 7.5 Hz, 2H, OTs), 7.23 (d, ^3J = 7.5 Hz, 12H, Ar-H), 7.17

(d, ^3J = 7.5 Hz, 2H, OTs), 7.07 (t, ^3J = 8.0 Hz, 12H, Ar-H), 6.62 (d, ^3J = 6.5 Hz, 12H, Ar-H), 6.31 (t, ^3J = 7.5 Hz, 12H, Ar-H), 2.51 (s, 2H, CH_2, encaps.), 2.20 (s, 1H, CH, encaps.), 1.34 (s, 2H, CH_2, encaps.), 0.50 (q, ^3J = 12.8 Hz, 2H, CH_2, encaps.), 0.10 (s, 3H, CH_3, encaps.), 0.01 (s, 3H, CH_3, encaps.), -0.70 (s, 3H, CH_3, encaps.), -0.82 (s, 3H, CH_3, encaps.) ppm. **TOF MS ES** (-): (♦ denotes the host-guest species **K$_{11}$[5 ⊂ Ga$_6$L$_6$]**). Calc'd (found) m/z: Ga$_4$C$_{156}$H$_{109}$N$_{13}$O$_{36}$K$_8$ (♦ − 3K$^+$)$^{3-}$ 1110.035 (1110.044), Ga$_4$C$_{156}$H$_{110}$N$_{13}$O$_{36}$K$_7$ (♦ − 4K$^+$)$^{4-}$ 822.784 (822.781).

K$_{11}$ [6 ⊂ Ga$_6$L$_6$]. **^{1}H NMR** (500 MHz, D$_2$O): δ 8.07 (d, ^3J = 6.5 Hz, 12H, Ar-H), 7.72-7.67 (m, 14H, Ar-H + OTs), 7.36 (d, ^3J = 8.0 Hz, 12H, Ar-H), 7.29 (d, ^3J = 8.0 Hz, 12H, Ar-H), 7.01 (t, ^3J = 8.0 Hz, 12H, Ar-H), 6.74 (d, ^3J = 7.0 Hz, 12H, Ar-H), 6.59 (t, ^3J = 8.0 Hz, 12H, Ar-H), 1.70 (s, 1H, CH, encaps.), 1.19 (d, 1H, CH, encaps.), 1.10 (s, 3H, CH_3, encaps.), 1.03 (s, 1H, CH, encaps.), 0.73 (s, 3H, CH_3, encaps.), -0.36 (d, 1H, CH, encaps.), -1.03 (s, 3H, CH_3, encaps.), -1.48 (s, 3H, CH_3, encaps.), -1.60 (s, 3H, CH_3, encaps.) ppm. **TOF MS ES** (-): (♦ denotes the host-guest species **K$_{11}$[6 ⊂ Ga$_6$L$_6$]**). Calc'd (found) m/z: Ga$_4$C$_{156}$H$_{109}$N$_{13}$O$_{36}$K$_8$ (♦ − 3K$^+$)$^{3-}$ 1110.036 (1110.009), Ga$_4$C$_{156}$H$_{110}$N$_{13}$O$_{36}$K$_7$ (♦ − 4K$^+$)$^{4-}$ 822.784 (822.757).

Na$_{11}$[7 ⊂ Ga$_6$L$_6$]. **^{1}H NMR** (500 MHz, D$_2$O): δ 8.06 (d, ^3J = 7.5 Hz, 12H, Ar-H), 7.75 (d, ^3J = 8.5 Hz, 12H, Ar-H), 7.70 (d, ^3J = 8.5 Hz, 2H, OTs), 7.36 (d, ^3J = 8.0 Hz, 2H, OTs), 7.33 (d, ^3J = 8.0 Hz, 12H, Ar-H), 6.99 (t, ^3J = 8.0 Hz, 12H, Ar-H), 6.79 (d, ^3J = 7.0 Hz, 12H, Ar-H), 6.62 (t, ^3J = 7.5 Hz, 12H, Ar-H), 2.01 (s, 1H, CH, encaps.), 1.49 (d, ^3J = 1.5 Hz, 1H, CH, encaps.), 1.24 (s, 3H, CH_3, encaps.), 0.66 (d, ^3J = 35.0 Hz, 6H, (CH_3)$_2$, encaps.), -0.05 (d, ^3J = 15.5 Hz, 1H, CH, encaps.), -0.206 (s, 2H, CH_2, encaps.), -0.958 (s, 3H, CH_3, encaps.), -1.042 (s, 3H, CH_3, encaps.), -1.42 (d, ^3J = 58.5 Hz, 2H, CH_2, encaps.), -1.71 (s, 2H, CH_2, encaps.) ppm. **TOF MS ES** (-): (♦ denotes the host-guest species **Na$_{11}$[7 ⊂ Ga$_6$L$_6$]**). Calc'd (found) m/z: Ga$_4$C$_{157}$H$_{111}$N$_{13}$O$_{36}$Na$_8$ (♦ − 3Na$^+$)$^{3-}$ 1071.7742 (1071.7858),   Ga$_4$C$_{157}$H$_{108}$N$_{13}$O$_{36}$Na$_7$ (♦ − 4Na$^+$)$^{4-}$ 798.0843 (798.0863), Ga$_4$C$_{157}$H$_{108}$N$_{13}$O$_{36}$Na$_6$, (♦ − 5Na$^+$)$^{5-}$ 633.8695 (633.8650).

K$_{11}$ [8 ⊂ Ga$_6$L$_6$]. **^{1}H NMR** (500 MHz, D$_2$O): δ 8.06 (d, ^3J = 7.5 Hz, 12H, Ar-H), 7.75 (d, ^3J = 8.5 Hz, 12H, Ar-H), 7.70 (d, ^3J = 8.5 Hz, 2H, OTs), 7.36 (d, ^3J = 8.0 Hz, 2H, OTs), 7.33 (d, ^3J = 8.0 Hz, 12H, Ar-H), 6.99 (t, ^3J = 8.0 Hz, 12H, Ar-H), 6.79 (d, ^3J = 7.0 Hz, 12H, Ar-H), 6.62 (t, ^3J = 7.5 Hz, 12H, Ar-H), 2.90 (s, 1H, CH, encaps.), 1.15 (s, 2H, CH_2, encaps.), 0.62 (s, 3H, CH$_3$, encaps.), 0.51 (s, 3H, CH$_3$, encaps.), -0.45 (br, 1H, CH, encaps.), -1.0 (s, 3H, CH$_3$, encaps.), -1.3 − (-1.5) (br, 5H, CH$_3$ + CH_2, encaps.), -1.89 (br, 6H, 2 x CH_3, encaps.) ppm. **TOF MS ES** (-): (♦ denotes the host-guest species **K$_{11}$[8 ⊂ Ga$_6$L$_6$]**). Calc'd (found) m/z: Ga$_4$C$_{157}$H$_{112}$N$_{13}$O$_{36}$K$_7$ (♦ − 4K$^+$)$^{4-}$ 826.288 (826.013), Ga$_4$C$_{157}$H$_{113}$N$_{13}$O$_{36}$K$_6$ (♦ − 5K$^+$ + H$^+$)$^{4-}$ 816.799 (816.529), Ga$_4$C$_{157}$H$_{114}$N$_{13}$O$_{36}$K$_5$ (♦ − 6K$^+$ + 2H$^+$)$^{4-}$ 807.310 (807.776).

K$_{11}$ [9 ⊂ Ga$_6$L$_6$]. **^{1}H NMR** (500 MHz, D$_2$O): δ 8.06 (d, ^3J = 7.5 Hz, 12H, Ar-H), 7.75 (d, ^3J = 8.5 Hz, 12H, Ar-H), 7.70 (d, ^3J = 8.5 Hz, 2H, OTs), 7.36 (d, ^3J = 8.0 Hz, 2H, OTs), 7.33 (d, ^3J = 8.0 Hz, 12H, Ar-H), 6.99 (t, ^3J = 8.0 Hz, 12H, Ar-H), 6.79 (d, ^3J = 7.0 Hz, 12H, Ar-H), 6.62 (t, ^3J = 7.5 Hz, 12H, Ar-H), -0.3 − (-1.1) (many overlapping peaks, encaps.), -1.25 (s, 3H, CH$_3$, encaps.), -1.55 (s, 2H, CH_2, encaps.), -1.79 (s, 6H, CH_3, encaps.), -1.8 − (-2.0) (broad

overlapping peaks, encaps.), -2.18 (s, 6H, 2 x CH_3, encaps.) **TOF MS ES** (-): (♦ denotes the host-guest species **K$_{11}$[8 ⊂ Ga$_6$L$_6$]**). Calc'd (found) *m/z*: Ga$_4$C$_{157}$H$_{112}$N$_{13}$O$_{36}$K$_7$ (♦ − 4K$^+$)$^{4-}$ 826.288 (826.266), Ga$_4$C$_{157}$H$_{113}$N$_{13}$O$_{36}$K$_6$ (♦ − 5K$^+$ + H$^+$)$^{4-}$ 816.799 (816.529), Ga$_4$C$_{157}$H$_{114}$N$_{13}$O$_{36}$K$_5$ (♦ − 6K$^+$ + 2H$^+$)$^{4-}$ 807.310 (807.786).

Data for Aldehyde Products. Isolation of the product aldehydes from the thermal reaction was simpler than isolation from the **1**-catalyzed reaction, so the following procedure was followed: In an NMR tube, ~100 mg of the propargyl enammonium salt was dissolved in 1.0 mL D$_2$O and sealed under vacuum. The tube was heated at 135 ˚C for 14 hours, at which point the reactant was judged to be consumed by ^{1}H-NMR analysis. A layer of oil formed above the water over the course of the reaction, which was extracted as the pure aldehyde product in 26-44% yield. Samples for FAB mass spectrometry were prepared employing a procedure similar to the one described, except that H$_2$O was used as the reaction solvent, and the product was extracted with pentane.

2,2-Dimethylpenta-3,4-dienal. This compound prepared as described above for NMR analysis yielded material quantitatively deuterated in the 3 position. This is presumably due to the acidity of the terminal alkyne in the starting material **2**, which exchanges with D$_2$O over the course of the reaction. Deuterium incorporation was not observed for the material prepared in H$_2$O for FAB-MS analysis. **^{1}H NMR** (600 MHz, CDCl$_3$): δ 9.39 (s, 1H, CHO), 4.88 (s, 2H, C=C=CH_2), 1.18 (s, 6H, 2 CH_3) ppm. **^{13}C{^{1}H} NMR** (150.9 MHz, CDCl$_3$): δ 208.4, 202.6, 123.2 (t, *J* = 32 Hz, C-3), 78.2, 46.0, 21.9 ppm. **HRFAB-MS:** Exact mass for C$_7$H$_9$O [M-H]$^+$. Calc'd: 109.0653; Found: 109.0650.

2,2,3-Trimethylpenta-3,4-dienal. **^{1}H NMR** (600 MHz, CDCl$_3$): δ 9.33 (s, 1H, CHO), 4.75 (q, ^{5}*J* = 3.2 Hz, 2H, C=C=CH_2), 1.61 (t, ^{5}*J* = 3.1 Hz, 3H, C=C-CH_3) 1.16 (s, 6H, 2 CH_3) ppm. **^{13}C{^{1}H} NMR** (150.9 MHz, CDCl$_3$): δ 207.3, 202.8, 100.0, 76.5, 48.4, 20.7, 15.4 ppm. **HRFAB-MS:** Exact mass for C$_8$H$_{12}$O. Calc'd: 124.0888; Found: 124.0880.

3-Ethyl-2,2-dimethylpenta-3,4-dienal. **^{1}H NMR** (600 MHz, CDCl$_3$): δ 9.32 (s, 1H, CHO), 4.89 (t, ^{5}*J* = 4.0 Hz, 2H, C=C=CH_2), 1.83 (m, 2H, C=C-CH_2-CH$_3$), 1.16 (s, 6H, 2 CH_3), 0.98 (t, ^{3}*J* = 7.3 Hz, 3H, CH$_2$-CH_3) ppm. **^{13}C{^{1}H} NMR** (150.9 MHz, CDCl$_3$): δ 206.7, 203.0, 107.1, 79.3, 48.6, 20.9, 20.6, 12.5 ppm. **HRFAB-MS:** Exact mass for C$_9$H$_{13}$O [M-H]$^+$. Calc'd: 137.0966; Found: 137.0965.

3-Propyl-2,2-dimethylpenta-3,4-dienal. **^{1}H NMR** (600 MHz, CDCl$_3$): δ 9.31 (s, 1H, CHO), 4.85 (t, ^{5}*J* = 3.8 Hz, 2H, C=C=CH_2), 1.78 (m, 2H, C=C-CH_2-CH$_2$), 1.40 (m, 2H, C=C-CH$_2$-CH_2), 1.15 (s, 6H, 2 CH_3), 0.88 (t, ^{3}*J* = 7.4 Hz, 3H, CH$_2$-CH_3) ppm. **^{13}C{^{1}H} NMR** (150.9 MHz, CDCl$_3$): δ 206.7, 203.0, 105.3, 78.8, 48.6, 29.7, 21.2, 20.9, 14.0 ppm.

3-Isopropyl-2,2-dimethylpenta-3,4-dienal. **^{1}H NMR** (600 MHz, CDCl$_3$): δ 9.33 (s, 1H, CHO), 4.89 (s, 2H, C=C=CH_2), 2.01 (sep, 1H, ^{3}*J* = 6.7 Hz, C=C-CH-(CH$_3$)$_2$), 1.17 (s, 6H, 2

C*H*$_3$), 0.99 (d, 6H, ^3J = 6.8 Hz, C=C-CH-(C*H*$_3$)$_2$) ppm. **^{13}C{^{1}H} NMR** (150.9 MHz, CDCl$_3$): δ 206.4, 203.1, 112.4, 79.9, 49.0, 27.0, 23.7, 21.0 ppm. **HRFAB-MS:** Exact mass for C$_{10}$H$_{15}$O [M-H]$^+$. Calc'd: 151.1123; Found: 151.1120.

3-Secbutyl-2,2-dimethylpenta-3,4-dienal. **^{1}H NMR** (600 MHz, CDCl$_3$): δ 9.31 (d, ^6J = 1.4 Hz, 1H, C*H*O), 4.85 (dt, ^5J = 3.5 Hz, ^6J = 1.4 Hz, 2H, C=C=C*H*$_2$), 1.75-1.66 (m, 3H, C=C-C*H*$_2$-C*H*), 1.15 (s, 6H, 2 C*H*$_3$), 0.87 (d, ^3J = 6.3 Hz, 6H, CH-(C*H*$_3$)$_2$) ppm. **^{13}C{^{1}H} NMR** (150.9 MHz, CDCl$_3$): δ 207.1, 203.1, 104.3, 78.6, 48.6, 37.2, 26.8, 22.7, 20.9 ppm. **HRFAB-MS:** Exact mass for C$_{11}$H$_{18}$O. Calc'd: 166.1358; Found: 166.1343.

Kinetic Analyses of Enammonium Rearrangements. Kinetic analyses using an equimolar amount of **1** with respect to the enammonium substrate (Table 2.1) were performed in D$_2$O on a Bruker AVB 400 spectrometer. Due to the long reaction times associated with these reactions, kinetic runs were monitored by taking individual time points, and the reaction temperature was maintained outside the probe in a circulating oil bath. The concentration of all samples was 15 mM; the solutions were buffered with 100 mM phosphate and adjusted to pD 8.09. All samples were degassed by performing three vacuum/N$_2$ backfill cycles and sealed under vacuum to prevent the oxidation of **1**. The benzylic methyl peak of the tosylate counterion served as an internal standard for integration. The background reactions of unencapsulated substrates were monitored under the same conditions with regard to substrate concentration, buffer strength, and pD. For the majority of experiments, the decay of starting material was monitored using 2 scans with a delay time of 25 seconds and a 90° pulse of 8.15 μsec.

When the assembly **1** is subjected to three or more equivalents of any given propargyl enammonium substrate, significant precipitation occurs. For this reason DMSO-d$_6$ (20% by volume) was used as a cosolvent in experiments where substoichiometric amounts of **1** were used with respect to substrate. Kinetic runs using substoichiometric amounts of **1** were performed on Bruker AVB 400, AVQ 400, DRX 500 and AV 500 spectrometers. The concentration of all samples was 1.7 mM in **1**, and the mixed-solvent experiments were conducted without buffer.

Catalytic Kinetics of the Rearrangement of 3 in D$_2$O/DMSO-d$_6$. Samples for kinetic analysis with the concentrations of **3** given in Table 2.2 were prepared by dissolving **1** (4.2 mg, 0.00102 mmol) in 4:1 D$_2$O:DMSO-d$_6$, and adding the appropriate amount of **3** as a 63 mM solution in D$_2$O. The total sample volume was adjusted to 600 μL with 4:1 D$_2$O:DMSO-d$_6$. Point kinetics were taken for runs where more than 3 equivalents of **3** were used; all other runs were performed inside the NMR probe. All rates are either initial rates or zeroth order rates, and all values are reported as the average of the two kinetic runs.

equiv. **3**	Concentration of **3** (mM)	Reaction rate (mM/s)
0.26	0.4	4.53×10^{-5}
0.69	1.2	8.58×10^{-5}
1.7	2.9	9.85×10^{-5}
3.1	5.3	1.10×10^{-4}
4.5	7.7	1.20×10^{-4}
9.1	15.5	1.15×10^{-4}
17.0	28.9	1.19×10^{-4}
19.3	32.8	1.15×10^{-4}

Table 2.2. Rate vs. substrate concentration of the **1**-catalyzed rearrangement of **3** with no added inhibitor.
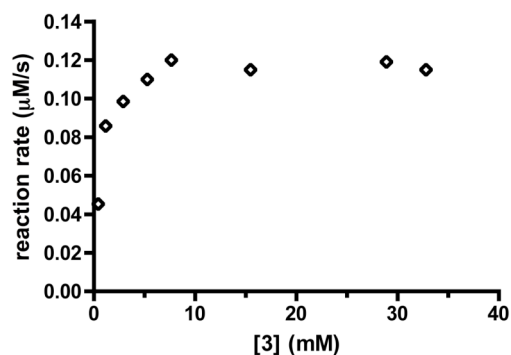

Figure 2.11. Substrate saturation curve of **1**-catalyzed rearrangement of **3** with no added inhibitor.

Competitive Inhibition Kinetics. Competitive inhibition kinetic runs were performed by analogy to the experiments described above. In the competitive inhibition experiments employing 10 equivalents of NPr$_4$Br, it was necessary to use in-probe NMR kinetics monitoring, and 6 scans were taken per time point to ensure accurate integrations. In these experiments it was also necessary to take time points less frequently (6 minutes per time point).

equiv. **3**	Concentration of **3** (mM)	Reaction rate (mM/s)
1.2	2.0	2.26×10^{-5}
1.9	3.2	6.63×10^{-5}
2.5	4.3	7.89×10^{-5}
3.0	5.1	8.76×10^{-5}
4.5	7.7	9.56×10^{-5}
7.2	12.2	1.03×10^{-4}
9.6	16.3	1.06×10^{-4}

Table 2.3. Rate vs. substrate concentration of the **1**-catalyzed rearrangement of **3** with 4 equivalents of added inhibitor (6.8 mM NPr$_4$Br).

Figure 2.12. Substrate saturation curve of the **1**-catalyzed rearrangement of **3** with 4 equivalents of added inhibitor

equiv. **3**	Concentration of **3** (mM)	Reaction rate (mM/s)
0.94	1.6	2.74×10^{-5}
2.03	3.5	5.03×10^{-5}
3.78	6.4	7.80×10^{-5}
7.5	12.8	1.01×10^{-4}
11.3	19.2	1.08×10^{-4}
20.1	34.2	1.26×10^{-4}
29.2	49.6	1.24×10^{-4}

Table 2.4. Rate vs. substrate concentration of the **1**-catalyzed rearrangement of **3** with 10 equivalents of added inhibitor (17.0 mM NPr$_4$Br).
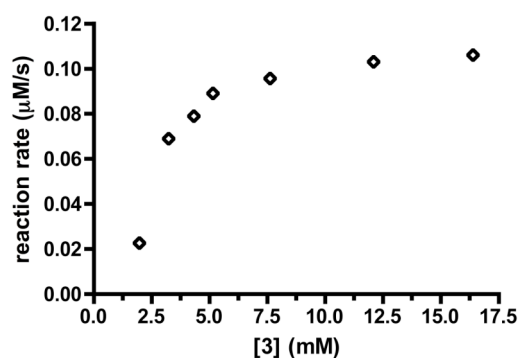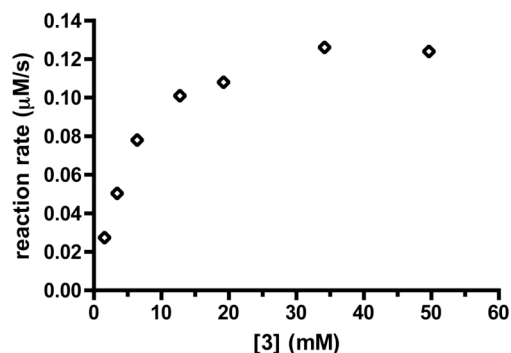
Figure 2.13. Substrate saturation curve of **1**-catalyzed rearrangement of **3** with 10 equivalents of added inhibitor.

Determination of Activation Parameters. Variable temperature kinetic runs of the encapsulated reaction were set up identically to the other catalytic kinetic runs, using 12 equivalents (18 mM) of substrate **3** with respect to **1**. Rates were measured at 40.2, 45.0, 55.0, 60.0 and 65.0 °C (±0.1 °C), and values are reported as an average of two runs. An average of the saturation rate constants determined at 60.0 °C were used. The temperature dependence of the background reaction was measured by point kinetics at 60.0, 75.0, 96.0, 105.0, 120.0, and 135.0 °C (±0.1 °C). Kinetics at 135.0 °C were measured by heating 12 identical samples and transferring one sample to an ice bath every 20 minutes. After the final tube was withdrawn from heating, the samples were each analyzed by ^{1}H-NMR.

T (°C)	T (°K)	Rate (mM/s)	K_{obs} (s^{-1})
65.0	338.3	2.3×10^{-4}	1.4×10^{-4}
60.0	333.3	4.2×10^{-4}	7.2×10^{-5}
55.0	328.3	6.6×10^{-4}	4.1×10^{-5}
45.0	318.3	1.7×10^{-4}	1.1×10^{-5}
40.2	313.5	3.6×10^{-6}	6.1×10^{-5}

Table 2.5. Temperature dependence of the rate of the **1**-catalyzed rearrangement of **3**.

T (^{o}C)	T (^{o}K)	Rate (s^{-1})
60	333	8.30 x 10^{-7}
85	358	4.24 x 10^{-6}
96	369	3.25 x 10^{-5}
105	378	4.04 x 10^{-5}
120	393	1.46 x 10^{-4}
127	400	2.70 x 10^{-4}
135	408	5.13 x 10^{-4}

Table 2.6. Rate vs. temperature dependence of the uncatalyzed rearrangement of **3.**

References

(1)   Kang, J. M.; Hilmersson, G.; Santamaria, J.; Rebek, J. Jr. *J. Am. Chem. Soc.* **1998**, *120*, 3650.

(2)   Kang, J. M.; Rebek, J. Jr. *Nature* **1997**, *385*, 50.

(3)   Kang, J. M.; Santamaria, J.; Hilmersson, G.; Rebek, J. Jr. *J. Am. Chem. Soc.* **1998**, *120*, 7389.

(4)   Nishioka, Y.; Yamaguchi, T.; Yoshizawa, M.; Fujita, M. *J. Am. Chem Soc.* **2007**, *129*, 7000.

(5)   Yoshizawa, M.; Tamaru, M.; Fujita, M. *Science* **2006**, *312*, 251

(6)   Fiedler, D.; Bergman, R. G.; Raymond, K. N. *Angew. Chem. Int. Ed.* **2004**, *43*, 6748.

(7)   Fiedler, D.; van Halbeek, H.; Bergman, R. G.; Raymond, K. N. *J. Am. Chem. Soc* **2006**.

(8)   Elkik, E.; Francesch, C. *Bull. Soc. Chim.* **1968**, *3*, 903.

(9)   Opitz, G. *Justus Liebigs Ann. Chem.* **1961**, 122.

(10)   Corey, E. J.; Fuchs, P. L. *Tetrahedron Lett.* **1972**, 3769.

(11)   Andersen, U. N.; Seeber, G.; Fiedler, D.; Raymond, K. N.; Lin, D.; Harris, D. *J. Am. Soc. Mass Spectrom.* **2006**, *17*, 292-296.

(12)   McKee, T.; McKee, J. R. *Biochemistry: The Molecular Basis of Life*; Third ed.; McGraw-Hill: New York, 2003.

(13)   Eadie, G. S. *J. Biol. Chem.* **1942**, *146*, 85.

(14)   Hofstee, B. H. J. *Science* **1952**, *116*, 329.

(15)   Pluth, M. D.; Bergman, R. G.; Raymond, K. N. *Science* **2007**, *316*, 85.

(16)   Viola, A.; MacMillan, J. H. *J. Am. Chem. Soc.* **1970**, *92*, 2404.

(17)   Gottlieb, H. E.; Kotlyar, V.; Nudelman, A. *J. Org. Chem.* **1997**, *62*, 7512.

(18)   Alaimo, P. J.; Peters, D. W.; Arnold, J.; Bergman, R. G. *J. Chem. Educ.* **2001**, *78*, 64.

(19)   Caulder, D. L.; Powers, R. E.; Parac, T. N.; Raymond, K. N. *Angew. Chem. Int. Ed.* **1998**, *37*, 1840.

(20)   Ellenberger, M. R.; Dixon, D. A.; Farneth, W. E. J. *J. Am. Chem. Soc.* **1981**, *103*, 5377.

(21)   Corey, E. J.; Fuchs, P. L. *Tett. Lett.* **1972**, *36*, 3769.

(22)   Capon, R. J.; Barrow, R. A. *J. Org. Chem.* **1998**, *63*, 75.

(23)   Russell, G. A.; Ngoviwatchai, P.; Wu, Y. W. *J. Am. Chem Soc.* **1989**, *111*, 4921.

(24)   Kavvadias, D.; Beuerle, T.; Wein, M.; Boss, B.; Konig, T.; Schwab, W. *J. Agric. Food Chem.* **1999**, *47*, 5178.

(25)   Yoshida, Y.; Sakakura, Y.; Aso, N.; Okada, S.; Tanabe, Y. *Tetrahedron* **1998**, *55*, 2183.

(26)   Condon-Gueugnot, S.; Linstrumelle, G. *Tetrahedron* **2000**, *56*, 1851.

Chapter 3
Catalysis of the Nazarov Cyclization of Pentadienols by a Self-Assembled Supramolecular Assembly

Introduction

Supramolecular catalysis has much in common with many enzymatic reactions, chiefly the use of both spatially appropriate binding pockets and precisely oriented functional groups to recognize and activate specific substrate molecules.[1-3] Although there are now many examples which demonstrate how selective encapsulation in a host cavity can enhance the reactivity of a bound guest, all have failed to reach the degree of increased reactivity typical of enzymes.[4] This chapter describes the development of the **1**-catalyzed dehydration/cyclization reaction of pentadienols, commonly known as the Nazarov cyclization. The catalytic rate enhancement of the Nazarov cyclization of 1,4-pentadien-3-ol is on the order of 10^6, which is the largest reported for supramolecular catalysis and the first to reach enzyme-like levels of reactivity.

Several catalytic reactions exploit the polyanionic nature of the self-assembled Ga_4L_6 host **1** (where L = N,N'-bis(2,3-dihydroxybenzoyl)-1,5-diaminonaphthalene) for encapsulating monocationic guests. Encapsulation in **1** can perturb acid-base equilibria to favor the protonation of a wide range of amines and phosphines, even at strongly basic pH.[5,6] These investigations led to the development of proton-catalyzed hydrolysis reactions inside of **1**, in which a protonated transition-state is stabilized in the host interior. These reactions are remarkable in that there are no functional groups in the interior of **1**; the protonation of bound guests is favorable due to the charge of the host assembly and cation-pi interactions with the naphthalene rings of the host walls.[6-11] The stabilization of transient protonated species produces a several thousandfold rate acceleration of orthoformate and acetal hydrolysis under basic conditions. However, even this substantial acceleration does not reach that typically seen in enzyme-catalyzed reactions.

Results and Discussion

1,4-Pentadien-3-ol Reactivity. Having demonstrated the ability of 1 to perform acid-catalyzed hydrolysis reactions, the application of this reactivity to more synthetically useful acid-catalyzed reaction types was an appealing goal. Acid-catalyzed cyclizations are particularly interesting, since **1** could accelerate such a reaction both by enhancing the basicity of the bound substrate and by preorganizing the substrate in a reactive conformation.[12,13] The enzymatic cyclization of several important classes of natural products are catalyzed in this fashion.[14,15] The Nazarov cyclization, an acid-catalyzed reaction in which a 1,4-dien-3-ol forms a cyclopentadiene (e.g. the example shown in Figure 3.1) is attractive from this perspective. In this reaction, protonation of the starting alcohol is followed by loss of water. The resulting diallylic carbocation undergoes a conrotatory electrocyclic ring closure, followed by deprotonation to yield the cyclopentadiene.[16,17] This reaction is used in synthetic organic chemistry as well as in organometallic chemistry where it has provided a route to substituted polymethylcyclopentadienyl ligands.[18,19]
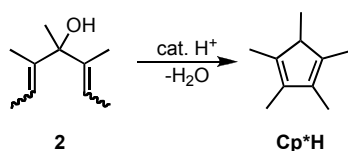
Figure 3.1. General Scheme for the Nazarov Cyclization of pentadienols to form cyclopentadienes.

As proof of principle, 10 equivalents of 3,4,5-trimethylhepta-2,5-dien-4-ol (**2**, obtained as a mixture of the three possible olefin stereoisomers, Figure 3.2), were added to a solution of **1** in H_2O (buffered to pH 11.0), and heated at 50 °C. Under these reaction conditions new peaks were observed by ^{1}H-NMR that were shifted upfield by several parts per million, which indicates guest binding. After 12 hours, the organic products were extracted into CH_2Cl_2 whereupon GC-MS analysis showed the complete consumption of the starting material and the quantitative formation of the Nazarov product, Cp*H (**3**). The reaction is inhibited with 1.1 equivalents of a strongly binding guest (NEt_4^+), which blocks access to the host interior.[6,13]
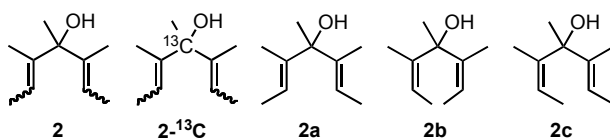

Figure 3.2. Nazarov Substrates used in this study.

Having obtained preliminary results, the kinetic analysis of the **1**-catalyzed Nazarov cyclization was identified as an important objective for providing both mechanistic information and quantification of the catalytic rate enhancement. The use of **2** as a model substrate for kinetic studies of the reaction was non-ideal due to its insolubility in water. For this reason, water-soluble pentadienols were investigated as substrates for this reaction. The simplest substrate, 1,4-pentadien-3-ol (**4**), is soluble in D_2O, and its reactivity with catalytic quantities of **1** was monitored. The ^{1}H-NMR resonances of **4** are broadened and shifted slightly upfield in the presence of **1**, indicating rapid guest exchange. The ^{1}H-NMR resonances of **4** are restored to their original width and chemical shift when a strongly-binding guest is added to **1**, which prevents transient binding of **4**. While **4** apparently interacts with the assembly interior, no cyclization was observed after 12 hours at 45 °C in unbuffered D_2O (Figure 3.3a). After heating for this period of time, the host assembly decomposed significantly. Because the acid-catalyzed conversion of **4** to cyclopentadiene has not been reported in the literature, this reaction was attempted. While pentamethyl substrate **2** is immediately converted to Cp*H in the presence of catalytic *p*-toluenesulfonic acid (TsOH), 1,4-pentadien-3-ol **4** does not react under identical conditions (Figure 3.4). The different reactivity of these two compounds is presumably due to the substitution at the hydroxyl position: the reactive **2** forms a tertiary carbocation after ionization of water, while the unreactive **4** substrate would form a less stable secondary carbocation.
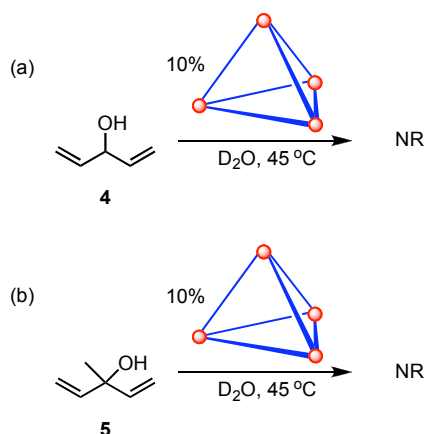
Figure 3.3. Attempted 1-catalyzed Nazarov cyclization of water-soluble substrates (a) 1,4-pentadien-3-ol (**4**) and (b) 3-methyl-1,4-pentadien-3-ol (**5**). Both reactions were conducted in unbuffered solution.
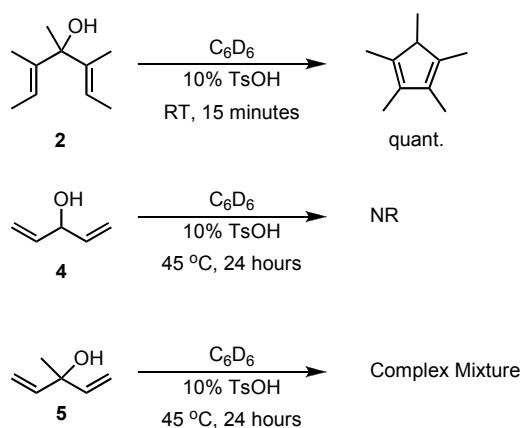

Figure 3.4. Acid-catalyzed reactivity of pentadienols.

We hypothesized that methyl substitution in the 3-position was necessary for the **1**-catalyzed Nazarov reaction to proceed. Thus, the tertiary alcohol 3-methyl-1,4-pentadien-3-ol (**5**) was synthesized, and its reactivity was evaluated. This compound is also soluble in D_2O, and its reactivity was tested with 10% **1** at 45 °C (Figure 3.3b). Like substrate **4**, substrate **5** appears to be transiently encapsulated, but no reaction occurs and the host assembly eventually decomposes. In the presence of *p*-toluenesulfonic acid, **5** reacts to form a complex mixture of products (Figure 3.4). The tertiary alcohol **5** is more reactive in the presence of catalytic acid than secondary alcohol **4**; however, it remained inert to catalysis by encapsulation in **1**. At this point, attempts to identify water-soluble substrates for mechanistic studies were abandoned.

Substrate Synthesis. In order to acquire interpretable kinetic data, it was necessary to obtain the three possible stereoisomers of **2** (Figure 3.2). Attempts to separate the individual stereoisomers **2a**, **2b**, and **2c** from the mixture **2** were unsuccessful using silica chromatography, alumina chromatography, preparative gas chromatography, and reverse-phase HPLC. Compound **2a** could be prepared in reasonably high purity using commercially available (*E*)-2-

bromo-2-butene (Figure 3.5a).[17] Although **2b** can be prepared from (*Z*)-2-bromo-2-butene, it can be obtained more conveniently and in higher purity via dienone **7b** (Figure 3.5b).   (It was not possible to purchase (*Z*)-2-bromo-2-butene at the time of this work, so it was purified by preparative gas chromatography. Obtaining the necessary amount of (*Z*)-2-bromo-2-butene to prepare **2b** is very time-consuming, and the synthesis described here proved to be more convenient.)   The isomer **2c** was synthesized via the unsymmetrical alcohol **6c**, which was prepared by the addition of (*Z*)-2-bromo-2-butene to tiglaldehyde (Figure 3.5c). Oxidation to dienone **7c**, followed by addition of methyllithium, gave the desired product (Figure 3.5c). Attempts to synthesize **2c** directly from 3-methyl-3-penten-2-one and (*Z*)-2-bromo-2-butene were unsuccessful.
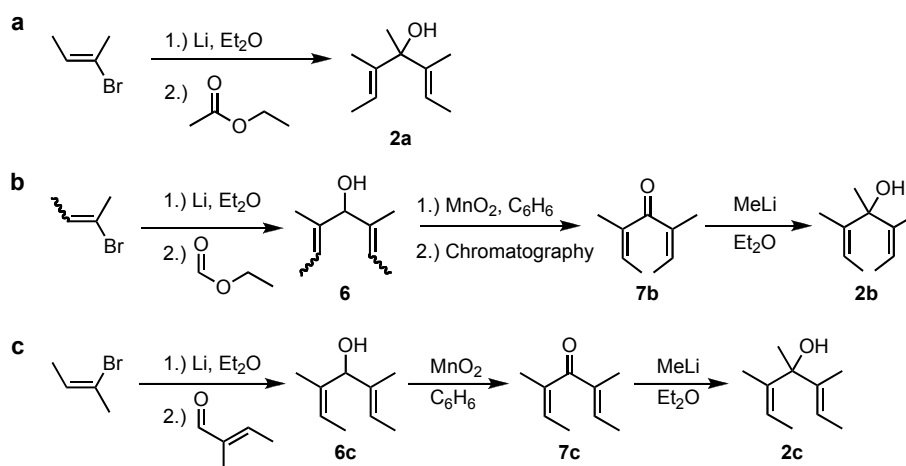

Figure 3.5. (a) Synthesis of *E,E* isomer **2a**. (b) Synthesis of *Z,Z* isomer **2b**. (c) Synthesis of *E,Z* isomer **2c**.

Identification of Encapsulated Species.   The identity of the encapsulated species observed during the reaction was sought, as it is potentially the resting state of the catalyst. The ^{13}C-labeled compound **2-[13]C** was prepared as a mixture of three stereoisomers and used for this purpose (Figure 3.6). When **2-[13]C** is exposed to **1**, the enriched ^{13}C resonances are shifted by only a few ppm upfield compared to those of the unencapsulated alcohol (Figure 3.7). This is consistent with encapsulation of the alcohol **2-[13]C** and is not consistent with an encapsulated carbocation, whose ^{13}C-NMR resonances would be dramatically shifted.[20] The hydrophobic binding of neutral alkanes and arenes in **1** has been reported, and it is likely that the encapsulation of **2** is driven by similar factors.[21,22] The encapsulated, neutral substrate was observed as the resting state of the **1**-catalyzed hydrolysis of orthoformates and acetals, and suggests a certain degree of generality in the mechanisms of acid-catalyzed reactions within **1**.[9]
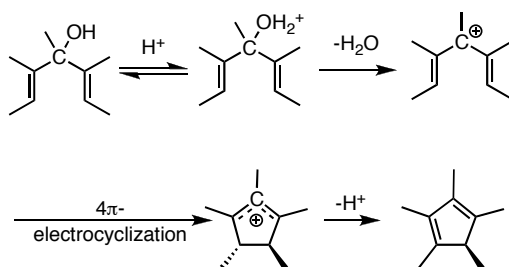
Figure 3.6. Mechanism of the Nazarov cyclization, showing possible intermediates that are encapsulated in **1** as the catalyst resting state.
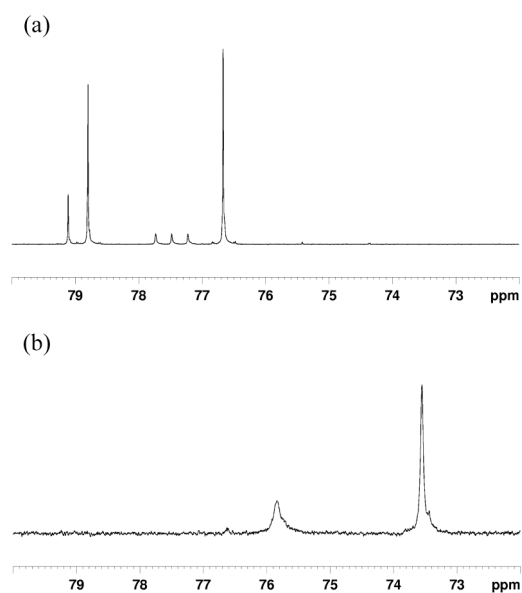

Figure 3.7. $^{13}C\{^1H\}$-NMR of (a) **2-^{13}C** in CDCl$_3$ and (b) Host-guest complex **1 ⊂ 2-^{13}C** in D$_2$O.

In the $^{13}C\{^1H\}$-NMR spectrum of **1 ⊂ 2-^{13}C** (where ⊂ denotes encapsulation), only two resonances are observed, though three resonances are present in the spectrum of the unencapsulated stereoisomers (Figure 3.7). The possibility that two of the ^{13}C resonances of encapsulated material were overlapping, or that two of the stereoisomers of **2** were bound selectively over the third were both considered. The exclusion of one stereoisomer was supported by the ^{1}H-NMR of **1 ⊂ 2**, which appears to contain two species with five resonances each. The three independently synthesized stereoisomers were added to an aqueous solution of **1**, and a ^{1}H-NMR spectrum of each encapsulated isomer was recorded (Figure 3.8). The spectrum of **1 ⊂ 2b** (Figure 3.8b) corresponds exactly to the major species observed in the spectrum of **1 ⊂ 2**. Because the unsymmetrical dienol **2c** is chiral, its encapsulation in the chiral assembly **1** results in two diastereomeric host-guest complexes, which are observed in the spectrum of **1 ⊂ 2c** and assigned using an EXSY experiment (Figure 3.8c). The resonances in this spectrum correspond to the minor peaks observed in the spectrum of **1 ⊂ 2**. The resonances observed in the spectrum of **1 ⊂ 2a** (Figure 3.8d) are not seen at all in the spectrum of **1 ⊂ 2**.

These binding experiments show that the there are marked differences in the binding of the three stereoisomers of **2**, and that the order of the binding strength is **2b**>**2c**>**2a**.
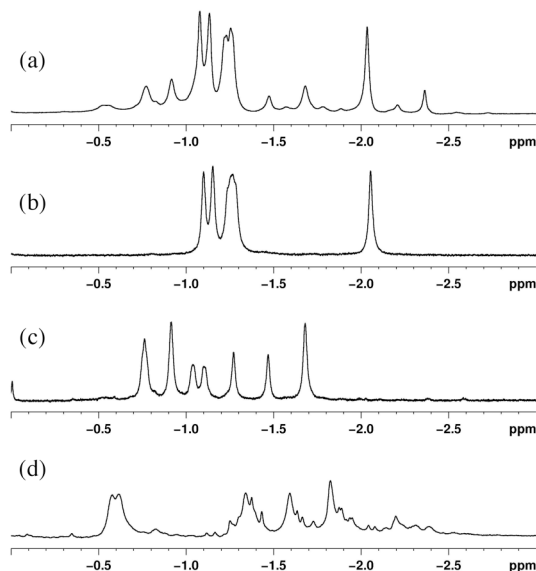

Figure 3.8. ^{1}H-NMR spectra of encapsulated Nazarov substrates. (a) Mixture of stereoisomers, **1** $\subset$ **2** (b) **1** $\subset$ **2b** (c) **1** $\subset$ **2c** (d) **1** $\subset$ **2a**.

Reaction Kinetics. Due to the low solubility of these substrates in water, further studies were carried out in D_2O (buffered at pD 8.0) with 50% added DMSO-d_6, in which **2** is soluble at concentrations below 60 mM. It was also possible to conduct the reaction in D_2O with 50% added methanol-d_4. When the reaction was attempted in pure DMSO-d_6 or methanol-d_4, no reaction occured, and no guest encapsulation was observed. This confirms that the hydrophobic effect contributes to guest binding, which is necessary for catalysis. Under these mixed solvent conditions the disappearance of each of the three stereoisomers of **2** catalyzed by 7% **1** was monitored by ^{1}H-NMR spectroscopy. The product of these reactions, Cp*H (**3**), is not soluble under these conditions and was not observed during the course of the reaction, but can be extracted into organic solvent after the reaction is complete. Again, no reaction was observed when a strongly-binding guest was added to exclude the substrate from the interior of **1**.

For all three stereoisomers of **2**, the initial reactions were rapid, but a deviation from first-order kinetic behavior was seen as the reaction progressed. In each case k_{obs} of starting material disappearance (calculated from the natural log plot of concentration versus time) was constant at the beginning of the reaction, and then decreased as the reaction proceeded (Figure 3.9). This effect was especially severe for the reaction of the weakly-binding substrate **2a**, which nearly halted after 25% conversion (Figure 3.10). The observed decrease in reaction rate is consistent with product inhibition, a common occurrence in both synthetic and enzymatic catalysis when the host does not bind the reactant substantially more strongly than it binds the product.[23-25] Competition experiments between Cp*H and the stereoisomers of **2** show that Cp*H is a competitive guest. Adding a full equivalent of Cp*H to the **1**-catalyzed reaction of **2b** shuts

down the Nazarov cyclization. These experiments clearly implicate product inhibition as the cause of the decrease of k_{obs} that is observed as the reaction progresses.
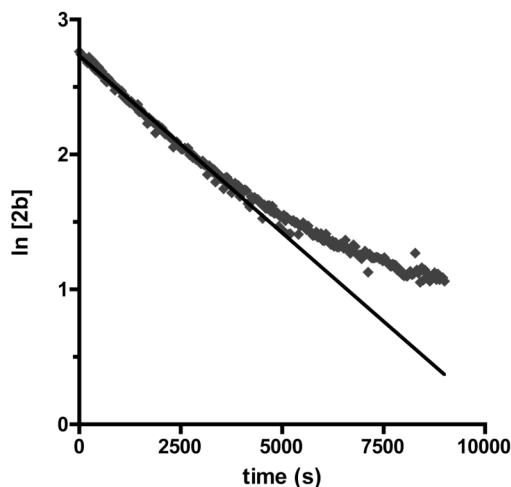

Figure 3.9. Natural log of concentration vs. time plot for the **1**-catalyzed reaction of **2b** in D$_2$O/DMSO-d_6 at 45 °C, showing a deviation from pseudo-first order kinetics.
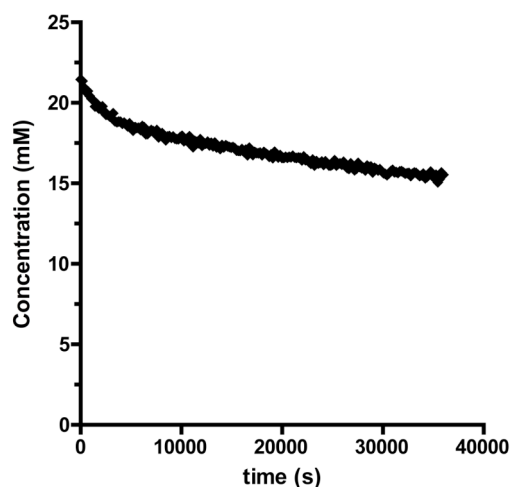
Figure 3.10. Concentration vs. time plot for the **1**-catalyzed reaction of **2a** in D$_2$O/DMSO-d_6 at 45 °C, demonstrating severe product inhibition by product Cp*H (**3**).

Rapid conversion of the product into a poorly bound guest is a strategic solution to product inhibition that has been used in other examples of supramolecular catalysis.[12,13,26] A similar strategy was applied to the **1**-catalyzed Nazarov cyclization. Cyclic dienes such as Cp*H participate in Diels-Alder reactions with electron-deficient alkenes under ambient conditions.[27] To implement this strategy, we sought to identify an appropriate dienophile that would react rapidly with Cp*H and form a species that is not bound by **1**. Ideally, the trapping reaction

would proceed much faster than the **1**-catalyzed reaction, so that Cp*H never builds up in solution. Additionally it is necessary for the trapping agent to be soluble under the reaction conditions (1:1 D_2O/DMSO-d_6) to ensure homogeneity of the reaction mixture. With these requirements in mind, the solubility and the reactivity of Cp*H toward a series of activated alkenes was evaluated (Table 3.1). The reactions of Cp*H with the dienophiles were conducted in DMSO-d_6 due to the insolubility of Cp*H in the mixed solvent system. Maleimide (**8**, entry 3) possessed the most favorable characteristics for use as a trapping reagent for Cp*H, reacting quickly and having good solubility in D_2O/DMSO-d_6. Maleic anhydride (entry 7) and *N*-phenyltriazoline dione (entry 2) were unsuitable because they react with water (via hydrolysis) and DMSO, respectively. Tetracyanoethylene (entry 1), *N*-4-(nitrophenyl)-maleimide (entry 4), and diethylacetylene dicarboxylate (entry 6) have limited solubility in D_2O/DMSO-d_6, while acetylene dicarboxylic acid (entry 5) does not react immediately with Cp*H.

Entry	Dienophile	Reaction time (to >95% conversion)	Solubility in D$_2$O/DMSO
1		< 5 minutes	Insoluble
2		-	-
3		< 5 minutes	Soluble
4		< 5 minutes	Low Solubility
5		2 hours	Soluble
6		< 5 minutes	Low Solubility
7		-	-

Table 3.1. Screen of dienophiles for the trapping of Cp*H. Reaction time was measured in DMSO-d_6, while solubility was evaluated in 1:1 D$_2$O:DMSO-d_6. Entries 2 and 7 were not evaluated due to the instability of the dienophile under the reaction conditions.

The addition of maleimide (**8**) to the **1**-catalyzed Nazarov cyclization completely alleviated product inhibition by converting Cp*H into the Diels-Alder adduct **9**, which was formed as a 1:4 mixture of *syn* to *anti* diastereomers (Figure 3.11). In the reaction using maleimide as a trapping agent, the rate of Diels-Alder adduct formation was equal to rate of starting material consumption, and implies that no Cp*H builds up in solution. The concentration versus time plots for reactions with added maleimide subsequently showed no deviation from first order behavior, indicating that product inhibition was eliminated (Figure 3.12). Adduct **9** is a suitable guest in **1**, and the host-guest complex forms in 46% yield (based

60

on total host concentration) in water. The ratio of encapsulated *syn* to *anti* diastereomer is 1:4, implying that there is no diastereoselectivity in binding the diastereomers of **9**. In a competitive binding experiment between Cp*H and **9** in water, the concentration of Cp*H $\subset$ **1** is four times as high as the concentration of **9** $\subset$ **1**. In this experiment the solution is saturated with both Cp*H and **9**. Since **9** presumably has a higher solubility in water than Cp*H (as it does in D$_2$O/DMSO-d_6), the binding constant of **9** is certainly lower by a factor of more than four relative to that of Cp*H.
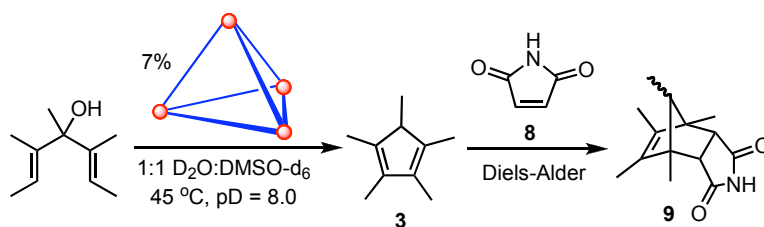

Figure 3.11. Conversion of Cp*H into a noncompetitive guest (**9**) via Diels-Alder reaction with maleimide (**8**) to alleviate product inhibition.
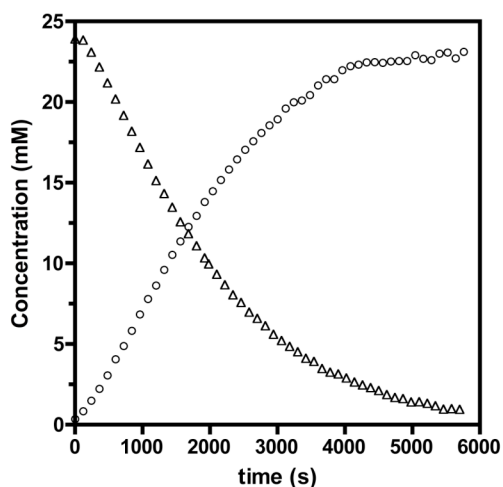

Figure 3.12. Concentration vs. time plot of the reaction of substrate **2b** ($\triangle$) to form **9** ($\bigcirc$), catalyzed by 1.5 mM **1** at 45 °C with added maleimide. No deviation from first-order kinetic behavior is observed, and no intermediate species are detected.

Catalysis under these conditions is quite efficient, and turnover numbers of up to 160 are achieved. The observed rate constants for the catalyzed cyclization of Z,Z substrate **2b** and E,Z substrate **2c** are an order of magnitude larger than that of the cyclization of E,E substrate **2a** (Table 3.2). It is remarkable that the reactivity of these three substrates is so different when they only differ in stereochemistry at positions remote to the forming carbocation. Rate constants were calculated from initial rate data (first 15% conversion) using the Michaelis-Menten equation:

$d[P]/dt = (k_{cat}[\mathbf{1}]_{tot}[SM])/([SM] + K_M)$, where [SM] is the average starting material concentration and $K_M = (k_{cat} + k_{-1})/k_1$.

In the Michaelis-Menten model, the dissociation constant (K_d) of the host-guest complex is equal to K_M when guest exchange is fast relative to the reaction rate k_{cat}. The self-exchange rate k_{exch} of substrate **2b** in **1** is 2.4 s^{-1}, which is orders of magnitude faster than the rates of cyclization for **2a**, **2b**, or **2c**. Thus, experimentally measured K_d values were used in place of the Michaelis constant.

Substrate **2a** is too weakly bound under the mixed-solvent conditions for the K_d value to be measured, so its k_{cat} value cannot be calculated directly. It was possible however, to measure the binding constant of **2a** relative to that of **2c** in pure D_2O, in which binding is much stronger. It is possible that the relative binding in **1** of **2a** versus **2c** is different in D_2O and in mixed D_2O/DMSO-d_6. To determine whether this solvent composition significantly affects the relative binding of two stereoisomeric substrates, the relative binding of **2b** and **2c** (whose binding constants are known) were measured in D_2O. In a D_2O solution saturated with a 1:1 mixture of **2b** and **2c**, there is a 2.1:1.0 ratio of **2b** $\subset$ **1** to **2c** $\subset$ **1**. The ratio of the independently-measured binding constant of **2b** to that of **2a** in D_2O/DMSO-d_6 is 2.2:1.0, which validates the comparison of relative binding constants between the two solvent systems. In D_2O (with 5% DMSO-d_6 added, which prevents guest peaks from overlapping) there is a 12.8:1 ratio of **2c** $\subset$ **1** to **2a** $\subset$ **1**, so the estimated K_d of **2a** in D_2O/DMSO-d_6 is 1.2 M. Interestingly, the k_{cat} for **2a** based on the estimated K_d is slightly larger than that of **2b**, even though the k_{obs} for the reaction of **2a** is nearly an order of magnitude smaller than the k_{obs} for the reaction of **2b**. In other words, each stereoisomer is similarly reactive once bound in **1**, and the differences in the observed rate are due to encapsulation ability. The specificity constant k_{cat}/K_M (M^{-1}s^{-1}) corresponds to a second-order rate constant for the conversion of unbound substrate into product, and is used to quantify the efficiency of the catalytic process. Substrates **2a** and **2b** have specificity constants of 2.4 x 10^{-2} M^{-1}s^{-1} and 3.8 x 10^{-1} M^{-1}s^{-1} respectively, showing that **2b** is more efficiently converted by **1** by a factor of 16:1.

Substrate	Initial rate d[P]/dt (M/s)	k_{obs} (s^{-1})	K_d (mM)	k_{cat} (s^{-1})	k_{cat}/K_M (s^{-1}M^{-1})
2a	4.0(5) x 10^{-7}	5.1(1) x 10^{-5}	(1200)	(2.9(4) x 10^{-2})	(2.4 x 10^{-2})
2b	7.6(2) x 10^{-6}	4.2(1) x 10^{-4}	42(1)	1.6(1) x 10^{-2}	3.8 x 10^{-1}
2c	1.64(4) x 10^{-5}	1.08(2) x 10^{-3}	91(1)	5.7(1) x 10^{-2}	6.3 x 10^{-1}

Table 3.2. Kinetic data for the **1**-catalyzed Nazarov reaction at 45 °C in 1:1 D_2O:DMSO-d_6 at pD 8.0. K_d and k_{cat} values (in parentheses) for **2a** were estimated from competitive binding experiments with **2c** in D_2O.

While the Michaelis-Menten model is for the catalysis of a unimolecular reaction, the **1**-catalyzed Nazarov reaction is complicated by the protonation step that is necessary for reaction. Thus, the k_{cat} calculated from the Michaelis-Menten equation implicitly includes both the equilibrium constant for protonation and the concentration of D$^+$ in solution. While the [D$^+$] in

bulk solution can be estimated from the pD of the aqueous buffer used in the experiment, the pK_a of the protonated substrate cannot be measured. Furthermore, it is certain that the pK_a of the encapsulated, protonated substrate is different from that of the unencapsulated molecule.[5,9] For that reason, the reported k_{cat} and k_{uncat} are not corrected for $[D^+]$ and the equilibrium constant for protonation. Using uncorrected values of k_{cat} and k_{uncat} is appropriate in determining the catalytic rate acceleration. The uncorrected values take into account any basicity shift that occurs as a consequence of encapsulation. Moreover, the comparison includes any change in the local $[D^+]$ within the cavity of **1** compared to bulk solution, which could play a role in catalysis.

In order to quantify the rate acceleration attributable to catalysis, the background reaction rates of each substrate were measured in the absence of **1**. During initial attempts to measure the uncatalyzed reaction rate of **2a**, the data obtained were erratic, exhibiting an apparent induction period (e.g., there was little or no reaction for a period of time, followed by a decrease in substrate concentration, Figure 3.13). A likely explanation is that the glass from the NMR tube is slowly acidifying the reaction mixture over the course of days, at which point the reaction proceeds more rapidly. The measurements were repeated using silylated NMR tubes, in which the acidic functional groups on the interior glass surface are protected as silyl ethers. The rate data collected in silylated tubes were very erratic, and it was suspected that the hydrophobic substrate was adsorbing to the silylated surface in the upper portion of the tube, which is outside of the NMR probe during measurement. To address this problem, partially silylated tubes were prepared, in which only the portion of the NMR tube that contacts the reaction mixture was silylated and the remainder is unmodified. The partially silylated NMR tubes yielded consistent results, and over the course of many weeks low (2-3%), but reproducible, levels of conversion of **2a**, **2b**, and **2c** was observed (Figure 3.14).
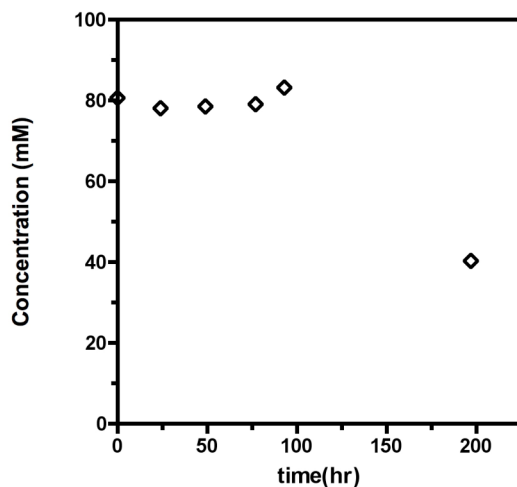

Figure 3.13. Concentration vs. time plot for the background reaction of **2b**, conducted in 1:1 D$_2$O/DMSO-d_6 at 45 °C, showing an induction period for the reaction.
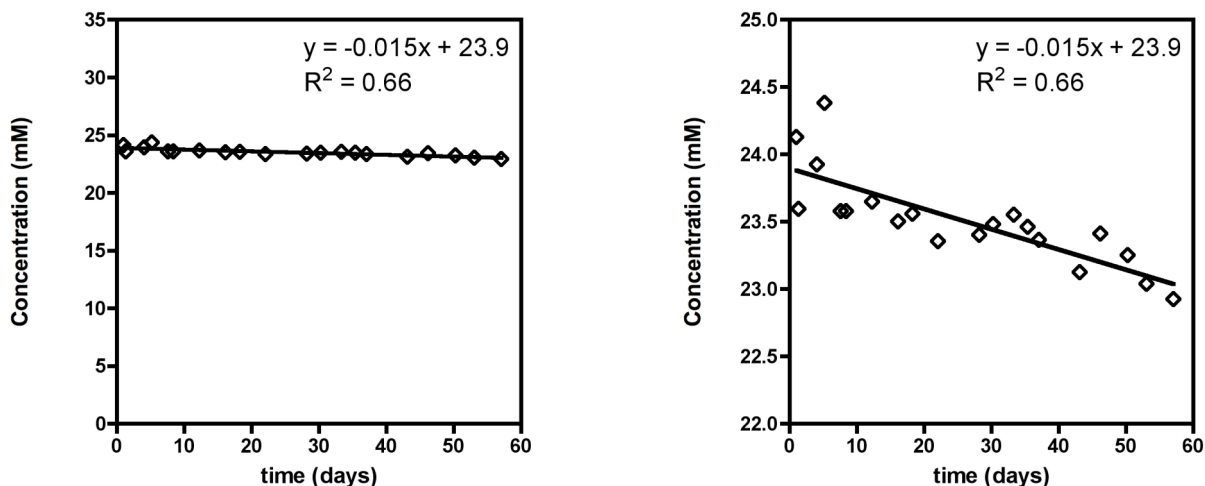
Figure 3.14. Concentration versus time plot for the uncatalyzed reaction of **2b**, conducted in 1:1 D$_2$O/DMSO-d_6 at 45 °C in a partially-silylated NMR tube. Both plots represent the same data.

Although rate constants measured under these conditions were reproducible, kinetic data obtained under conditions where higher levels of conversion occur were desired. Between 10 and 20% conversion is observed when the uncatalyzed reaction is conducted at elevated temperature (between 60 and 105 °C). The predicted value for the reaction rate at 45 °C, obtained from an Eyring plot of the high-temperature data, is identical to the experimental value (Figure 3.15). Similarly, the reaction is accelerated at lower pD, and >50% conversion is observed over the course of several hours when the pD of the aqueous buffer is between 3.5 and 4.5. A Brønsted plot of the uncatalyzed reaction rates shows that the reaction is first-order in D$^+$, and that extrapolating from the low pD data to pD 8.0 predicts a rate similar to the experimentally-determined value (Figure 3.16). The variable temperature and variable pD studies on the uncatalyzed reaction rate both clearly validate the low-conversion rate data obtained at 45 °C and pD 8.0.
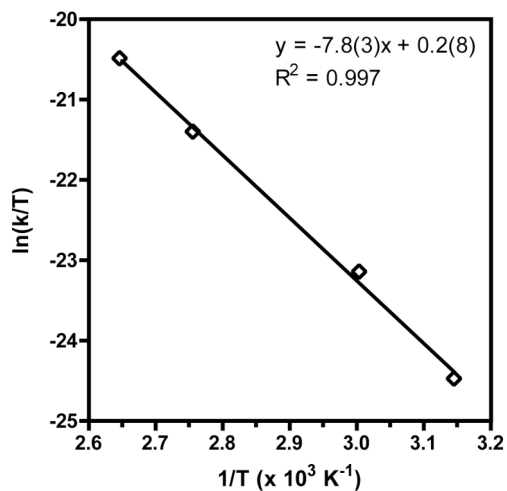
Figure 3.15. Eyring plot used to determine activation parameters for the uncatalyzed reaction of **2b**.
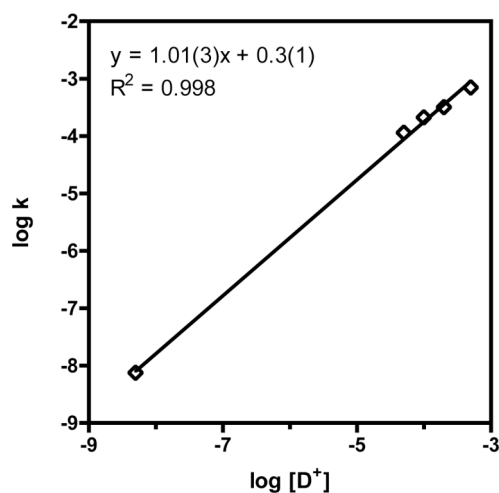

Figure 3.16. Brønsted plot of pD-dependence kinetics for the uncatalyzed reaction of **2b**.

The uncatalyzed reaction rates are strongly dependent on the substrate stereochemistry, with methyl groups in the Z configuration giving the slowest reaction (Table 3.3). This suggests that the reacting molecule must adopt a U-shaped conformation in order to react prior to or at the transition state of the rate-determining step. This compact conformation necessary for reaction is sterically disfavored by Z methyl groups when compared to the linear conformation of the same molecule (Figure 3.17).
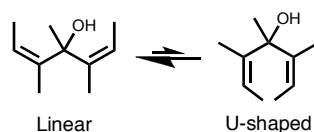
Figure 3.17. Linear and U-shaped conformations of substrate 2b.

The rate accelerations of the catalyzed reaction over the uncatalyzed reaction are on the order of 10^6 (Table 3.3), the largest measured for supramolecular catalysis by orders of magnitude.[28-32] This very high level of catalytic activity is reminiscent of enzymatic catalysis. The observed rate acceleration is too large to be explained only by an increase of the basicity of the bound substrate. In previous studies a maximum of four orders of magnitude in equilibrium shift of protonated amines, and thousandfold rate acceleration in the hydrolysis of orthoformates were observed.[5,6] It is proposed that the additional rate enhancement in this system is due to constrictive binding in the pocket of 1, which favors both the U-shaped conformation of the substrate and the compact transition state of the electrocyclization. Constrictive binding is responsible for rate enhancements of nearly three orders of magnitude in the 1-catalyzed aza-Cope rearrangement of enammonium cations, where encapsulation preorganizes the substrate into a reactive conformation.[12,13,26] These factors are discussed in further detail in Chapter 5.

substrate	k_{cat} (s^{-1})	k_{uncat} (s^{-1})	rate acceleration (k_{cat}/k_{uncat})
2a	$(2.9(4) \times 10^{-2})$	$4.0(3) \times 10^{-8}$	(730,000)
2b	$1.6(1) \times 10^{-2}$	$7.7(8) \times 10^{-9}$	2,100,000
2c	$5.7(1) \times 10^{-2}$	$3.3(1) \times 10^{-8}$	1,700,000

Table 3.3. Kinetic data for Nazarov substrates at 45 °C in 1:1 D$_2$O:DMSO-d_6. The k_{cat} and rate acceleration values for substrate 2a (in parentheses) were estimated from competitive binding experiments with 2c in D$_2$O.

Conclusion

In conclusion, the efficient catalysis of the Nazarov cyclization of 1,4-pentadien-3-ols by a self-assembled host in aqueous solution has been demonstrated. The reaction product, Cp*H, is a suitable guest for 1, and causes product inhibition in the catalyzed reaction. Adding maleimide to the reaction mixture converts Cp*H into the corresponding Diels-Alder adduct, whose binding constant is significantly lower than that of the reactant. The catalyst resting state was identified as the encapsulated, neutral substrate. Kinetic studies reveal that the rate of the catalyzed reaction is up to 2,100,000 times larger than that of the uncatalyzed reaction, representing the first instance of supramolecular catalysis that achieves rate enhancements comparable in size to those seen in enzymatic systems.

Experimental Section

General Experimental Procedures. Unless otherwise noted, reactions and manipulations were performed using standard Schlenk and high-vacuum techniques at room temperature. All glassware was dried in an oven at 150 °C for at least 12 h or flame-dried under vacuum prior to use. Column chromatography was performed on a Biotage SP1 MPLC instrument using pre-packed silica gel columns.

Instrumentation. NMR spectra were obtained on Bruker Avance AV 300 (300 MHz), AV 400 (400 MHz), AV 500 (500 MHz), or AV 600 (600 MHz) spectrometers as indicated. Chemical shifts are reported as δ in parts per million (ppm) relative to residual protonated solvent resonances. In the case of D_2O samples, ^{13}C shifts were referenced to an internal standard of CH_3OH.[33] NMR data are reported in the following format: (s = singlet, d = doublet, t = triplet, q = quartet, m = multiplet, b = broad; integration; coupling constant). The temperatures of the kinetics experiments carried out in a circulating oil bath were measured using a calibrated mercury thermometer and varied ±0.1 °C. The temperatures of the kinetics experiments carried out in an NMR probe were determined from the ^1H NMR chemical shifts of ethylene glycol and CH_3OH samples, and varied ±0.1 °C. IR spectra were measured neat on a Nicolet iS10 FT-IR spectrometer with a diamond attenuated total reflective (ATR) accessory. Peak intensities are reported as broad (b), weak (w), medium (m), or strong (s). Only peaks in the functional group region $(4000-1300 \text{ cm}^{-1})$ are reported. Mass spectral data were obtained at the QB3 Mass Spectrometry Facility operated by the College of Chemistry, University of California, Berkeley. Fast atom bombardment mass spectra were recorded on a Micromass ZAB2-EQ magnetic sector instrument. Electron impact (EI) and chemical ionization (CI) mass spectra were recorded on a Micromass ProSpec magnetic sector instrument equipped with an EI and a CI source.

Materials. Unless otherwise noted, reagents were obtained from commercial suppliers and used without further purification. Ethyl ether (Et_2O), tetrahydrofuran (THF), and pentane were dried by passing through columns of activated alumina under nitrogen pressure and were sparged with nitrogen before use.[34] The two isomers of 2-bromo-2-butene could be separated by preparative gas chromatography (Varian Aerograph 970, using a 0.38" x 10' column packed 10% Carbowax chemically bonded to Chromsorb stationary phase). The helium flow rate was 60 mL/min, the column temperature was 60 °C, the injector temperature was 100 °C, and the detector temperature was 150 °C. Prior to injection, the *E* and *Z* isomers of 2-bromo-2-butene were passed through a column of basic alumina. Total recovery of the two isomers was approximately 45%, and both isomers were >99% pure by ^{1}H-NMR. Although the photoisomerization of pure (*E*)- or (*Z*)-2-bromo-2-butene has been reported, the pure compounds can tolerate ambient light for several minutes with no apparent erosion of stereochemical purity.[35] As a precaution, however, all operations involving either pure compound were performed with as much light excluded as possible. The *E* and *Z* isomer of 2-bromo-2-butene are occasionally available commercially from Sigma-Aldrich. 1,2,3,4,7–pentamethylbicyclo[2.2.1]hept-2-ene-5,6-dicarboximide (**9**),[36] 3-methyl-1,4-pentadien-3-ol (**5**)[37] and $K_{12}Ga_4L_6$ (K_{12}**1**)[38] were prepared according to literature procedures.

2
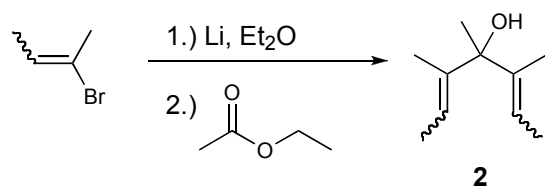
3,4,5-Trimethyl-2,5-pentadien-4-ol (2), mixture of stereoisomers. This procedure was adapted for a small scale (5-50 mmol) from a published procedure for the large-scale preparation of **2**.[19] A 2-necked round-bottomed flask equipped with a magnetic stir bar and a reflux condenser was charged with lithium wire (310 mg, cut into 1 cm lengths, 44.8 mmol) and 1.5 mL dry Et$_2$O. 2-bromo-2-butene was purified and dried immediately before use by passage through a pipette column of basic alumina. The first 1.0 mL of 2-bromo-2-butene (total of 2.3 mL, 22.4 mmol) was added to the stirred solution via syringe dropwise over the course of several minutes. At this point, the reaction initiated, as indicated by the evolution of heat and bubbling of the reaction mixture. An additional 15 mL of fresh Et$_2$O was added, and the remainder of the 2-bromo-2-butene was added slowly to keep the reaction at reflux. After the addition was complete, stirring was continued for one additional hour. The reaction mixture was then cooled to 0 °C in an ice bath and quenched by the slow addition of ethyl acetate (1.1 mL, 11.2 mmol) diluted to 50% with Et$_2$O. The reaction mixture was poured into saturated aqueous NH$_4$Cl and extracted five times with 20 mL Et$_2$O. The combined organic layers were washed with brine and dried over MgSO$_4$, and the solvent was removed by rotary evaporation to obtain the title compound (1.35 g, 8.75 mol) as a yellow liquid in 78% yield. This mixture contains **2a**, **2b**, and **2c** (*vide infra*) according to analysis by ^{1}H- NMR, ^{13}C{^{1}H}-NMR and GC-MS.
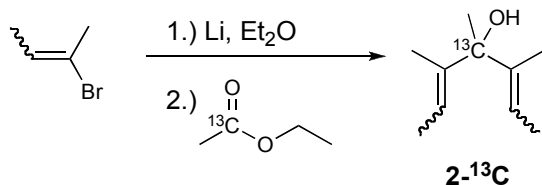
2-^{13}C

[4-^{13}C]3,4,5-Trimethyl-2,5-pentadien-4-ol (2-^{13}C), mixture of stereoisomers. The above procedure was followed using 313 mg lithium wire (45.2 mmol), 2.3 mL 2-bromo-2-butene (22.6 mmol), and 1.0 g ethyl acetate-1-^{13}C (11.3 mmol). The title compound was obtained as a yellow liquid (1.40 g, 9.01 mmol) in 80% yield. This material is identical to **2** by ^{1}H and ^{13}C{^{1}H}-NMR, except that the following peaks are enriched: ^{13}C{^{1}H}-NMR (125.8 MHz, CDCl$_3$): δ 78.9, 78.5, 76.4 ppm.

2a
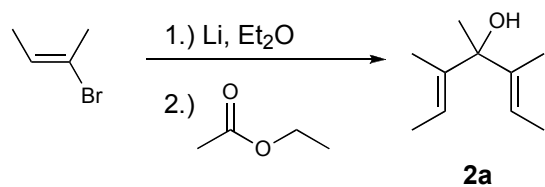
3,4,5-Trimethylhepta-2-*cis*-5-*cis*-dien-4-ol (2a). The above procedure for preparing **2** was followed using 192 mg lithium wire (27.7 mmol), 1.87 g (*E*)-2-bromo-2-butene (13.9 mmol), and 0.680 mL ethyl acetate (6.95 mmol). The title compound was obtained in 90%

purity in 87% yield (928 mg, 6.0 mmol) as a yellow liquid, with **2c** as the contaminant. ^{1}**H NMR** (500 MHz, CDCl$_3$): δ 5.55 (m, 2H, $^3J = 6.6$ Hz, $^4J = 1.3$ Hz), 1.56 (d, 6H, $^3J = 6.6$ Hz), 1.43 (br, 6H), 1.32 (s, 3H) ppm; ^{13}**C{^{1}H} NMR** (125.8 MHz, CDCl$_3$): δ 139.7, 118.4, 78.9, 26.2, 13.7, 12.6 ppm; **IR**: 3459 (br), 2922 (s), 2859 (m), 1731 (w), 1452 (m), 1378 (s), 1366 (m), 1310 (w) cm^{-1}; **HRMS (CI)**: Exact mass calcd for C$_{10}$H$_{17}$O [M-H]$^+$: 153.1279, found 153.1276.


7b
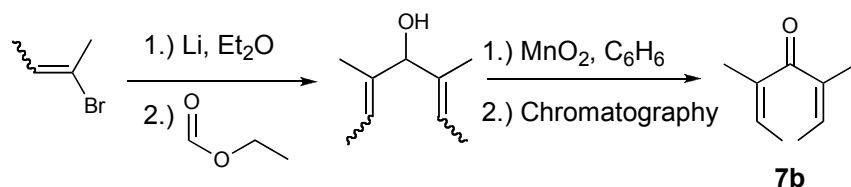
3,4,5-Trimethylhepta-2-*trans*-5-*trans*-dien-4-one (7b).   Purification of 2-bromo-2-butene was performed as described above.   A 3-necked round-bottomed flask equipped with a magnetic stir bar, reflux condenser and addition funnel was charged with lithium wire (5.94 g, cut into 1 cm lengths, 0.86 mol) and 30 mL dry Et$_2$O. The first 1.5 mL of 2-bromo-2-butene (total of 43 mL, 0.43 mol) was added to the stirred solution via syringe in three 0.5 mL portions spaced at one minute intervals. At this point, the reaction initiated as indicated by the evolution of heat and bubbling of the reaction mixture. An additional 125 mL of fresh Et$_2$O was added, and the remainder of the 2-bromo-2-butene was added slowly via addition funnel to keep the reaction at reflux. After the addition was complete, the reaction mixture was stirred for one additional hour. The reaction mixture was cooled to 0 ^{o}C in an ice bath, and quenched slowly with ethyl formate (17 mL, 0.21 mol) diluted to 50% with Et$_2$O, added via addition funnel. The reaction mixture was poured into saturated aqueous NH$_4$Cl and extracted five times with 100 mL Et$_2$O. The combined organic layers were washed with brine and dried over MgSO$_4$, and the solvent was removed by rotary evaporation to obtain the crude alcohol **6** (22.4 g, 0.16 mol) as a red liquid. This material was used in the subsequent reaction without further purification.

A round bottom flask equipped with a stir bar was charged with the crude alcohol (3.00 g, 21.4 mmol) and 200 mL pentane. To this mixture was added MnO$_2$ (37.0 g, 428 mmol), and the reaction mixture was stirred for one hour, at which point the reaction was complete as judged by TLC analysis (using 10% ethyl acetate in hexane as eluent). The reaction mixture was filtered through Celite over a medium frit and concentrated by rotary evaporation to obtain compound **7b** as a mixture with the other two stereoisomers. Pure **7b** was obtained by automated column chromatography using a solvent gradient of 2 to 8% ethyl acetate in hexanes over 10 column volumes. The other two stereoisomers are copolar. The title compound was isolated as a yellow liquid in 3% yield (90.5 mg, 0.65 mmol). ^{1}**H NMR** (500 MHz, CDCl$_3$): δ 5.80 (q, 2H, $^3J = 7.3$ Hz), 1.87 (s, 6H), 1.76 (d, 6H, $^3J = 7.3$ Hz) ppm; ^{13}**C{^{1}H} NMR** (125.8 MHz, CDCl$_3$): δ 203.1, 138.0, 131.0, 20.4, 15.3 ppm; **IR:** 2973 (m), 2921 (m), 1717 (m), 1640 (s), 1455 (s), 1378 (m) cm^{-1}; **HRMS (FAB)**: Exact mass calcd for C$_9$H$_{14}$O [M]$^+$: 138.1045, found 138.1041.
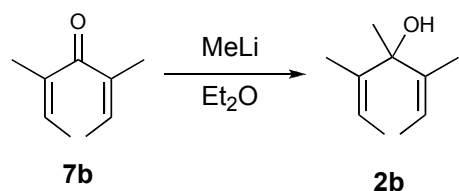
3,4,5-Trimethylhepta-2-*trans*-5-*trans*-dien-4-ol (2b). A flame-dried, 50 mL round-bottom flask was charged with 161 mg **7b** (1.16 mmol) and 25 mL Et$_2$O. The reaction mixture was cooled to -78 °C in a dry ice/acetone bath, at which point 0.91 mL methyllithium (1.6 M in pentane, 1.5 mmol) was added dropwise to the stirred solution by syringe. The reaction flask was removed from the cold bath and allowed to warm to room temperature, and the mixture was stirred for an additional two hours. The reaction mixture was quenched by addition to saturated aqueous NH$_4$Cl solution and extracted with three portions of 50 mL Et$_2$O. The combined organic fractions were washed with three portions of brine and dried over MgSO$_4$, and the solvent was removed by rotary evaporation to obtain 167 mg of the title compound (1.08 mmol) in 93% yield. **^{1}H NMR** (500 MHz, CDCl$_3$): δ 5.27 (q, 2H, ^3J = 7.5 Hz), 1.81 (s, 6H), 1.58 (d, 6H, ^3J = 7.5 Hz), 1.35 (s, 3H) ppm; **^{13}C{^{1}H} NMR** (125.8 MHz, CDCl$_3$): δ 141.8, 121.6, 76.4, 27.2, 22.1, 14.9 ppm; **IR:** 3480 (br), 2969 (s), 2941 (m), 2918 (m), 2860 (w), 1452 (m), 1376 (m) cm^{-1}; **HRMS (CI)**: Exact mass calcd for C$_{10}$H$_{17}$O [M-H]$^+$: 153.1279, found 153.1280.
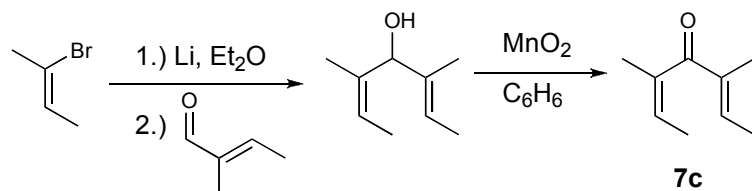
3,4,5-Trimethylhepta-2-*cis*-5-*trans*-dien-4-one (7c). The procedure described above for preparing **7b** was followed using 1.3 mL (*Z*)-2-bromo-2-butene (12.8 mmol), 208 mg Li (30.0 mmol), and 1.35 mL tiglaldehyde (14.1 mmol) to quench the organolithium reagent in the first step. The resulting crude alcohol **6c** was oxidized without purification using 34 g MnO$_2$ (384 mmol). The resulting crude ketone was purified by automated chromatography using a 5% ethyl acetate in hexane. The title compound was obtained as a yellow liquid in 45% yield (862 mg, 6.2 mmol). **^{1}H NMR** (600 MHz, CDCl$_3$): δ 6.72 (q, 1H, ^3J = 7.0 Hz), 5.52 (q, 1H, ^3J = 7.0 Hz), 1.86 (d, 3H, ^3J = 7.0 Hz), 1.81 (s, 3H), 1.79 (s, 3H), 1.47 (d, ^3J = 7.0 Hz) ppm; **^{13}C{^{1}H} NMR** (150.9 MHz, CDCl$_3$): δ 203.09, 142.27, 137.66, 137.11, 124.33, 21.67, 15.24, 15.18, 10.34 ppm; **HRMS (EI)**: Exact mass calcd for C$_9$H$_{14}$O [M]$^+$: 138.1045, found 138.1044.
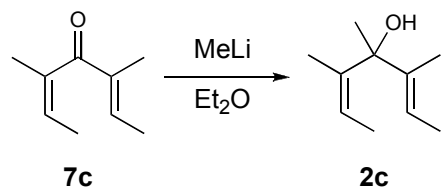
3,4,5-Trimethylhepta-2-*trans*-5-*cis*-dien-4-ol (2c). The procedure described above for preparing **2b** was followed, using 100 mg **7c** (0.72 mmol) and 0.50 mL methyllithium (1.6 M in diethyl ether, 0.79 mmol). The title compound was obtained in 81% yield (90 mg, 0.58 mmol) as

a yellow liquid. **¹H NMR** (600 MHz, CDCl₃): δ 5.62 (q, 1H, ^3J = 7.4 Hz), 5.32 (q, 1H, ^3J = 7.2 Hz), 1.70 (br, 6H), 1.65 – 1.61 (m, 9H), 1.43 (s, 3H) ppm; **¹³C{¹H} NMR** (150.9 MHz, CDCl₃): δ 140.7, 140.0, 121.7, 118.0. 78.6, 26.8, 23.1, 14.5, 13.5, 12.8 ppm; **IR**: 3470 (br), 2969 (m), 2920 (m), 2862 (w), 1450 (s), 1378 (m), 1303 (m) cm⁻¹; **HRMS (CI)**: Exact mass calcd for $C_{10}H_{17}O$ [M-H]⁺: 153.1279, found 153.1276.

General Procedure for Encapsulation Reactions. The potassium salt of **1** (15.0 mg, 4.0 μmol) was dissolved in 0.6 mL D₂O (buffered to pD 11.3 with 0.1 M K₂CO₃ to slow **1**-catalyzed reaction of guest), and the resulting solution was then mixed thoroughly with the guest (12.0 μmol). The solution was transferred to an NMR tube, and the spectrum of the host-guest complex was recorded within 20 minutes. The NMR resonances for the encapsulated guests are shifted upfield by 2 to 3 ppm because of shielding by the aromatic walls of the host. Due to the chirality of the host, diastereotopic atoms become inequivalent upon binding and two diastereomeric host-guest complexes were observed for the chiral guest **2c**. Quantitative guest binding was not observed in these experiments, so the reported binding efficiency represents the relative ¹H-NMR integrations of the guest to host peaks. Resonances corresponding to encapsulated guests were not observed by ¹³C{¹H}-NMR after obtaining hundreds of scans unless ¹³C-enriched material was used. However, host resonances in the ¹³C{¹H}-NMR are easily observed. The unencapsulated guest is sparingly soluble in D₂O, and only broad resonances were observed. Encapsulated peaks were assigned by 2-D NMR Exchange Spectroscopy (EXSY) experiment acquired using an optimized 90° pulse and a 150 msec mixing time.

K₁₂[2a ⊂ 1]. Host-guest complex prepared as above with a binding efficiency of 47%. **¹H NMR** (500 MHz, D₂O): δ 7.81 (br, 12H, Ar-*H*), 7.78 (d, 12H, ^3J = 8.7 Hz, Ar-*H*), 7.27 (d, 12H, ^3J = 8.7 Hz, Ar-*H*), 6.95 (t, 12H, ^3J = 7.0 Hz, Ar-*H*), 6.73 (d, 12H, ^3J = 7.1 Hz, Ar-*H*), 6.57 (t, 12H, ^3J = 7.6 Hz, Ar-*H*), -0.48 (br, 6H, encaps.), -1.22 (br, 3H, encaps.), -1.47 (br, 3H, encaps.), -1.71 (br, 3H, encaps.) ppm.

K₁₂[2b ⊂ 1]. Host-guest complex prepared as above with a binding efficiency of 86%. **¹H-NMR** (400 MHz, D₂O): δ 7.91 (d, 12H, ^3J = 6.3 Hz, Ar-*H*), 7.80 (d, 12H, ^3J = 8.1 Hz, Ar-*H*), 7.32 (d, 12H, ^3J = 7.6 Hz, Ar-*H*), 7.01 (t, 12H, ^3J = 7.5 Hz, Ar-*H*), 6.74 (d, 12H, ^3J = 6.8 Hz, Ar-*H*), 6.59 (t, 12H, ^3J = 7.4 Hz, Ar-*H*), -0.99 (s, 3H, encaps.), -1.04 (s, 3H, encaps.), -1.16 (br, 6H, encaps.), -1.94 (s, 3H, encaps.) ppm.

K₁₂[2c ⊂ 1]. Host-guest complex prepared as above with a binding efficiency of 83%. A 1:1 mixture of two diastereomeric host-guest complexes is formed. **¹H-NMR** (500 MHz, D₂O): δ 7.86 (br, 12H, Ar-*H*), 7.79 (d, 12H, ^3J = 8.5 Hz, Ar-*H*), 7.28 (d, 12H, ^3J = 7.9 Hz, Ar-*H*), 7.00 (t, 12H, ^3J = 8.0 Hz, Ar-*H*), 6.73 (d, 12H, ^3J = 7.1 Hz, Ar-*H*), 6.57 (t, 12H, ^3J = 7.8 Hz, Ar-*H*), -0.69 (s, 6H, encaps.), -0.85 (s, 6H, encaps.), -0.97 (s, 3H, encaps.), -1.03 (s, 3H, encaps.), -1.20 (s, 3H, encaps.), -1.40 (s, 3H, encaps.), -1.61 (s, 6H, encaps.) ppm.

K$_{12}$[2-^{13}C ⊂ 1]. The host-guest complex was prepared as above. By ^{1}H-NMR analysis, peaks corresponding to **2b ⊂ 1** and **2c ⊂ 1** are observed. The weaker-binding **2a** is not encapsulated in the presence of the other two stereoisomers. **^{13}C{^{1}H} NMR** (150.9 MHz, CDCl$_3$): δ 170.1, 167.0, 158.9, 155.0, 133.7, 127.3, 126.3, 119.8, 118.4, 115.9, 115.2, 114.9, 75.8 (encaps.), 73.6 (encaps.) ppm. The encapsulated peaks are not present in the ^{13}C{^{1}H} NMR of **K$_{12}$[2 ⊂ 1]** (prepared in an analogous fashion), which is otherwise identical by ^{1}H and ^{13}C{^{1}H} NMR.

Kinetic Analysis of Catalyzed Reactions. General procedure for kinetic runs: 2.0 mg substrate alcohol (13.0 μmol), 3.5 mg K$_{12}$**1** (0.9 μmol), 2.0 mg maleimide (20.6 μmol), and 3.0 mg sodium *p*-toluenesulfonate (15.4 μmol, added as an integration standard) were dissolved in 0.3 mL DMSO-*d$_6$* and 0.3 mL D$_2$O (buffered with 100 mM phosphate buffer, adjusted to pD = 8.0). The solution was transferred to an NMR tube and inserted into the NMR probe preheated to 45 °C. After allowing the sample temperature to equilibrate for two minutes, ^{1}H-NMR spectra were acquired every 20 seconds (for **2b** and **2c**) or every 240 seconds (for **2a**) until >95% of the starting material was consumed. Concentration versus time plots for the **1**-catalyzed reactions of **2a**, **2b**, and **2c** are given in Figure 3.18, Figure 3.12, and Figure 3.19 respectively. Standard errors for all reported values are given in parentheses.

Since guest exchange is fast in this system, the reciprocal of the dissociation constant (1/K$_d$) of the host-guest complex is substituted for K$_M$. In the case of substrate **2b**, the concentration of host-guest complex **2b ⊂ 1** can be measured during the kinetic run, and the K$_d$ is calculated from the observed concentration of **1**, **2b**, and **2b ⊂ 1**. In the case of substrates **2a** and **2c**, concentrations of the respective host-guest complexes are too low to measure under the reaction conditions of the kinetic runs. The K$_d$ for **2c ⊂ 1** can be determined by preparing samples that are more highly concentrated than those used for the kinetic runs, and buffered to a higher pD to slow the **1**-catalyzed Nazarov reaction. The K$_d$ for **2a ⊂ 1** could not be determined using this method.
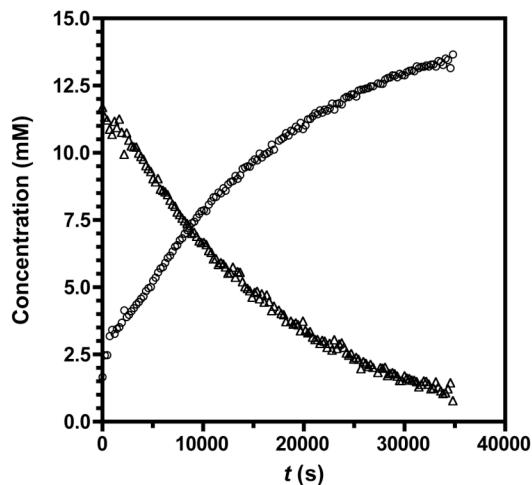
Figure 3.18. Concentration vs. time plot of the reaction of substrate **2a** (△) to form **4** (○), catalyzed by 1.5 mM **1** at 45 °C with added maleimide. The sample of **2a** in this experiment was contaminated by a small quantity of product **3**. This material immediately reacted under the reaction conditions to form the small quantity of **4** that is observed at the beginning of the reaction.

Figure 3.19. Concentration vs. time plot of the reaction of substrate **2c** (△) to form **4** (○), catalyzed by 1.5 mM **1** at 45 °C with added maleimide. The sample of **2c** in this experiment was contaminated by a small quantity of product **3**. This material immediately reacted under the reaction conditions to form the small quantity of **4** that is observed at the beginning of the reaction.
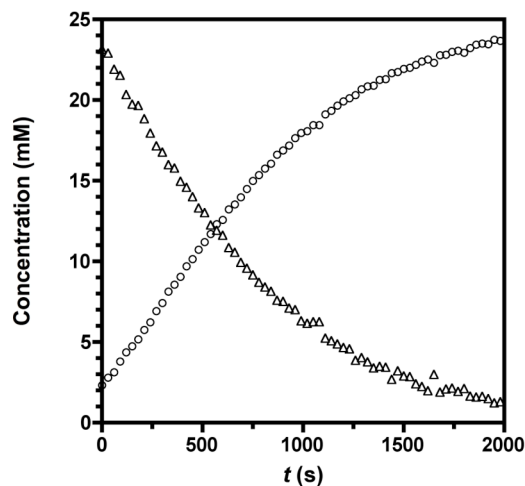
Typical procedure for binding constant determination: 22.0 mg K_{12}**1** (5.8 μmol), 3.0 mg substrate alcohol (19.4 μmol), and 3.0 mg sodium *p*-toluenesulfonate (15.4 μmol, added as

an integration standard) were dissolved in 0.3 mL DMSO-d_6 and 0.3 mL D_2O (buffered with 100 mM carbonate, adjusted to pD = 11.0). The solution was transferred to an NMR tube and inserted into the NMR probe preheated to 45 °C. A single scan ^{1}H-NMR spectrum was obtained using a calibrated 90° pulse and a 6.0 second relaxation time.

Kinetic Analysis of Uncatalyzed Reactions. The procedure for sample preparation is analogous to that used for the catalyzed reaction, except that **1** and maleimide are omitted and silylated glassware is used. For experiments conducted at lower pD values (between 3.0 and 4.0) the aqueous portion of solvent was buffered with 100 mM potassium hydrogen phthalate. The sample was sealed under vacuum in a thin-walled NMR tube and heated at 45 °C in circulating oil bath. Partially silylated tubes, in which only the portion of the NMR tube that contacts the reaction mixture was silylated and the remainder is unmodified, were prepared in the following fashion:
Hexamethyldisilazane (0.7 mL, purified by distillation) was transferred by syringe into a thin-walled NMR tube, with care being taken so that the reagent did not contact any part of the tube except the bottom portion. The NMR tube was capped and heated at 70 °C in a circulating oil bath for twelve hours. The hexamethyldisilazane was then pipetted out of the NMR tube and discarded, and the tube was heated in an oven for at least 24 hours at 150 °C.

This modification yielded consistent results, and over the course of many weeks at 45 °C low but reproducible levels of conversion of all three Nazarov substrates was observed. By treating the initial reaction rate as the derivative of a first-order process, the rate constant is calculated from the equation d[SM]/dt = - k_{uncat} [SM]. Kinetics data measured at lower pD were monitored by in-probe NMR spectroscopy as described above.

Entry	Substrate	Temp. (°C)	pD	k_{uncat} (s^{-1})	Half-life (h)
1	**2a**	45	8.0	2.7(3) x 10^{-8}	2.6(3) x 10^7
2	**2a**	45	8.0	3.4(3) x 10^{-8}	2.0(2) x 10^7
3	**2b**	45	8.0	8(2) x 10^{-9}	9(2) x 10^7
4	**2b**	45	8.0	7(1) x 10^{-9}	1.0(1) x 10^8
5	**2c**	45	8.0	5(1) x 10^{-8}	1.4(3) x 10^7
6	**2b**	60	8.0	2.2(7) x 10^{-8}	3(1) x 10^7
7	**2b**	60	8.0	2.5(7) x 10^{-8}	2.8(8) x 10^7
8	**2b**	60	8.0	2.9(5) x 10^{-8}	2.4(4) x 10^7
9	**2b**	60	8.0	3.8(7) x 10^{-8}	1.8(3) x 10^7
10	**2b**	60	8.0	2.2(7) x 10^{-8}	3(1) x 10^7
11	**2b**	60	8.0	4.2(5) x 10^{-8}	1.6(2) x 10^7
12	**2b**	90	8.0	1.8(2) x 10^{-7}	3.9(2) x 10^6
13	**2b**	90	8.0	1.9(1) x 10^{-7}	3.6(2) x 10^6
14	**2b**	105	8.0	4.8(3) x 10^{-7}	1.44(9) x 10^6
15	**2b**	105	8.0	5.0(3) x 10^{-7}	1.39(8) x 10^6
16	**2b**	105	8.0	4.6(2) x 10^{-7}	1.51(7) x 10^6
17	**2b**	45	3.0	6.95(9) x 10^{-4}	9.9(1) x 10^2
18	**2b**	45	3.4	3.19(5) x 10^{-4}	2.17(3) x 10^3

| 19 | **2b** | 45 | 3.7 | $2.12(3) \times 10^{-4}$ | $3.27(5) \times 10^{3}$ |
| 20 | **2b** | 45 | 4.0 | $1.14(2) \times 10^{-4}$ | $6.1(1) \times 10^{3}$ |

References:

(1)   Jencks, W. P. *Catalysis in Chemistry and Enzymology*; McGraw-Hill: New York, 1969.

(2)   Kirby, A. *Angew. Chem. Int. Ed.* **1996**, *35*, 708.

(3)   Breslow, R.; Dong, S. *Chem. Rev.* **1998**, *98*, 1997.

(4)   Radzicka, A.; Wolfenden, R. *Science* **1995**, *267*, 90.

(5)   Pluth, M. D.; Bergman, R. G.; Raymond, K. N. *J. Am. Chem. Soc.* **2007**, *129*, 11459.

(6)   Pluth, M. D.; Bergman, R. G.; Raymond, K. N. *Science* **2007**, *316*, 85.

(7)   Pluth, M. D.; Bergman, R. G.; Raymond, K. N. *Angew. Chem. Int. Ed.* **2007**, *46*, 8587.

(8)   Pluth, M. D.; Bergman, R. G.; Raymond, K. N. *J. Am. Chem. Soc.* **2008**, *130*, 11423.

(9)   Pluth, M. D.; Bergman, R. G.; Raymond, K. N. *Acc. Chem. Res.* **2009**, *42*, 1650.

(10) Pluth, M. D.; Bergman, R. G.; Raymond, K. N. *J. Org. Chem.* **2009**, *74*, 58.

(11) Ma, J.; Dougherty, D. *Chem. Rev.* **1997**, *97*, 1303.

(12) Fiedler, D.; Van Halbeek, H.; Bergman, R. G.; Raymond, K. N. *J. Am. Chem. Soc.* **2006**, *128*, 10240.

(13) Hastings, C. J.; Fiedler, D.; Bergman, R. G.; Raymond, K. N. *J. Am. Chem. Soc.* **2008**, *130*, 10977.

(14) Abe, I.; Rohmer, M.; Prestwich, G. D. *Chem. Rev.* **1993**, *93*, 2189.

(15) Gallimore, A. R. *Nat. Prod. Rep.* **2009**, *26*, 266.

(16) Woodward, R. B.; Hoffmann, R. *J. Am. Chem. Soc.* **1965**, *87*, 395.

(17) Campbell, P. H.; Chiu, N. W. K.; Deugau, K.; Miller, I. J.; Sorensen, T. S. *J. Am. Chem. Soc.* **1969**, *91*, 6404.

(18) King, R. B.; Bisnette, M. B. *J. Organomet. Chem.* **1967**, *8*, 287.

(19) Threlkel, R. S.; Bercaw, J. E.; Seidler, P. F.; Stryker, J. M.; Bergman, R. G. In *Organic Syntheses*; Wiley: New York, 1993; Vol. VIII, p 505.

(20) Sorensen, T. S. *J. Am. Chem. Soc.* **1967**, *89*, 3782.

(21) Biros, S. M.; Bergman, R. G.; Raymond, K. N. *J. Am. Chem. Soc.* **2007**, *129*, 12094.

(22) Hastings, C. J.; Pluth, M. D.; Biros, S. M.; Bergman, R. G.; Raymond, K. N. *Tetrahedron* **2008**, *64*, 8362.

(23) Kang, J.; Hilmersson, G.; Santamaria, J.; Rebek Jr, J. *J. Am. Chem. Soc* **1998**.

(24) Yoshizawa, M.; Takeyama, Y.; Kusukawa, T.; Fujita, M. *Angew. Chem. Int. Ed.* **2002**, *41*, 1347.

(25) Nishioka, Y.; Yamaguchi, T.; Yoshizawa, M.; Fujita, M. *J. Am. Chem. Soc.* **2007**, *129*, 7000.

(26) Fiedler, D.; Bergman, R. G.; Raymond, K. N. *Angew. Chem. Int. Ed.* **2004**, *43*, 6748.

(27) Letourneau, J.; Wellman, M.; Burnell, D. *J. Org. Chem.* **1997**, *62*, 7272.

(28) Mock, W. L.; Irra, T. A.; Wepsiec, J. P.; Adhya, M. *J. Org. Chem.* **1989**, *54*, 5302.

(29) Zhang, B.; Breslow, R. *J. Am. Chem. Soc.* **1997**, *119*, 1676.

(30)   Marinescu, L. G.; Bols, M. *Angew. Chem. Int. Ed.* **2006**, *45*, 4590.

(31)   Very large rate accelerations were observed in the stoichiometric acylation of cyclodextrins: Trainor, G. L.; Breslow, R. *J. Am. Chem. Soc.* **1981**, *103*, 154.

(32)   Million-fold rate enhancements were observed using an enzyme-mimicking polymer catalyst: Skouta, R.; Wei, S.; Breslow, R. *J. Am. Chem. Soc.* **2009**, *131*, 15604.

(33)   Gottlieb, H.; Kotlyar, V.; Nudelman, A. *J. Org. Chem.* **1997**, *62*, 7512.

(34)   Alaimo, P.; Peters, D.; Arnold, J.; Bergman, R. *J. Chem. Educ.* **2001**, *78*, 64.

(35)   Paquette, L.; Morwick, T. *J. Am. Chem. Soc.* **1997**, *119*, 1230.

(36)   Struga, M.; Kossakowski, J.; Kedzierska, E.; Fidecka, S.; Stefanska, J. *Chem. Pharm. Bull.* **2007**, *55*, 796.

(37)   Shing, T. K. M.; Zhu, X. Y.; Yeung, Y. Y. *Chem. Eur. J.* **2003**, *9*, 5489.

(38)   Caulder, D.; Powers, R.; Parac, T.; Raymond, K. *Angew. Chem. Int. Ed.* **1998**, *37*, 1840.

Chapter 4
Kinetic Deprotonation of Carbocationic Intermediates in the Host-Catalyzed Nazarov
Cyclization.

Introduction

Acid-base reactions are among the fastest chemical reactions, and as such they are typically reversible and under thermodynamic control. However, under the appropriate conditions some deprotonation reactions form kinetically favored products instead of the most thermodynamically stable species. For example, treatment of an unsymmetrical ketone with a bulky base at low temperatures will deprotonate at the more sterically-accessible position instead of forming the thermodynamic product.[1] A sterically hindered base and low temperature are both necessary to ensure that the energetic difference between the two competing transition states is large enough for complete kinetic selectivity.

Some enzymes involved in terpene biosynthesis exert kinetic control over the deprotonation of allyl cation intermediates, determining which products are ultimately formed. For instance, the acid-catalyzed ionization of geraniol or geranyl pyrophosphate produces the gernanyl cation, which can be deprotonated at one of two positions to form either myrcene or β-ocimene (Figure 4.1 – deprotonation is in competition with trapping by water and various cyclization reactions). In the absence of enzyme, there is little selectivity for deprotonation of the geranyl cation at one position over the other, and similar quantities of myrcene and β-ocimene are formed.[2,3] Two enzymes isolated from the snapdragon flower (*Antirrhinum majus*) catalyze the dehydration of geranyl pyrophosphate, and each exhibits a very high degree of regioselectivity in producing either myrcene and (*E*)-β-ocimene.[4] Although mechanistic studies of these reactions were not conducted, enzymatic control over the site of deprotonation is necessary for the formation of a single product, regardless of the exact mechanism. The amino acid sequences of the two enzymes are 93% identical, yet this small structural difference is responsible for completely switching the regioselectivity of geranyl cation deprotonation. In contrast to the kinetic deprotonation of unsymmetrical ketones, which requires low temperatures to achieve selectivity, the enzyme-controlled deprotonation of the geranyl cation is highly selective at room temperature.
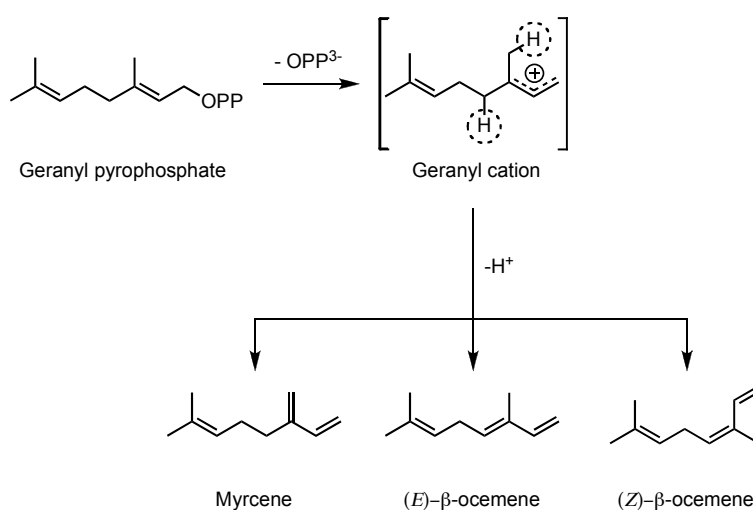

Figure 4.1. Possible products of geranyl cation deprotonation. Methyl deprotonation yields myrcene, while methylene deprotonation produces either stereoisomer of β-ocemene.

The high levels of selectivity achieved in enzymatic catalysis are the result of precise control over the substrate conformation and its interactions with catalytic functional groups or other reactants within the active site. Supramolecular encapsulation is similarly capable of enforcing a single conformation of a bound guest molecule and the orientation of two coencapsulated guests relative to one another.[5-13] This control over guest geometry can enhance the selectivity of reactions that proceed inside a molecular host by favoring specific reaction pathways. For instance, the cycloaddition of phenylacetylene with phenyl azide ordinarily produces a mixture of two regioisomers, but selectively forms the 1,5-substituted product when conducted inside a dimeric resorcinarene-derived capsule.[6] This regioselectivity is a direct consequence of the relative orientation of the two encapsulated reactants inside the oblong capsule, in which the phenyl groups of each guest are forced to orient in opposite directions. Similarly, the [2+2] photodimerization of several olefins produces just one regioisomer when two olefins are coencapsulated in a metal-ligand host, while two or more regioisomers are produced when the reactants are free in solution.[7]

This chapter describes the kinetically-controlled, regioselective deprotonation of encapsulated cyclopentenyl cation intermediates in the Nazarov cyclization of pentadienols catalyzed by a self-assembled host. The regiochemistry of the deprotonation step determines which one of two possible products is formed. Although this deprotonation step occurs at both possible positions outside the host interior, encapsulation in **1** renders the process >95% regioselective. Moreover, subtle differences in the stereochemistry of the encapsulated cyclopentenyl cation switch the product selectivity of this process. This reactivity shares several features with the regioselective, enzyme-controlled deprotonation of the geranyl cation involved in the biosynthesis of myrcene and β-ocimene.

Results and Discussion

Dihydrofulvene Formation. Chapter 3 describes the ability of the $[Ga_4L_6]^{12-}$ assembly (**1**, where L = *N,N'*-bis(2,3-dihydroxybenzoyl)-1,5-diaminonaphthalene) to catalyze the Nazarov cyclization of 1,3-pentadienols to form cyclopentadienes in aqueous solution (Figure 4.2).[14] In the initial experiments on the **1**-catalyzed Nazarov reaction of **2**, the identity of the product Cp*H (**3**) was confirmed by GC-MS analysis (Figure 4.2a). The quantitative formation of the Diels-Alder adduct of Cp*H with maleimide (**4**) was observed by ^{1}H-NMR analysis in each of the reactions studied for our rate and mechanism studies (Figure 4.2b). The **1**-catalyzed reaction of **2a** or **2b** in unbuffered D$_2$O at room temperature, however, led to the formation of the unexpected dihydrofulvene **5**, which is isomeric to Cp*H (Figure 4.3). The reaction of **2c** conducted under identical conditions yielded the expected product Cp*H. The isomeric relationship of **5** to Cp*H was verified by comparing the m/e and fragmentation patterns in the mass spectra of the two species, which are identical. The structural assignment of **5** was made on the basis of ^{1}H-NMR, ^{13}C-NMR, HSQC, and COSY analysis. Further confirmation was obtained by the independent synthesis of **5** and its diastereomer **6** (*vide infra*). Chiral gas chromatography of **5** allows for the resolution of the constituent enantiomers, which were present in the expected

12-

= Ga^{III}, **1**
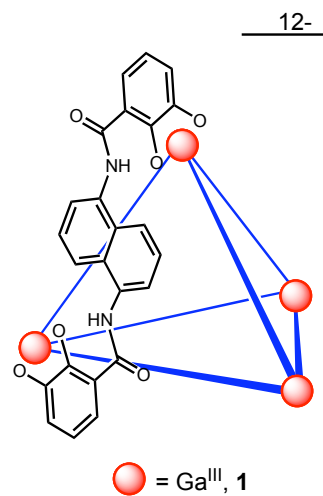
1:1 ratio. No data for either **5** or **6** have been reported in the literature, although a mixture of the two diastereomers was proposed as the minor product of a carbocation quenching reaction.[15]
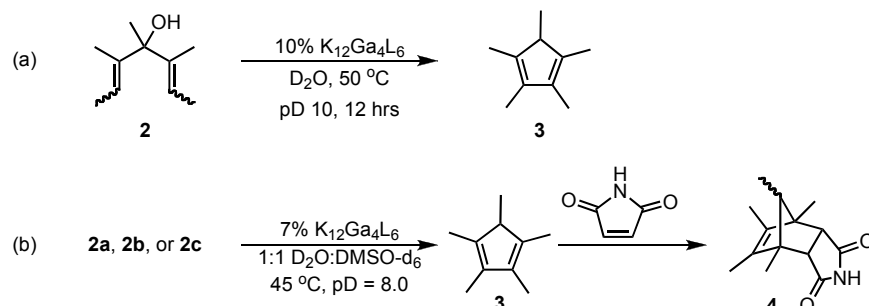

Figure 4.2. Products of the **1**-catalyzed Nazarov reaction under different conditions. (a) Prolonged heating in buffered D_2O (100 mM K_2CO_3, pD 11) yields Cp*H (**3**). (b) Mixed-solvent conditions lead to the Diels-Alder product of Cp*H.
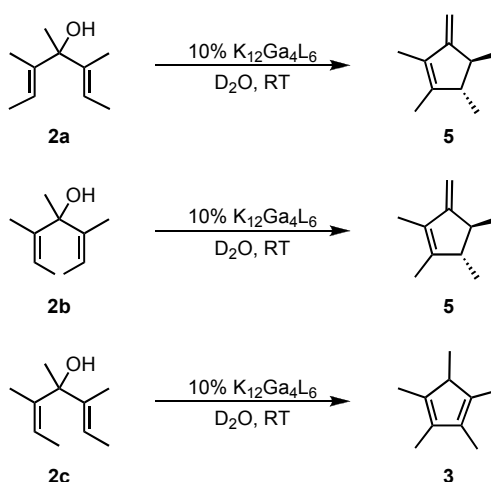

Figure 4.3. At room-temperature in unbuffered D_2O, the **1**-catalyzed Nazarov reaction of symmetrical substrates **2a** and **2b** produces **5**, while the reaction of **2c** forms Cp*H.

Mechanistic Rationale. The observation of **5** as a reaction product was initially puzzling, since it had not been detected when the reaction was conducted under other conditions. Kinetic analysis of the **1**-catalyzed reaction of **2a** or **2b** in 1:1 D_2O/DMSO-d_6 with added maleimide (which cannot react with **5**, due to the forced *trans* orientation of its diene fragment) displays clean conversion of reactant into **4** without the accumulation of significant quantities of any reaction intermediate (Figure 4.2b). It was considered that under the conditions of earlier mechanistic studies, **5** is initially produced from **2a** and **2b**, but is instantaneously converted into Cp*H and trapped by maleimide. It is also possible, although less likely, that **5** is not formed at all under those reaction conditions. With these possibilities in mind, the conversion of **5** to Cp*H was investigated. DFT calculations conducted using the B3LYP/6-31G level of theory predict that **5** is 3.87 kcal/mol higher in energy than Cp*H. This is expected, given the relative stability of tetrasubstituted alkenes compared to less substituted isomers. Addition of a

substoichiometric amount of TsOH immediately and quantitatively converted **5** to Cp*H. Next, the reactivity of **5** was evaluated under conditions similar to those used to measure kinetic data. Heating an 80 mM solution of **5** at 45 °C in 1:1 $D_2O/DMSO$-d_6 (aqueous portion buffered at pD 8.0 with 100 mM K_2HPO_4) in the absense of **1** for one hour caused quantitative conversion to Cp*H (Figure 4.4). This rate of reaction is sufficiently rapid that isomerization could occur without **5** being observed in the **1**-catalyzed conversion of **2** to **4**. Repeating the experiment under more basic conditions (aqueous portion buffered at pD 11.3 with 100 mM K_2CO_3) slowed the conversion of **5** to Cp*H, which is expected for this acid-catalyzed reaction. Interestingly, conversion was also slower when the aqueous portion was unbuffered, which suggests that increased ionic strength of the solvent also accelerates isomerization of **5**. A somewhat speculative explanation is that the carbocationic intermediates of the isomerization reaction are stabilized by increased ionic strength.
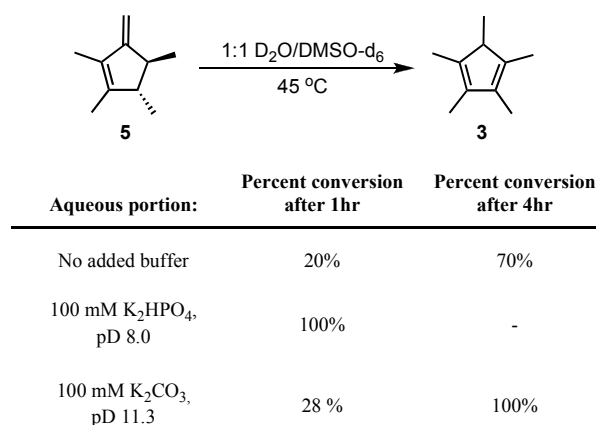

Aqueous portion:	Percent conversion after 1hr	Percent conversion after 4hr
No added buffer	20%	70%
100 mM K_2HPO_4, pD 8.0	100%	-
100 mM K_2CO_3, pD 11.3	28 %	100%

Figure 4.4. Experiments to determine the stability of **5** in 1:1 $D_2O/DMSO$-d_6 at 45 °C.

In considering the mechanism of the Nazarov cyclization (Figure 4.5a), the formation of **5** must occur via deprotonation of cyclopentenyl cation **9a**. While deprotonation at the cyclopentyl position generates the expected cyclopentadiene, deprotonation at the appropriate methyl group will place the double bond in the exocyclic position. A likely possibility was that the outcome of the **1**-catalyzed reactions of the three stereoisomers of **2** was dictated by the stereochemistry of the encapsulated cyclopentenyl cation intermediate (**9a** versus **9b**). The 4π electrocyclization of pentadienyl cations occurs in a conrotatory fashion,[16] so the alkene stereochemistry of the pentadienyl cations determines the stereochemistry of the resulting cyclopentenyl cation. Accordingly, the electrocyclization of pentadienyl cations **8a** and **8b** (derived from **2a** and **2b** respectively) yield cyclopentenyl cation **9a** with methyl groups in the *trans* orientation, while the E,Z pentadienyl cation **8c** (derived from **2c**) forms **9b** with methyl groups in *cis* orientation (Figure 4.5b).[15] This explanation is supported by the observation of **5** as the sole product of **1**-catalyzed dehydration of alcohol **10a** (Figure 4.6), whose methyl groups are set in the *trans* orientation. Like the Nazarov cyclization of **2a** and **2b**, **the** dehydration of **10a** proceeds through the intermediate cyclopentenyl cation **9a**.
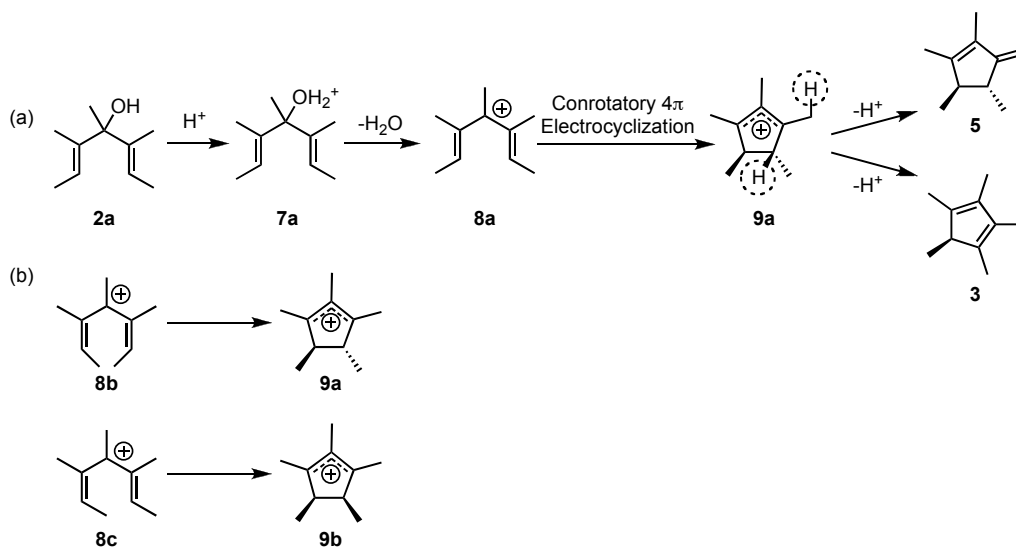
Figure 4.5. (a) Mechanism of the Nazarov cyclization, showing the mechanistic divergence that produces either **3** or **5**. (b) The stereochemistry of the cyclopentenyl cation is determined by the olefin geometry of the preceding pentadienyl cation.
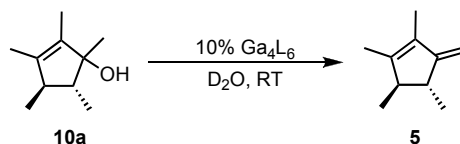

Figure 4.6. The **1**-catalyzed dehydration of cyclopentenyl alcohol **10a**.

We were intrigued by the possibility that encapsulation in **1** was responsible for the formation of either **5** or Cp*H, depending on the stereochemistry of the encapsulated cyclopentenyl cation (**9a ⊂ 1** or **9b ⊂ 1**, where ⊂ denotes encapsulation). To test this notion, it was necessary to evaluate the products of the deprotonation reaction of **9a** and **9b** in bulk solution, in case the formation of **5** from **9a** (or Cp*H from **9b**) is an intrinsic property of the molecule unaffected by encapsulation in **1**. Towards this end, the acid-catalyzed dehydration reactions of alcohols **10a** and **10b** were studied, which proceed through the cyclopentenyl cations of interest (Figure 4.7). The product distribution of these two dehydration reactions would indicate whether the regiochemistry of the deprotonation reaction in bulk solution is controlled by substrate stereochemistry. The desired cyclopentenyl alcohols were prepared by treating the corresponding enones (**11a** and **11b**) with methyllithium (Figure 4.8). The addition of methyllithium to **11b** produced a single diastereomer of the product, presumably delivering the nucleophile to the face of the ring opposite from the two other methyl groups. The formation of **10a** was not stereoselective, and a mixture of diastereomers was obtained. Ultimately, the stereochemistry of the alcohol is lost upon ionization of the alcohol, so the diastereoselectivity in forming these compounds is unimportant.
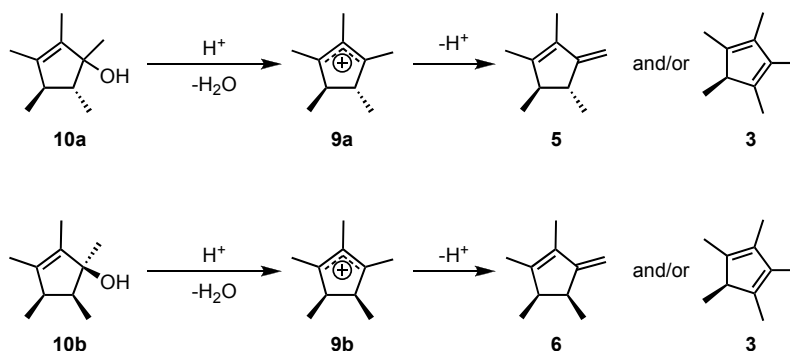
83

Figure 4.7. Dehydration of cyclopentenols **10a** and **10b**. The reaction can yield either Cp*H (**3**) or the dihydrofulvene isomer (**5** or **6**), depending on the deprotonation site on the intermediate cyclopentenyl cation (**9a** or **9b**).
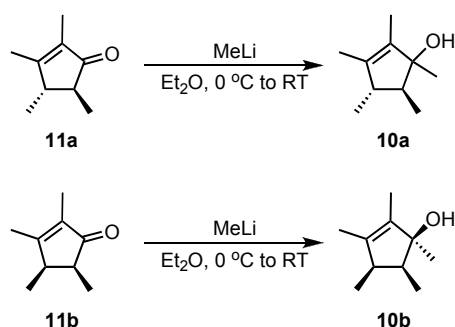

Figure 4.8. Synthesis of cyclopentenols **10a** and **10b**. Compound **10a** is formed as a mixture of diastereomers.

While acid catalysis was necessary for the dehydration reaction, it was crucial the acid catalyst not convert **5** (or **6**) to Cp*H. A survey of acid additives was undertaken, and benzoic acid was found to be optimal (Table 4.1), producing a 2:3 ratio of **5** to **3** in the dehydration of **10a**. The benzoic acid-catalyzed dehydration reaction was monitored by ^{1}H-NMR until the reactant was consumed, and only slight conversion of **5** to Cp*H was observed over the course of the reaction. Thus, the product ratio of this reaction reflects the kinetic selectivity for deprotonating the cyclopentenyl carbocation intermediate **9a**. The dehydration of **10b** was conducted under these conditions, which yielded a ~1:3 ratio of **6** to **3** (Figure 4.9). These data indicate that there is no significant kinetic preference for deprotonation at either of the two positions of cyclopentenyl cations **9a** and **9b** in free solution.

Table 4.1. Survey of acid catalysts for the dehydration of **10a**.
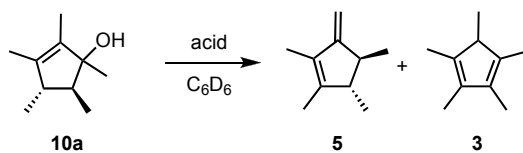
Entry	Acid	Reaction time	Result
1	Alumina	24 hours	No Reaction
2	Silica	< 5 minutes	100% Conversion to **3**
3	TsOH	< 5 minutes	100% Conversion to **3**
4	NH₄Cl	24 hours	No Reaction
5	NH₂Cl (piperidinium)	24 hours	No Reaction
6	acetic acid	24 hours	Low conversion, ~1:1 mixture of **5** to **3**
7	Ph CO₂H	24 hours	Complete conversion, 2:3 mixture of **5** and **3**
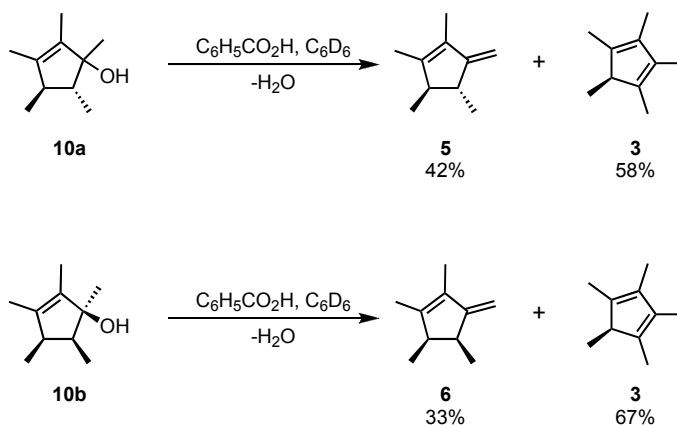
Figure 4.9. The acid-catalyzed dehydration reactions of cyclopentenyl alcohols **10a** and **10b**, which each produce roughly equal amounts of **3** and the corresponding dihydrofulvene isomer.

Based on the unencapsulated reactivity of cyclopentenyl cations **9a** and **9b**, it is concluded that encapsulation of these cations in **1** is directing the regiochemistry of deprotonation, producing Cp*H (**3**) from **9b** ⊂ **1**, and **5** from **9a** ⊂ **1** (Figure 4.10). Although we were unable to structural data of the short-lived host-guest complexes **9b** ⊂ **1** and **9a** ⊂ **1**, the most likely explanation is that the specific orientation of the carbocation within the cavity of **1** diminishes the accessibility of one proton, forcing deprotonation to occur at the other position exclusively. Changing from **9a** to **9b** could require a different orientation within **1**, switching the accessibility of the two possible deprotonation sites. Given the subtle structural difference

between **9a** and **9b**, this encapsulation-mediated inversion of regioselectivity is remarkable. This example of kinetically controlled deprotonation in supramolecular catalysis is strikingly similar to the enzymatic control of regiochemistry in deprotonating the geranyl cation in the biosynthesis of myrcene and ocimene (Figure 4.1). In both cases, deprotonation of an allyl carbocation can occur at multiple positions to form diene products, and minor structural changes are responsible for complete inversion of regioselectivity at room temperature. In fact, the cyclopentenyl cations from this study are constitutional isomers of the geranyl cation, and the products **3** and **5** are constitutional isomers of myrcene and ocimene. These similarities raise the possibility that **1** could act as a mimic for some of the cyclization reactions involved in terpene biosynthesis.
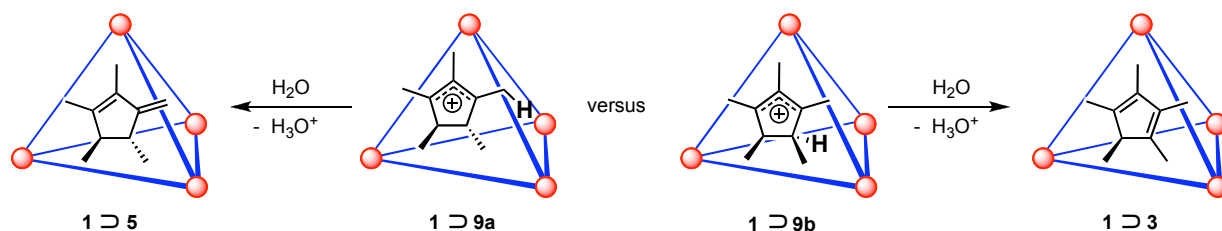
Figure 4.10. The stereochemistry of the encapsulated cyclopentenyl cation (**9a** versus **9b**) determines the site of deprotonation, and the regiochemistry of the diene product (**3** versus **5**).

Conclusion

The first example of selective, kinetic deprotonation mediated by supramolecular encapsulation has been demonstrated in the **1**-catalyzed Nazarov reaction of 1,4-pentadien-3-ols. The regiochemistry of deprotonation in the host-catalyzed reaction is determined by the stereochemistry of an intermediate cyclopentenyl cation, the structure of which is determined by the alkene stereochemistry of the reactant. Changing the relative stereochemistry of two methyl groups in the encapsulated carbocationic intermediate from *trans* (**9a**) to *cis* (**9b**) completely switches the regioselectivity of deprotonation, forming the corresponding diene regioisomer with greater than 95:5 selectivity. In contrast to their host-mediated reactivity, the deprotonation reactions of these carbocations in free solution were not selective at all, leading to a mixture of regioisomers in both cases. We propose that supramolecular encapsulation within **1** forces deprotonation to occur at a single position, which is similar to the regioselectivity in enzyme-mediated deprotonations involved in terpene biosynthesis.

Experimental Section

General Experimental Procedures. Unless otherwise noted, reactions and manipulations were performed using standard Schlenk and high-vacuum techniques at room temperature. All glassware was dried in an oven at 150 °C for at least 12 h or flame-dried under vacuum prior to use.

**Instrumentation**. NMR spectra were obtained on Bruker Avance AV 500 (500 MHz) or AV 600 (600 MHz) spectrometers at the frequencies indicated. Chemical shifts are reported as δ in parts per million (ppm) relative to residual protiated solvent resonances.[17] NMR data are reported in the following format: s = singlet, d = doublet, t = triplet, q = quartet, m = multiplet, b = broad; coupling constant; integration. Mass spectral data were obtained at the QB3 Mass Spectrometry Facility operated by the College of Chemistry, University of California, Berkeley. Fast atom bombardment (FAB) mass spectra were recorded on a Micromass ZAB2-EQ magnetic sector instrument. Electron impact (EI) mass spectra were recorded on a Micromass ProSpec magnetic sector instrument equipped with an EI source.

Materials. Unless otherwise noted, reagents were obtained from commercial suppliers and used without further purification. Ethyl ether (Et_2O), tetrahydrofuran (THF), and pentane were dried by passing through columns of activated alumina under nitrogen pressure and were sparged with nitrogen before use. The two stereoisomers of 2,3,4,5-tetramethyl-2-cyclopentenone were separated by preparative gas chromatography (Varian Aerograph 970, using a 0.38" x 10' column packed 10% Carbowax chemically bonded to Chromsorb stationary phase). The helium flow rate was 60 mL/min, the column temperature was 120 °C, the injector temperature was 100 °C, and the detector temperature was 210 °C. Prior to injection, the crude mixture was passed through a plug of silica gel. The retention times of the *trans* and *cis* isomers are 3.5 and 7.0 minutes, respectively, which are consistent with literature data on the separation of these compounds by preparative gas chromatography.[15] ^{1}H-NMR spectra of the separated isomers are consistent with data reported in the literature. $K_{12}Ga_4L_6$ (K_{12}**1**)[18] was prepared according to literature procedure.

11a   **11a**   **11b**
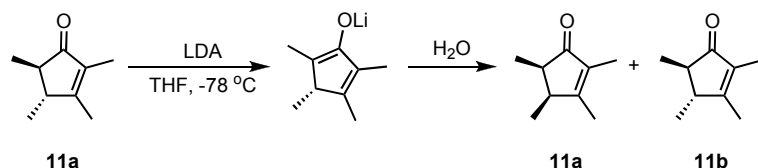
Cis and trans–2,3,4,5-tetramethyl-2-cyclopentenone (11a and 11b). Although this mixture can be obtained commercially, material purchased from Alfa-Aesar (described as a technical mixture of the two diastereomers) was >95% pure **11a** by ^{1}H-NMR analysis, so this step was necessary to generate significant quantities of **11b** for separation by preparative gas chromatography: To a flame-dried 250mL round-bottom flask under positive N_2 pressure was added 80 mL anhydrous THF and a magnetic stir bar, and the reaction vessel was cooled to -78 °C. *n*-Butyllithium (23 mL, 2.5 mM in pentane, 58 mmol) was added via syringe, and then 8.2 mL diisopropylamine (58 mmol) was added dropwise via syringe. The reaction mixture was allowed to stir for one hour, after which 8.0 mL **11a** (53 mmol) was added dropwise via syringe

over 15 minutes. The reaction mixture was allowed to warm to room temperature for one hour, and was then quenched by addition to water at 60 °C. This mixture was extracted three times with Et$_2$O, and the combined organic layers were washed once with saturated sodium bicarbonate, twice with brine, and dried over MgSO$_4$. Solvent was removed by rotary evaporation to give 7.2 g (52 mmol) of the title mixture (98% recovery), which was found to be 25% **11b** by ^{1}H-NMR analysis. The two stereoisomers were separated by preparative gas chromatography as described above, affording each stereoisomer in >98% purity.
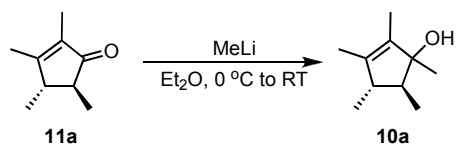
**(*trans*)-1,2,3,4,5-pentamethyl-2-cyclopentenol (10a).** A flame-dried 100mL round-bottom flask was charged with 30mL dry Et$_2$O, a magnetic stir bar and 11.4 mL methyllithium (1.4 M in Et$_2$O, 16.0 mmol). The solution was cooled to -78 °C and **11a** (2.0 mL, 13.3 mmol) was added dropwise as a solution in 10 mL Et$_2$O over 10 minutes. The reaction mixture was stirred at -78 °C for one hour, and was then allowed to warm to room temperature. After being stirred for an additional two hours at room temperature, the reaction mixture was quenched by pouring into a saturated solution of ice-cold sodium bicarbonate, which was then extracted three times with Et$_2$O. The combined organic extracts were washed three times with brine and solvent removed by rotary evaporation to give the title compound as a 3:2 mixture of diastereomers. **^{1}H NMR** (600 MHz, C$_6$D$_6$): δ 2.05 (m, 1H, major), 1.75 (m, 1H, minor), 1.61 (s, 3H, minor), 1.59 (s, 3H, major), 1.47 (s, 3H, major), 1.46 (s, 3H, minor), 1.27 (m, 1H, major), 1.19 (s, 3H, major), 1.09 (m, 1H, minor), 1.05 (d, ^{3}j = 7.0 Hz, 3H, major), 1.02 (d, ^{3}j = 7.0 Hz, 3H, minor), 0.99 (s, 3H, minor), 0.97 (d, ^{3}j = 6.8 Hz, 3H, minor), 0.92 (d, ^{3}j = 7.0 Hz, 3H, major) ppm. **^{13}C{^{1}H} NMR** (150.9 MHz, C$_6$D$_6$): δ 137.5, 137.2, 135.8, 133.6, 83.3, 82.2, 53.5, 50.9, 47.3, 46.6, 24.8, 19.4, 16.9, 16.8, 11.8, 11.6, 11.5 (two partially-resolved peaks), 9.2, 8.9 ppm. **HRMS (FAB)**: Exact mass calcd for C$_{10}$H$_{17}$O [M-H]$^+$: 153.1279 found 153.1277.
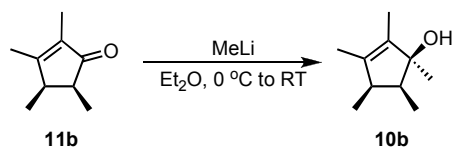
(*cis*)-1,2,3,4,5-pentamethyl-2-cyclopentenol (10b). The title compound was prepared by following the procedure used for **10a**, using 319 mg **11b** (2.3 mmol), 2.0 mL MeLi (1.4 M in Et$_2$O, 2.8 mmol), and 30 mL Et$_2$O. The title compound was obtained as a yellow liquid in 92% yield (346 mg). This material was contaminated with 5% of the minor diastereomer. **^{1}H NMR** (600 MHz, C$_6$D$_6$): δ 2.18 (m, 1H, ^{3}j = 7.4 Hz), 1.85 (m, 1H, ^{3}j = 7.4 Hz), 1.57 (s, 3H), 1.49 (s, 3H), 1.16 (s, 3H), 0.97 (d, 3H, ^{3}j = 7.4 Hz), 0.88 (d, 3H, ^{3}j = 7.3 Hz) ppm. **^{13}C{^{1}H} NMR** (150.9 MHz, C$_6$D$_6$): δ 139.5, 136.1, 84.0, 66.2, 45.7, 45.1 16.0, 13.0, 9.8, 9.7 ppm. **HRMS (FAB)**: Exact mass calcd for C$_{10}$H$_{17}$O [M-H]$^+$: 153.1279 found 153.1275.
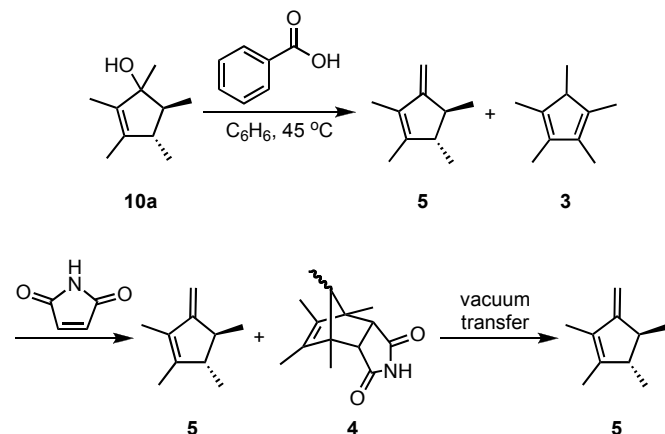
(*trans*)-1,2,3,4-tetramethyl-5-methylenecyclopentene (5). A 100mL round-bottom flask was charged with 50 mL benzene, a magnetic stir bar, 1.00 g **10a** (6.48 mmol), and 0.792 mg benzoic acid (6.48 mmol). The solution was stirred until all reagents were dissolved, and the flask was outfitted with a rubber stopper and oil bubbler outlet. The reaction mixture was heated at 45 °C for 14 hours, at which point the reaction was judged to be complete by GC-MS analysis. The reaction mixture was washed three times with saturated Na_2CO_3, dried over $MgSO_4$, and added to 1.26 g maleimide (12.96 mmol). The maleimide was dissolved and the reaction mixture stirred for ten minutes. The volatile portion was vacuum transferred to yield a solution of **5** in benzene. It was important during the vacuum transfer that the solution was frozen in a dry-ice/acetone bath instead of in liquid nitrogen to ensure that the solution would thaw in a reasonable period of time. The solvent was removed very carefully by rotary evaporation to yield the title compound as a clear, colorless liquid. The overall process yielded 5.0 mg (0.067 mmol, <1% yield from **10b**) of material. The isolated yield was low because the majority of the material was lost during the vacuum transfer and the removal of solvent. **^{1}H NMR** (600 MHz, C_6D_6): δ 4.87 (s, 1H), 4.76 (s, 1H), 2.21 (m, 3H, ^2j = 3.1 Hz), 2.00 (br, 3H), 1.64 (s, 3H), 1.54 (s, 3H), 1.14 (d, 3H, ^3j = 6.6 Hz), 0.92 (d, 3H, ^3j = 6.6 Hz) ppm. **^{13}C{^{1}H} NMR** (125.8 MHz, C_6D_6): δ 161.4, 145.7, 132.6, 98.2, 51.0, 45.5, 20.1, 19.0, 13.1, 10.6 ppm. **HRMS (EI)**: Exact mass calcd for $C_{10}H_{16}$ [M]$^+$: 136.1252 found 136.1253. The structural assignment of this compound is consistent with ^{1}H-^{13}C{^{1}H} HSQC (heteronuclear single quantum coherence) and ^{1}H-^{1}H COSY (correlational spectroscopy) NMR analysis (Figure 4.11 and 4.12).
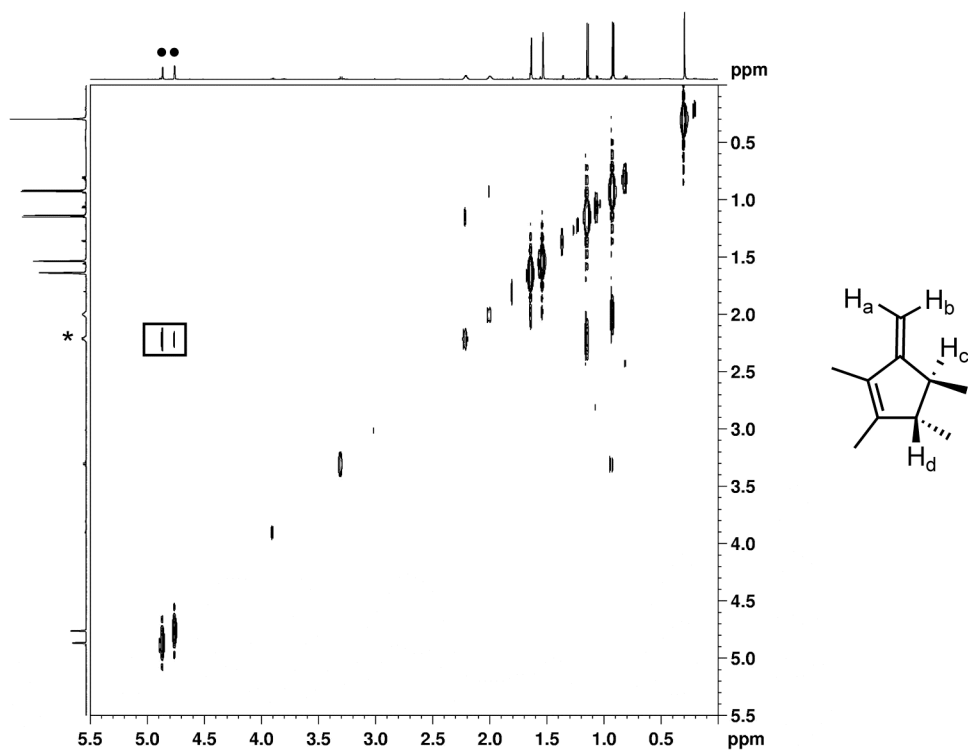
Figure 4.11. ^{1}H-^{1}H COSY NMR of **5**. Cross peaks between vinyl protons H$_a$ and H$_b$ (●) and H$_c$ (*) but not H$_d$ are consistent with the structural assignment.
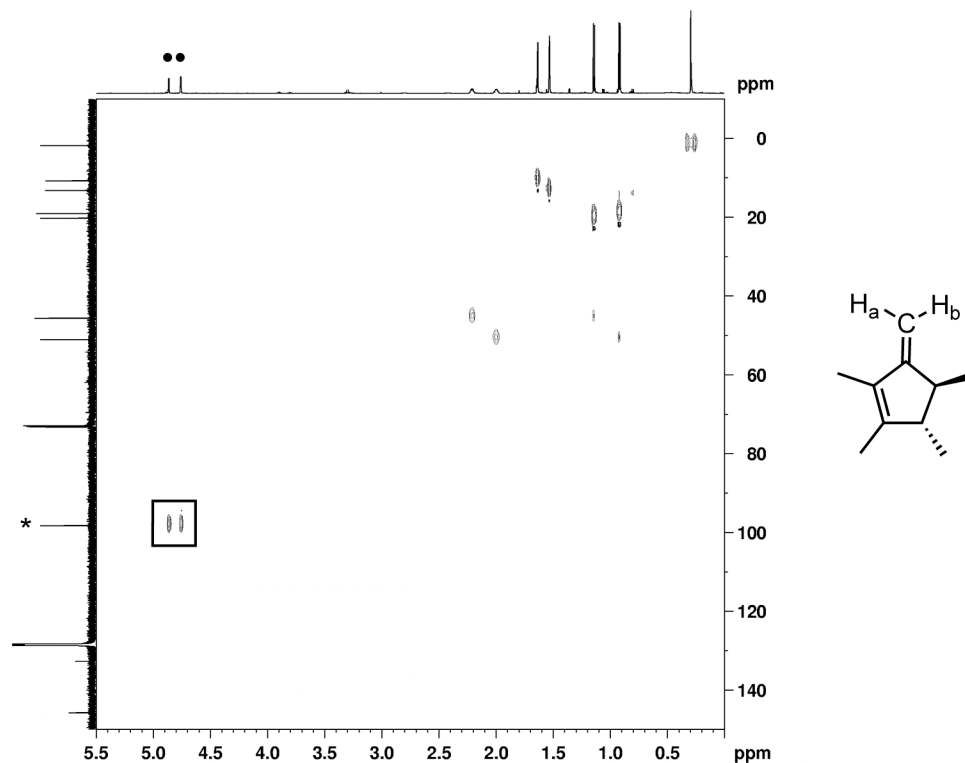
Figure 4.12. ^1H-$^{13}C\{^1H\}$ HSQC NMR spectrum of **5**. Cross peaks between an sp^2-hybridized carbon (*) and vinyl protons H$_a$ and H$_b$ (●) confirm the presence of a terminal alkene.
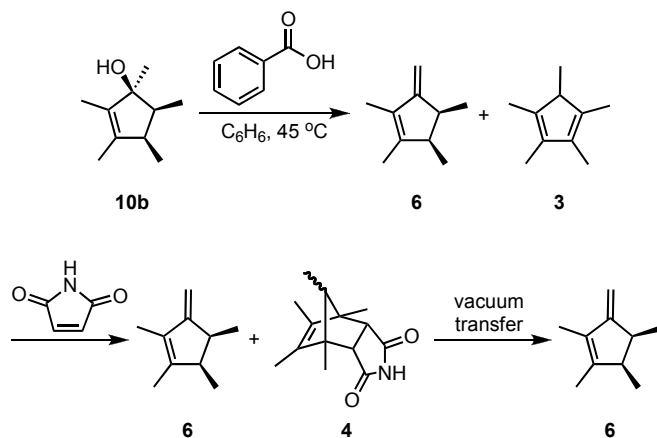
(***cis***)-**1,2,3,4-tetramethyl-5-methylenecyclopentene (6).** The procedure for preparing **5** was followed using 5 mL C$_6$D$_6$, 50 mg **10b** (0.32 mmol), 39 mg benzoic acid (0.32 mmol), and 45 mg maleimide (0.48 mmol). The solution obtained directly after the vacuum transfer step was used for NMR characterization of the title compound. ^{1}**H NMR** (600 MHz, C$_6$D$_6$): δ 4.98 (s, 1H), 4.85 (s, 1H), 2.90 (m, 3H, ^{3}j = 7.3 Hz), 2.52 (m, 3H, ^{3}j = 7.1 Hz), 1.74 (s, 3H), 1.66 (s, 3H), 1.19 (d, 3H, ^{3}j = 7.0 Hz), 0.91 (d, 3H, ^{3}j = 7.1 Hz) ppm. ^{13}**C{^{1}H} NMR** (125.8 MHz, C$_6$D$_6$): δ 161.4, 145.7, 132.6, 98.2, 51.0, 45.5, 20.1, 19.0, 13.1, 10.6 ppm. The structural assignment of this compound is consistent with HSQC NMR analysis (Figure 4.13).

91
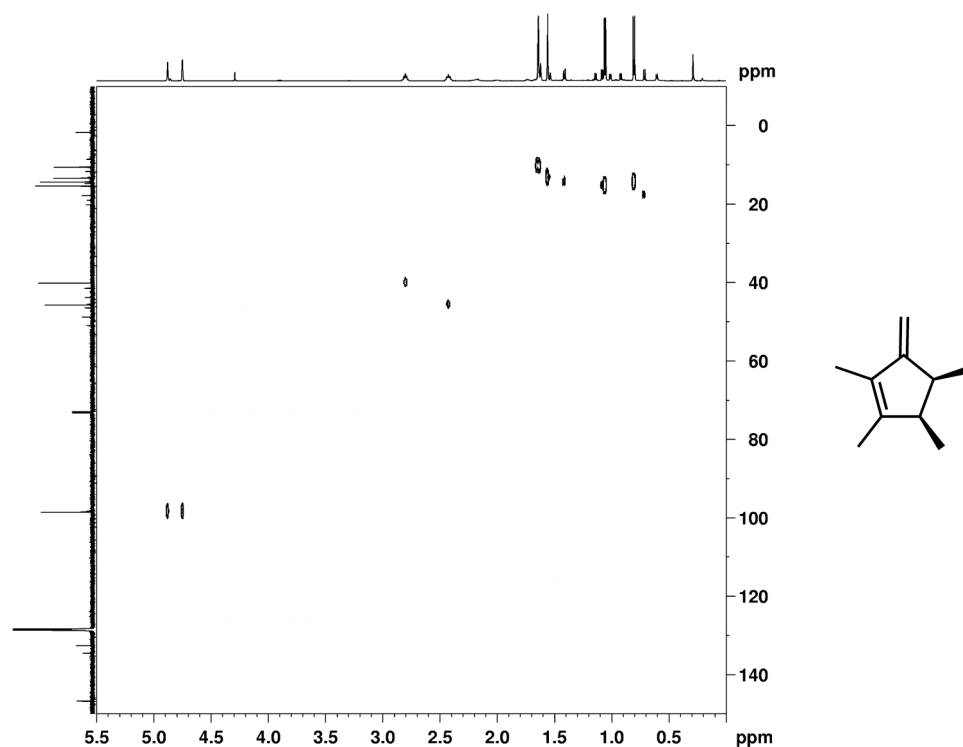
Figure 4.13. ^{1}H-^{13}C{^{1}H} HSQC NMR spectrum of **6**. The cross peaks in this spectrum are directly analogous to those observed in the HSQC spectrum of **5**.

General Procedure for the Acid-catalyzed Dehydration of 10a and 10b. A stock solution of 100 mg **10a** (0.65 mmol) in 6 mL C$_6$D$_6$ was prepared. NMR samples were prepared using 0.6 mL (0.065 mmol **10a**) of this stock solution, and ^{1}H-NMR spectra were obtained before and after exposure to the acid source. For soluble acids, the acid was added to the NMR tube and inverted five times to ensure mixing. For solid acids, such as silica gel and alumina, the sample was filtered through a plug (~25 mg) of the solid and transferred back into the NMR tube. If there was any **10a** remaining after the addition of acid, it was heated at 45 °C and monitored until no starting material remained. The procedure for the monitoring benzoic acid-catalyzed dehydration of **10b** was similar: 10 mg **10b** (0.065 mmol) and 8.0 mg benzoic acid (0.065 mmol) were dissolved in 0.6 mL C$_6$D$_6$, the reaction mixture was transferred into an NMR tube, and then heated at 45 °C until no starting material remained (approximately 12 hours). The relative quantities of **5** and **6** were determined from ^{1}H-NMR analysis, and are reported as the average of three experiments.

General Procedure for the 1-catalyzed Reactions of 2a, 2b and 2c. The following representative procedure for the **1**-catalyzed reaction of **2a** was also followed for the **1**-catalyzed reaction of **2b** and **2c**: 15 mg K$_{12}$**1** (0.0039 mmol) was dissolved in 0.6 mL D$_2$O, to which 1.8 mg **2a** (0.012 mmol) was added. The solution was mixed by pipette, and allowed to stand at room temperature for 3 hours. The reaction mixture was diluted with 3 mL brine and extracted three

92

times with CH_2Cl_2. The combined organic layers were dried over $MgSO_4$ and analyzed by ^{1}H-NMR. For the reaction of **2a** and **2b**, the ratio of **5** to **3** is greater than 95:5, and for **2c** the ratio of **3** to **5** is greater than 95:5.

References:

(1)   d'Angelo, J. *Tetrahedron* **1976**, *32*, 2979.

(2)   Bunton, C.; Cori, O.; Hachey, D.; Leresche, J. *J. Org. Chem* **1979**.

(3)   Cramer, F.; Rittersdorf, W. *Tetrahedron* **1967**, *23*, 3015.

(4)   Dudareva, N.; Martin, D.; Kish, C. M.; Kolosova, N.; Gorenstein, N.; Fäldt, J.; Miller, B.; Bohlmann, J. *Plant Cell* **2003**, *15*, 1227.

(5)   Mock, W. L.; Irra, T. A.; Wepsiec, J. P.; Adhya, M. *J. Org. Chem* **1989**, *54*, 5302.

(6)   Chen, J.; Rebek, J. *Org. Lett.* **2002**, *4*, 327.

(7)   Yoshizawa, M.; Takeyama, Y.; Kusukawa, T.; Fujita, M. *Angew. Chem. Int. Ed.* **2002**, *41*, 1347.

(8)   Yoshizawa, M.; Tamura, M.; Fujita, M. *Science* **2006**, *312*, 251.

(9)   Furusawa, T.; Kawano, M.; Fujita, M. *Angew. Chem. Int. Ed.* **2007**, *46*, 5717.

(10)   Nishioka, Y.; Yamaguchi, T.; Kawano, M.; Fujita, M. *J. Am. Chem. Soc.* **2008**, *130*, 8160.

(11)   Shenoy, S. R.; Pinacho Crisóstomo, F. R.; Iwasawa, T.; Rebek, J. Jr. *J. Am. Chem. Soc.* **2008**, *130*, 5658.

(12)   Yamaguchi, T.; Fujita, M. *Angew. Chem. Int. Ed.* **2008**, *47*, 2067.

(13)   Pinacho Crisóstomo, F. R.; Lledó, A.; Shenoy, S. R.; Iwasawa, T.; Rebek, J. Jr. *J. Am. Chem. Soc.* **2009**, *131*, 7402.

(14)   Hastings, C. J.; Pluth, M. D.; Bergman, R. G.; Raymond, K. N. *J. Am. Chem. Soc.* **2010**, *132*, 6938.

(15)   Campbell, P. H.; Chiu, N. W. K.; Deugau, K.; Miller, I. J.; Sorensen, T. S. *J. Am. Chem. Soc.* **1969**, *91*, 6404.

(16)   Woodward, R. B.; Hoffmann, R. *J. Am. Chem. Soc.* **1965**, *87*, 395.

(17)   Gottlieb, H.; Kotlyar, V.; Nudelman, A. *J. Org. Chem.* **1997**, *62*, 7512.

(18)   Caulder, D.; Powers, R.; Parac, T.; Raymond, K. *Angew. Chem. Int. Ed.* **1998**, *37*, 1840.

Chapter 5
Mechanistic Studies of the Host-Catalyzed Nazarov Cyclization

Introduction

Chapter 3 describes reactivity and kinetic studies of the Nazarov cyclization of 1,4-pentadien-3-ols (Figure 5.1a-b), a reaction that is catalyzed by supramolecular encapsulation within the self-assembled $[Ga_4L_6]^{12-}$ host **1** (where L = *N,N'*-bis(2,3-dihydroxybenzoyl)-1,5-diaminonaphthalene).[1] The reaction proceeds in aqueous or mixed water-DMSO solution at near-neutral pH and mild temperature. The reaction product, Cp*H, is a suitable guest for **1**, and causes product inhibition when the catalyzed reaction is carried out in mixed water-DMSO solution. Addition of maleimide to the reaction mixture traps Cp*H as the corresponding Diels-Alder adduct **5**, whose binding constant in **1** is low enough that it does not bind competitively with substrate (Figure 5.1c). The rate of the catalyzed reaction is up to 2,100,000 times larger than that of the uncatalyzed reaction, representing the largest reported rate acceleration for a reaction catalyzed by supramolecular encapsulation (Table 5.1). The unexpected formation of dihydrofulvene **6** in the **1**-catalyzed Nazarov cyclization of symmetrical substrates **2a** and **2b** is presented in Chapter 4 (Figure 5.1d). The formation of **6** instead of its expected regioisomer **3** is the result of a kinetically controlled, regioselective deprotonation of an intermediate cyclopentenyl carbocation. The regioselectivity of this deprotonation step is determined by encapsulation within **1**; no regioselectivity is observed when the reaction is conducted in free solution. This chapter presents mechanistic studies of the processes described in the two preceding chapters. A combined experimental and computational approach is used to elucidate the reaction mechanism of both the catalyzed and the uncatalyzed reaction. Additionally, quantifying the energetics of both reactions provides insight into the dramatic rate acceleration of the **1**-catalyzed reaction over the uncatalyzed reaction.
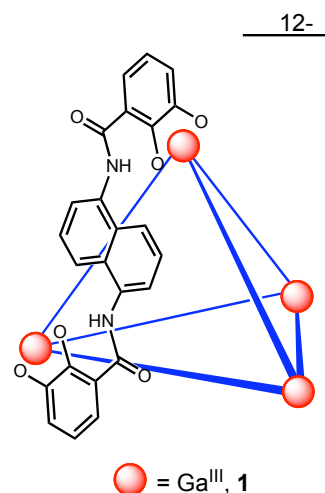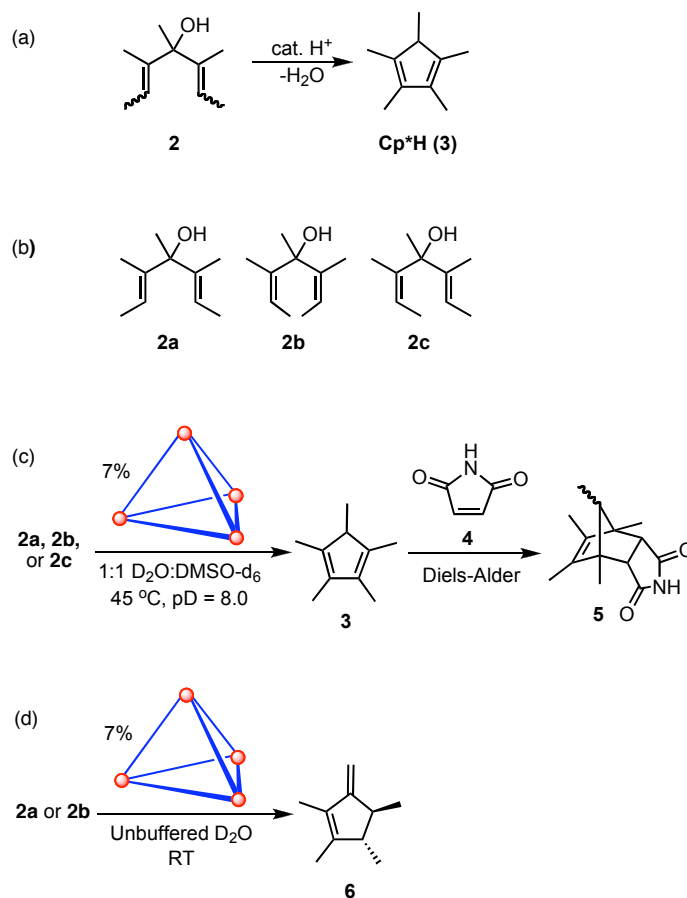
Figure 5.1. (a) General Scheme for the Nazarov cyclization of pentadienols to form cyclopentadienes. (b) Pentadienol stereoisomers used in this study. (c) **1**-Catalyzed Nazarov cyclization with maleimide (**8**) added to convert Cp*H (**3**) to weakly-binding Diels-Alder adduct **9**, alleviating product inhibition. (d) Formation of unexpected dihydrofulvene isomer **6** from the **1**-catalyzed reaction of symmetrical substrates **2a** or **2b**.

substrate	k_{cat} (s^{-1})	k_{uncat} (s^{-1})	rate acceleration (k_{cat}/k_{uncat})
2a	(2.9(4) x 10^{-2})	4.0(3) x 10^{-8}	(730,000)
2b	1.6(1) x 10^{-2}	7.7(8) x 10^{-9}	2,100,000
2c	5.7(1) x 10^{-2}	3.3(1) x 10^{-8}	1,700,000

Table 5.1. Kinetic data for Nazarov substrates at 45 °C in 1:1 D$_2$O/DMSO-d_6. The k_{cat} and rate acceleration values for substrate **2a** (in parentheses) were estimated from competitive binding experiments with **2c** in D$_2$O.

Results and Discussion

       Kinetic Studies of the 1-Catalyzed Reaction. In order to probe the origin of the rate enhancement of the **1**-catalyzed Nazarov cyclization, mechanistic analysis of both the **1**-

catalyzed and the uncatalyzed reaction were conducted, focusing on whether the transition state of the rate-determining step is stabilized by the constrictive interior of **1**. Mechanistic studies were conducted using **2b** as a substrate. Pseudo-first-order consumption of starting material was observed under **1**-catalyzed conditions (Figure 5.2). Variable-concentration kinetic studies of the catalytic reaction revealed a first-order dependence on [**1**] (Figures 5.3) and an apparent order of 0.5 on [D$^+$] (Figure 5.4). The catalyst resting state was determined to be the encapsulated, neutral substrate **2b** $\subset$ **1** (where $\subset$ denotes encapsulation) by ^{13}C-NMR analysis, and the self-exchange rate k_{exch} of **2b** in **1** is 2.4 s^{-1}, which is fast relative to the overall rate of the **1**-catalyzed reaction.[1] Kinetic studies of the uncatalyzed reaction of substrate **2b** were also conducted; these display first-order dependence on both substrate concentration and [D$^+$] (Figure 5.5). Additional data are provided by the reactivity of the substrate **2-CF$_3$**, which is similar in size to **2b**, but much less basic than **2b** owing to the electron-withdrawing trifluoromethyl substituent.[2-4] No reaction occurred when the **1**-catalyzed Nazarov cyclization of **2-CF$_3$** was attempted, although the expected host-guest complex **2-CF$_3$** $\subset$ **1** was immediately formed (Figure 5.6). Taken together, these data implicate a mechanism that involves rapid, reversible binding of substrate, followed by protonation of the bound guest. When the protonation step is made inaccessible by using the less basic substrate **2-CF$_3$**, no reaction occurs.
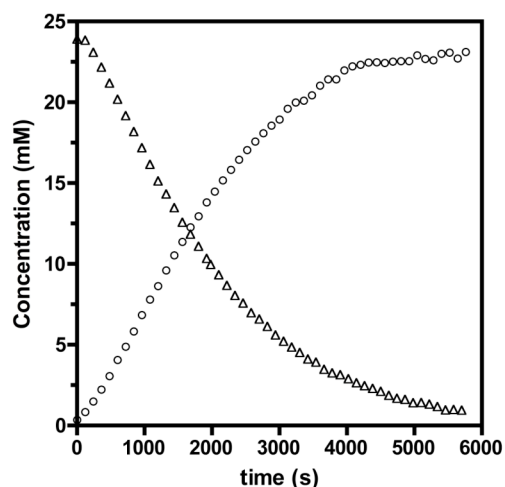
Figure 5.2. Concentration vs. time plot of the reaction of substrate **2b** ($\triangle$) to form **9** ($\bigcirc$), catalyzed by 1.5 mM **1** at 45 °C with added maleimide. Pseudo-first-order dependence on [**2b**] is observed.
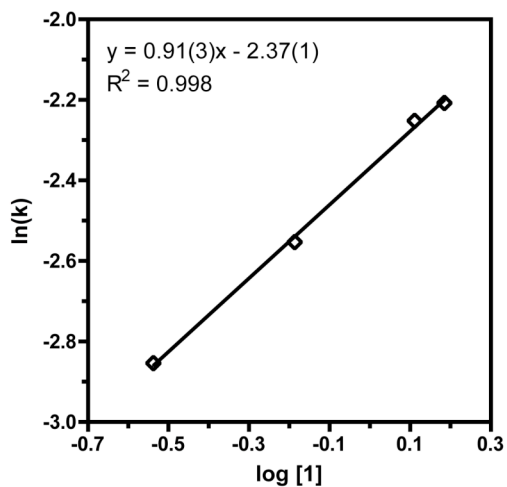
Figure 5.3. Rate dependence on [**1**] for the **1**-catalyzed Nazarov cyclization of **2b** in 1:1 D_2O/DMSO-d_6 at 45 °C.
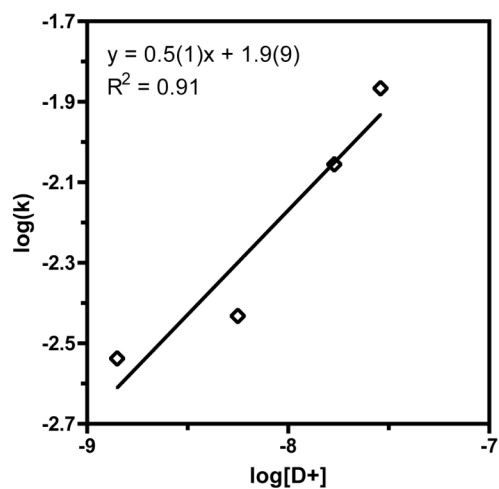
Figure 5.4. Rate dependence on [D^+] for the **1**-catalyzed Nazarov cyclization of **2b** in 1:1 D_2O/DMSO-d_6 at 45 °C.
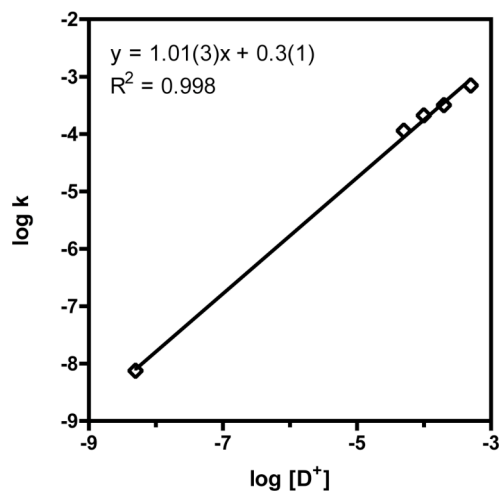
Figure 5.5. Rate dependence on $[H^+]$ for the uncatalyzed Nazarov cyclization of **2b** in 1:1 D_2O/DMSO-d_6 at 45 °C.
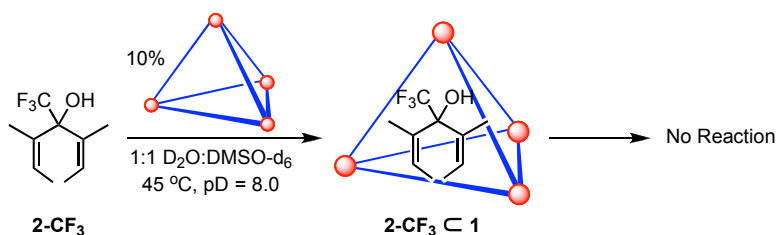
Figure 5.6. Attempted **1**-catalyzed Nazarov cyclization of substrate **2-CF$_3$**. Host-guest complex **2-CF$_3$ ⊂ 1** is observed, but no further reaction occurs.

Further studies of both the **1**-catalyzed and the uncatalyzed reaction were necessary, since these experiments do not provide any information about the reaction mechanism beyond the protonation steps, nor do they suggest which step is rate-determining. Earlier studies of the Nazarov cyclization conducted in superacidic media implicate a mechanism in which protonation and water loss is followed by rate-determining electrocyclization of a dienyl cation.[5,6] Upon quenching, the resulting cyclized allyl cation is deprotonated to give the product cyclopentadiene (Figure 5.7a). The relative rates of these steps are certainly different under the superacid conditions than they are in aqueous solution (**1**-catalyzed or acid-catalyzed); for example **8a** and **9a** are observed by NMR in superacid solution, but not in 1:1 D_2O/DMSO-d_6 at pD 8.0. Furthermore, it is possible that loss of water and electrocyclization occur in a concerted fashion under reaction conditions where proton concentration is extremely low (Figure 5.7b). While there is no direct precedent for this mode of reactivity, the concerted solvolysis and electrocyclic ring-opening of cyclopropyl tosylates is known.[7,8]
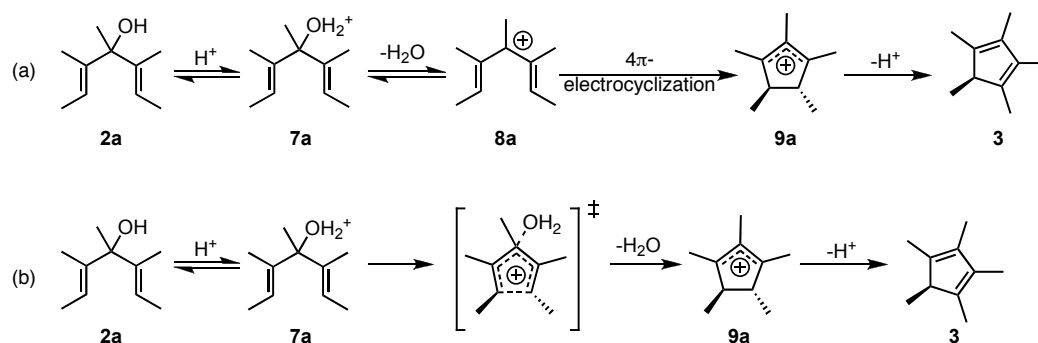
Figure 5.7. Possible mechanisms for the Nazarov cyclization. (a) Proposed mechanism in superacidic solution from reference 5. (b) Possible mechanism involving concerted water loss and electrocyclization.

Computational Studies of the Reaction Mechanism. Studies were conducted to explore the possibility that water loss occurs prior to electrocyclization (Figure 5.7a), or whether the two steps proceed in a concerted fashion from the protonated alcohol (Figure 5.7b). Initial studies were aimed at evaluating the two possible reaction pathways using density functional theory (DFT) calculations. In all attempts to optimize the structure of protonated substrate **7a** or **7b**, irreversible loss of water occured, forming the corresponding pentadienyl cation (**8a** or **8b**, respectively) as the minimized structure. This suggests that the kinetic barrier for water loss is very low, and provides some evidence against the concerted mechanism depicted in Figure 5.7b. While the water loss step may be nearly barrierless, it is likely that the reverse reaction also has a low barrier and that **7a** and **8a** are in equilibrium (Figure 5.8). This equilibrium in aqueous solvent cannot be modelled accurately by a gas-phase calculation. Although it was not possible to obtain quantitative information about water loss from the protonated substrate, the energetics of the electrocyclization step were calculated for **8a** and **8b** (Figure 5.9), which are derived from **2a** and **2b**, respecetively. The electrocyclization is predicted to be 20.2 and 30.2 kcal/mol downhill for **8a** and **8b** respectively, and would certainly be irreversible under the reaction conditions. Barriers of 3.8 and 7.1 kcal/mol were calculated for the transition state of this reaction for **8a** and **8b**, respectively. The higher calculated barrier calculated for **8b** is consistent with the slower reaction rate of **2b** compared to **2a** in the uncatalyzed Nazarov cyclization (Table 5.1).
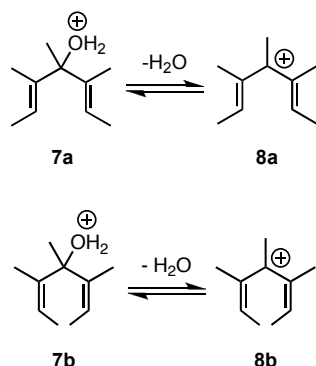
Figure 5.8. Equilibria between protonated pentadienol (**7a** and **7b**) and the corresponding dienyl cation (**8a** and **8b**).
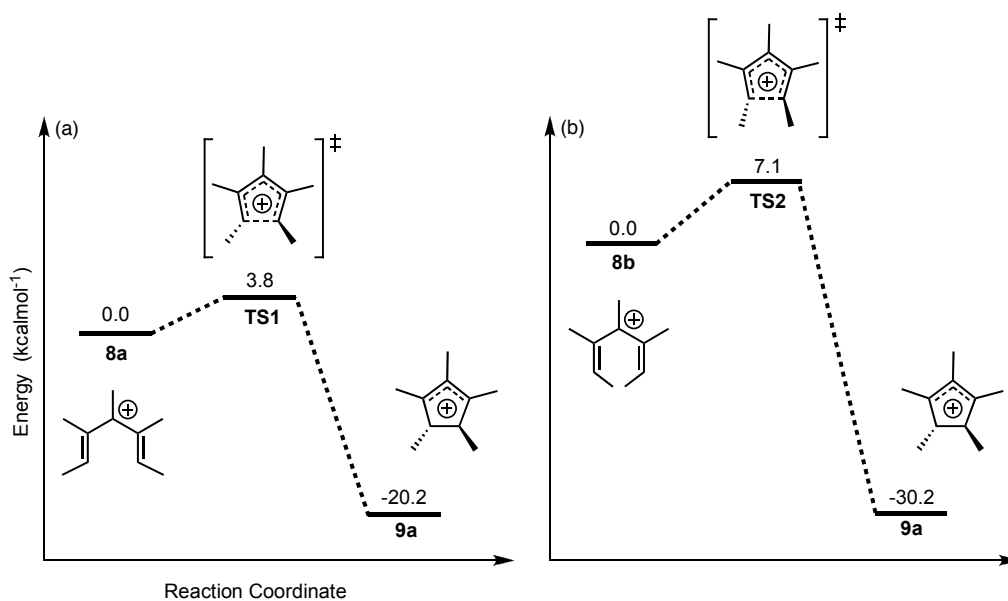
Figure 5.9. Calculated (B3LYP/6-31G) energy coordinate diagram for the formation of cyclopentenyl carbocation (**9a**) from (a) E,E pentadienyl carbocation **8a** and (b) Z,Z pentadienyl carbocation **8b**.

Clear evidence implicating one mechanism over the other was not obtained from the DFT calculations, although several insights were gained. The electrocyclization of dienyl cation **8a** is highly exothermic because one new C-C single bond is formed at the expense of a double bond. The same bonds are made and broken if electrocyclization and water loss are concerted, and this step should be quite exothermic as well. Such a step would be irreversible under the reaction conditions, regardless of its associated kinetic barrier.

[18]**O-Incorporation Studies.**   Determining whether water loss is reversible should differentiate between the two possible mechanisms; if water loss and electrocyclization are concerted then water loss should be irreversible. Both the **1**-catalyzed and the acid-catalyzed reaction of **2b** were run to partial conversion in ^{18}O-enriched water to probe the reversibility of

101

water loss. If the process were reversible, one would expect incorporation of ^{18}O into the recovered starting material (Figure 5.10). Incorporation of ^{18}O into the recovered starting material was observed in both reactions, proving that protonation and water loss are reversible, and in the **1**-catalyzed case, confirming that encapsulation is reversible (Figure 5.11a-b). No ^{18}O incorporation is observed when the reaction is run at pD 8.0 in the absence of **1**, ruling out any pathway for ^{18}O incorporation that does not involve acid catalysis (Figure 5.11c). These results in conjunction with our DFT calculations implicate the sequential loss of water and electrocyclization rather than the concerted mechanism (Figure 5.12).
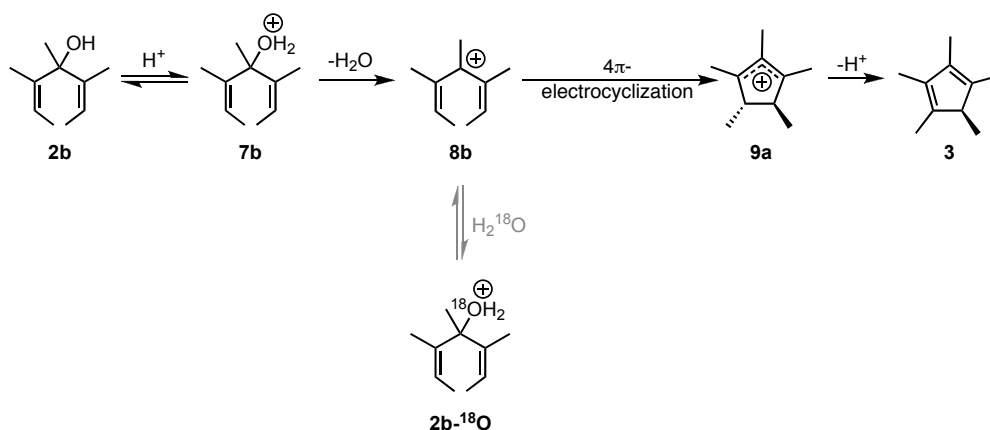
Figure 5.10. General scheme for the ^{18}O-incorporation experiment to determine whether loss of water is reversible in the Nazarov reaction.
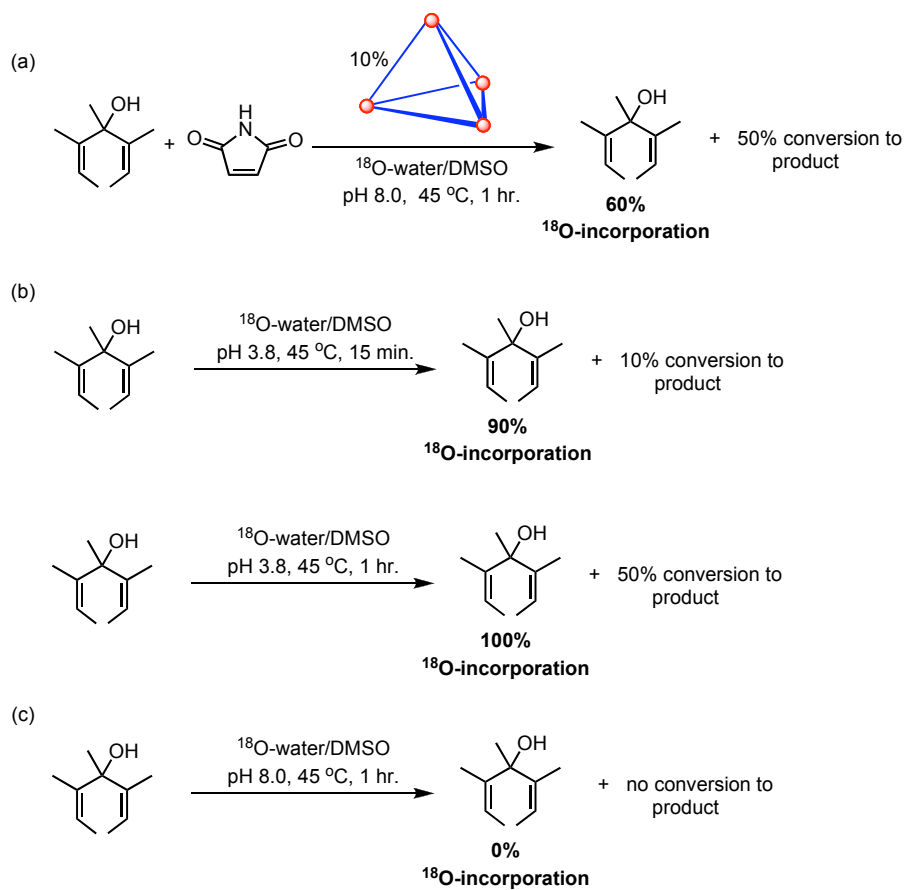
Figure 5.11. The Nazarov cyclization run in 1:1 $H_2{}^{18}O$/DMSO (a) with **1** as a catalyst, (b) under acidic conditions without **1**, and (c) under basic conditions without **1**.
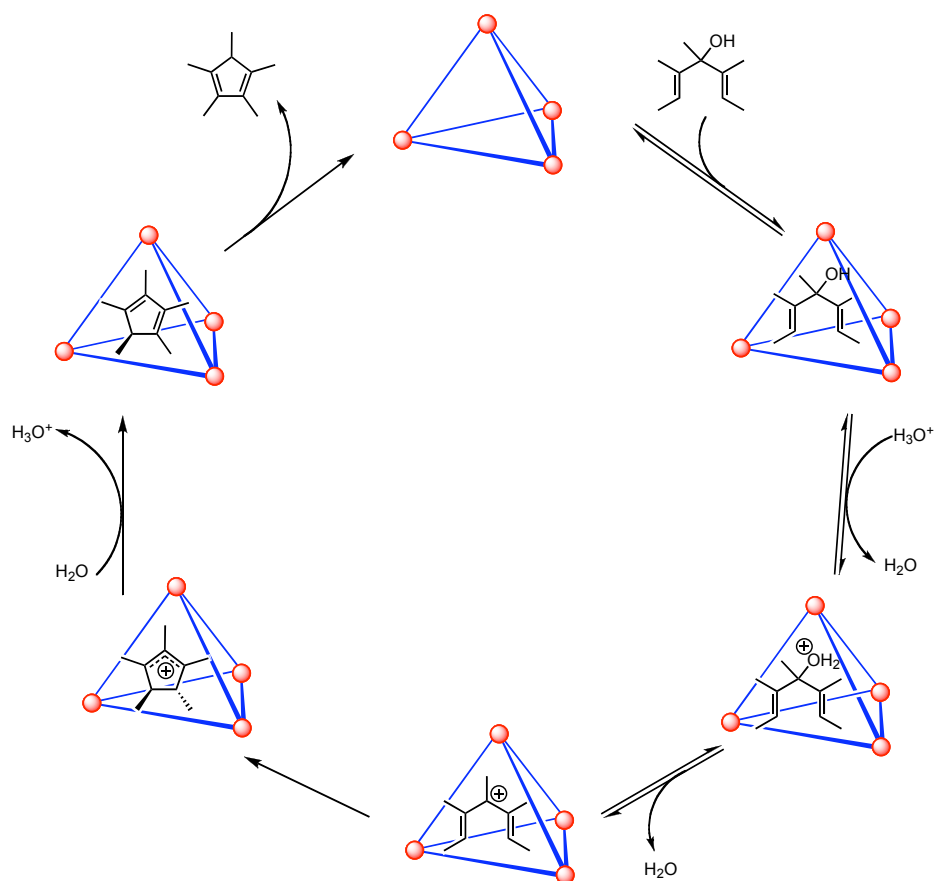
Figure 5.12. Proposed catalytic cycle for the **1**-catalyzed Nazarov cyclization of 1,4-pentadien-3-ols, with **2a** shown as a representative substrate.

The rates of ^{18}O incorporation versus the rate of product formation are not equal for the **1**-catalyzed and acid-catalyzed reaction. When the **1**-catalyzed reaction of **2b** was run to 50% conversion, 60% ^{18}O incorporation was observed. In the acid-catalyzed reaction, 90% ^{18}O incorporation was observed after only 10% conversion, and quantitative incorporation occurred after 50% conversion of **2b**. One explanation for this difference in relative exchange versus cyclization rates is that the recombination of **8b** $\subset$ **1** with water is faster than the analogous reaction of unencapsulated **8b**. It is possible that the effective concentration of water inside the host cavity is lower than in solution, or that **8b** is bound in a conformation that hinders recombination with water (Figure 5.13a). This effect was observed in a previous study in which the tropylium ion is protected from reacting with water by encapsulation within **1**, dramatically slowing the decomposition rate of the tropylium cation compared to that observed in free solution.[9,10] A second explanation is that encapsulation lowers the barrier for the electrocyclization of **8b**. Even slightly lowering the 7.1 kcal/mol barrier calculated for the electrocyclization of **8b** in the catalyzed reaction would account for the observed difference in ^{18}O incorporation (Figure 5.13b). It is not possible to determine which one of these factors is responsible for the ^{18}O incorporation results, or whether both water recombination and

electrocyclization are affected by encapsulation (Figure 5.13c). It is clear, however, that the barrier for the electrocyclization of **8b** ⊂ **1** is lowered relative to the recombination of water when compared to unencapsulated **8b**. Additionally, these results indicate that protonation and water loss are rapid compared to electrocyclization in the uncatalyzed reaction, and that electrocyclization is rate determining. In the **1**-catalyzed reaction, the formation of product **4** and labelled reactant **2b-^{18}O** are competitive, so the barrier heights for those two reactions must be similar. That there is no single rate-determining step for the **1**-catalyzed reaction could explain the unusual 0.5-order dependence on [D$^+$] observed in the **1**-catalyzed reaction (Figure 5.4).
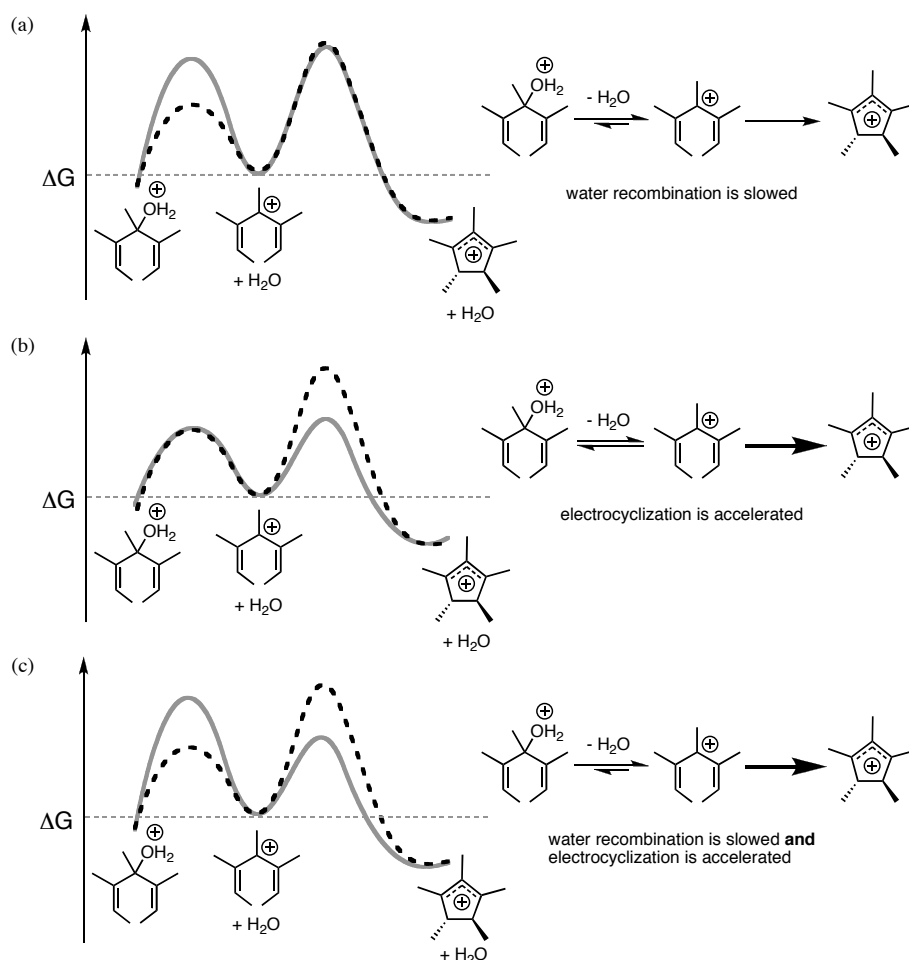
Figure 5.13. Qualitative energy coordinate diagrams illustrating how encapsulation might affect the reactivity of pentadienyl carbocation **8b**. The solid line represents the **1**-catalyzed reaction, the dotted line represents the acid-catalyzed reaction, and the diagrams are normalized such that **8b** ⊂ **1** and **8b** are equal in energy. (a) The rate of water recombination with **8b** ⊂ **1** is slow relative to recombination with **8b**. (b) The rate of electrocyclization for **8b** ⊂ **1** is fast relative to the electrocyclization of **8b**. (c) Encapsulation lowers the rate of water recombination and accelerates the rate of electrocyclization for **8b** ⊂ **1** relative to the analogous reactions of **8b**.

　　Reaction Energetics. To gain insight into the dramatic rate acceleration of the Nazarov cyclization that encapsulation in **1** provides, the energetic profiles of the catalyzed and uncatalyzed reaction were estimated and compared. The reactions of **2b** were compared for this purpose, since this substrate was used for the majority of experimental and computational studies. In the uncatalyzed reaction, a pK_a of -5.0 was estimated for protonated **2b** (**7b**), based on comparison to literature values. Although pK_a values for protonated aliphatic alcohols have been determined,[11,12] corresponding values for allylic and diallylic alcohols are not known. The effect of diallylic substitution on the pK_a of **7b** was estimated by comparing relevant ammonium compounds (Figure 5.14).[13] For instance the acidity of diallylammonium (**10**) is 1.7 pK_a units lower than that of either dipropylammonium (**11**) or diethylammonium (**12**). Similarly, the acidity of methyldiallylammonium (**13**) is 1.9 pK_a units lower than that of either triethylammonium (**14**) or tripropylammonium (**15**), and 1.5 pK_a units lower than that of methyldiethylammonium (**16**). Thus, the acidity of **7b** was estimated to be 1.8 pK_a units lower than that of protonated isopropanol (**17**). Protonation of **2b** under the experimental conditions, pD 8.0, is 18.9 kcal/mol uphill, and is assumed to have a low kinetic barrier (Figure 5.15). The activation energy of 30.4 kcal/mol for rate-determining electrocyclization was determined from the rate constant of the uncatalyzed reaction. The free energy of intermediate carbocations **8b** and **9a** relative to the transition state of the electrocyclization (-7.1 and -23.1 kcal/mol, respectively) were predicted by DFT calculations (Figure 5.9b).
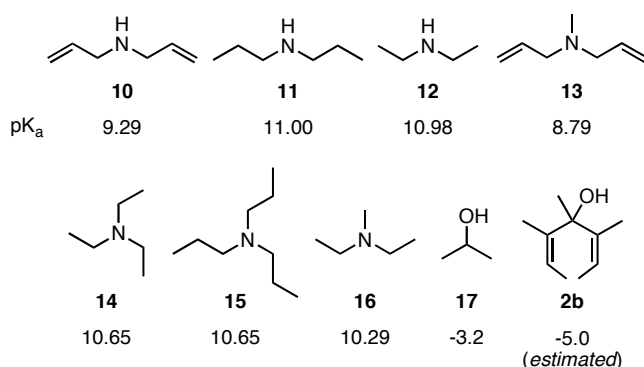
Figure 5.14. Reference compounds considered to estimate the pK_a of **7b**. The pK_a of the conjugate acid for each compound is given.

Figure 5.15. Proposed reaction coordinate diagram for the uncatalyzed Nazarov cyclization of **2b**, showing relative energies at the beginning of the reaction, at 318 K in 1:1 D_2O:DMSO-d_6 with 50 mM K_3PO_4 (pD 8.0) and 25 mM **2b**. Energies in italics were estimated (see text).

The energetics of binding **2b** in **1** were determined from the self-exchange rate of **2b** ⊂ **1** ($\Delta G_{exch}^{\ddagger}$ = 17.0 kcal/mol) and the extent to which **2b** is bound by **1** at the beginning of the reaction (Figure 5.16 represents the beginning of the **1**-catalyzed reaction). Previous studies demonstrated that encapsulation within **1** enhances the basicity of amines by up to 4.5 orders of magnitude, and that this basicity shift is responsible for thousand-fold rate enhancement in the hydrolysis of orthoformates.[14-17] Accordingly it is estimated that the acidity of **7b** ⊂ **1** is four pK_a units higher than that of unencapsulated **7b**, and that protonation of **2b** ⊂ **1** is 12.7 kcal/mol uphill. We assume that the energetics of water loss from **7b** ⊂ **1** shown in Figure 5.16 is 4.4 kcal/mol uphill, as it is in the uncatalyzed reaction. However, stabilization of the dienyl carbocation **8b** relative to **7b** by encapsulation is certainly possible; earlier studies demonstrate that favoring tropylium in its equilibrium with protonated 2,4,6-cycloheptatrien-1-ol by encapsulation in **1** could play a role in slowing the decomposition of the tropylium ion.[9] Thus, the energy of **7b** ⊂ **1** in Figure 5.16 is a rough estimate. The activation energy of 21.3 kcal/mol for electrocyclization of **8b** ⊂ **1** was determined from the rate constant of the **1**-catalyzed reaction. The free energy of **9a** ⊂ **1** was estimated by assuming moderate binding of **9a** (binding energy of -3.6 kcal/mol relative to unbound **9a**, corresponding to 10^2 binding). Although this value is speculative, the binding constant is unlikely to be below 10 or above 10^4, a range that

includes the majority of cationic guests bound by **1**,[18-21] and most guests bound by synthetic hosts in general.[22]

Figure 5.16. Proposed reaction coordinate diagram for the **1**-catalyzed Nazarov cyclization of **2b**, showing relative energies at the beginning of the reaction, at 318 K in 1:1 D$_2$O:DMSO-d_6 with 50 mM K$_3$PO$_4$ (pD 8.0), 1.5 mM **1** and 25 mM **2b**. Energies in italics were estimated (see text).

In previous studies on the basicity enhancement of **1**-bound guests, the protonation equilibrium of bound amines were shifted by a maximum of 4.5 orders of magnitude, and the rate of acid-catalyzed orthoformate hydrolysis was accelerated by a maximum of 3.5 orders of magnitude. Based on this precedent it is clear that the acceleration o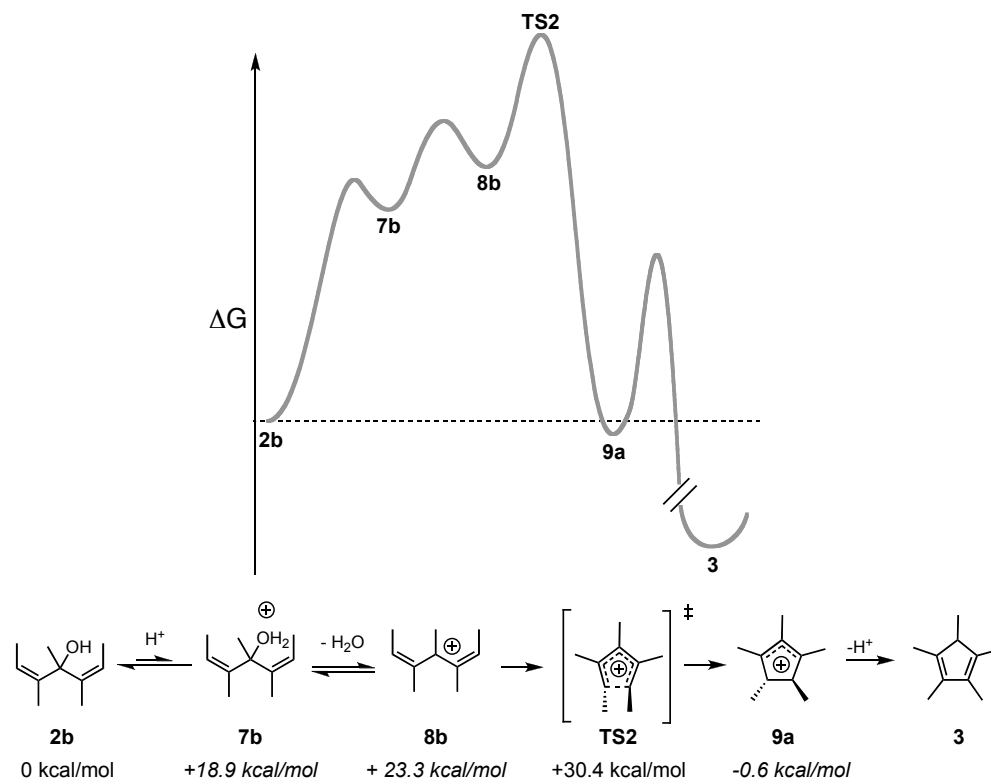f the **1**-catalyzed Nazarov cyclization is not simply due to increasing the basicity of the bound substrate. According to the energetics estimated for the **1**-catalyzed and uncatalyzed reaction, the reaction barrier for electrocyclization of **8b** ⊂ **1** is lowered by 3 kcal/mol relative to **8b** (Figure 5.17). We considered that either encapsulation within **1** could bind a reactive conformation of **2b** that is disfavored in bulk solution, or that encapsulation could stabilize the transition state itself. Encapsulation in **1** and in other supramolecular assemblies is known to favor folded conformations of acyclic molecules that are otherwise disfavored in bulk solution,[23-29] and conformational selection is responsible for a nearly thousand-fold rate acceleration in the **1**-catalyzed aza Cope rearrangement of enammonium cations.[30-32] Examining the rate constants for the uncatalyzed Nazarov cyclization of **2a**, **2b**, and **2c** indicates that substrate conformation affects the rate of electrocyclization (Table 5.1); the reaction rate is slowest for **2b**, whose methyl

groups are in the Z configuration. The cisoid conformer of **8b** necessary for rate-determining electrocyclization is sterically disfavored relative to the analogous cisoid conformer of **8a**. This effect is relatively small, only lowering the reaction rate of **2b** by a factor of 5 relative to that of **2a**, corresponding to an energetic difference of only 1 kcal/mol. Encapsulation in **1** could further lower the electrocyclization barrier by stabilizing the compact transition state **TS2**. Based on the small contribution of conformational selection towards the overall rate acceleration, we conclude that transition state stabilization is the dominant factor in lowering the reaction barrier **8b ⊂ 1** relative to **8b**.
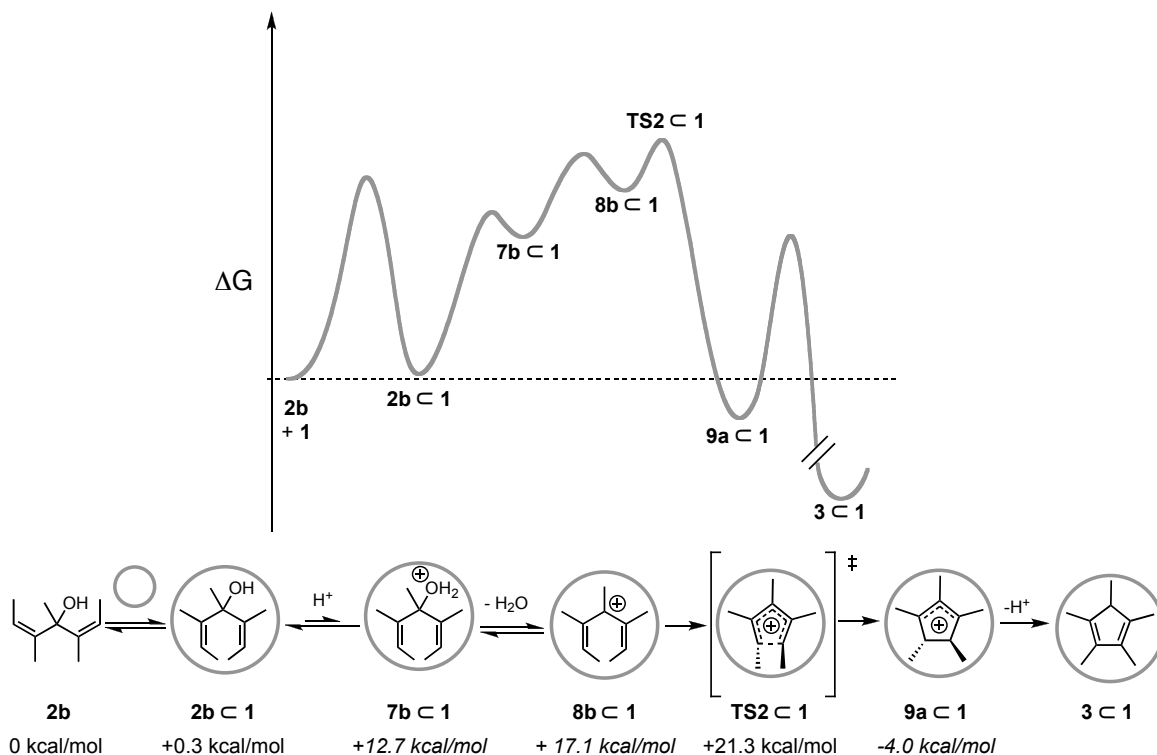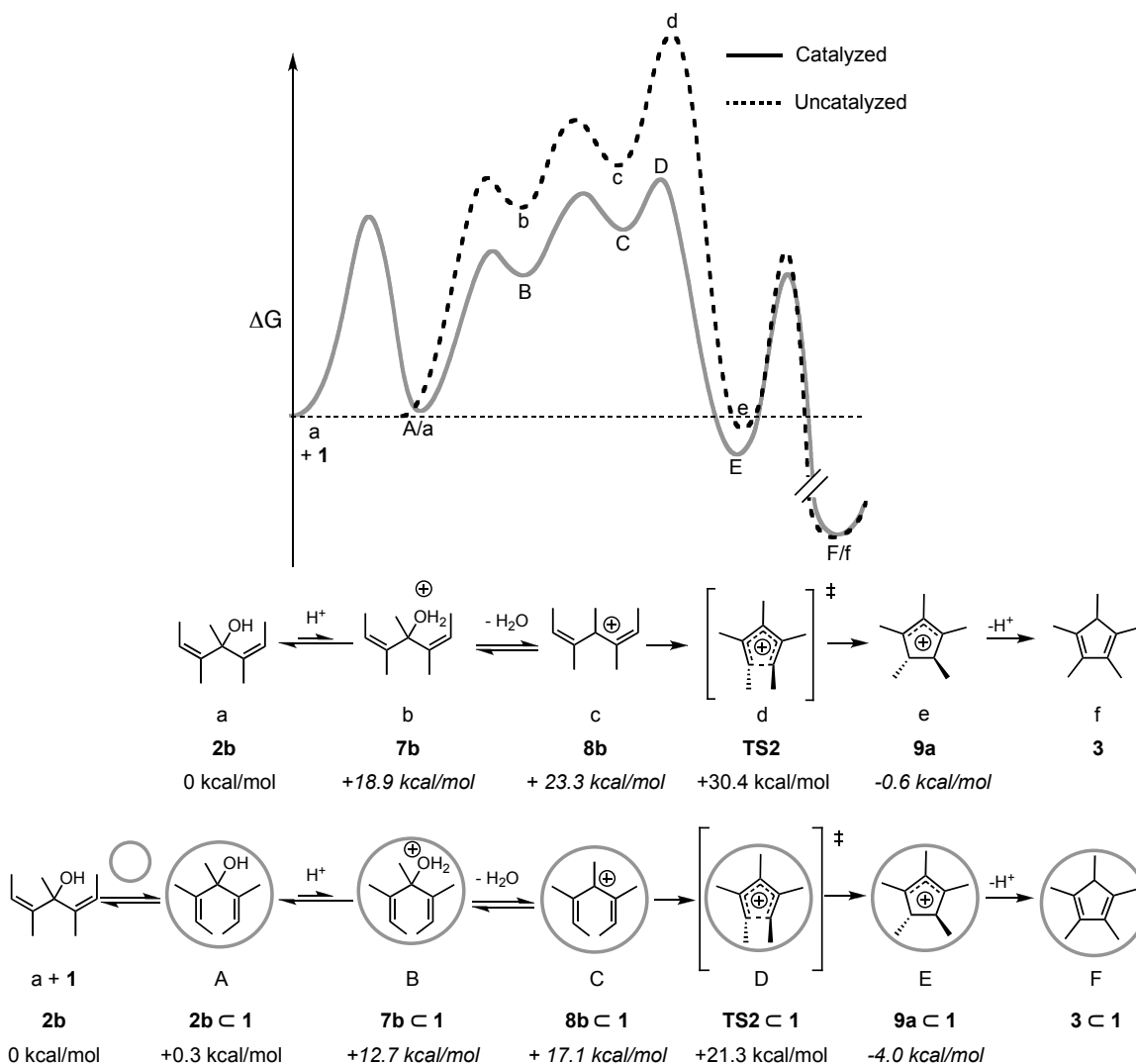

Figure 5.17. Proposed reaction coordinate diagram for the **1**-catalyzed and the uncatalyzed Nazarov cyclization of **2b**, showing relative energies at the beginning of the reaction, at 318 K in 1:1 D_2O:DMSO-d_6 with 50 mM K_3PO_4 (pD 8.0), 1.5 mM **1** and 25 mM **2b**. Energies in italics were estimated (see text).

The activation parameters for both the **1**-catalyzed and the uncatalyzed reaction of **2b** were determined in order to gain insight into the transition state of these reactions. As discussed in Chapter 3, it was not possible to deconvolute the protonation and electrocyclization steps of the reaction, and the measured rate constants implicitly include both the equilibrium constant for protonation and the concentration of D^+ in solution. This complicates the interpretation of activation parameters significantly, since each value represents the sum of both processes. Nevertheless, a comparison between the apparent activation parameters for the catalyzed and uncatalyzed reaction could yield useful information even if the absolute values are not meaningful. The measured activation parameters for the uncatalyzed reaction of **2b** are $\Delta H^{\ddagger} =$ 15.5(8) kcal/mol and $\Delta S^{\ddagger} = -48(1)$ e.u. (Figure 5.18), and the values for the catalyzed reaction of **2b** are $\Delta H^{\ddagger} = 14.8(8)$ kcal/mol and $\Delta S^{\ddagger} = -20(1)$ e.u. (Figure 5.19). Multiplication of rate constants by a constant factor will affect the $\Delta S^{\ddagger}$ in Eyring analysis, but not the $\Delta H^{\ddagger}$. Inclusion of $[D^+]$ and the equilibrium constant for the protonation reaction in the overall rate constants is presumably responsible for the unusually large, negative values of $\Delta S^{\ddagger}$. Interestingly, the $\Delta H^{\ddagger}$ values for both reactions are within the standard error, while the entropic barrier is reduced by 28 e.u. in the catalyzed reaction relative to the uncatalyzed reaction. A lowered entropic barrier is consistent with some degree of organization in the transition state of the reaction being provided by encapsulation within **1**; this is the effect that is responsible for catalysis in the **1**-catalyzed aza Cope rearrangement. Protonation of neutral, encapsulated substrate (**2b** $\subset$ **1**) could also contribute to the lowered entropic barrier; a large, positive change in the entropy of hydration occurs as the host charge is reduced from -12 to -11.[21,33] Considering the large reduction in the entropy of activation in the catalyzed reaction relative to the uncatalyzed reaction, it is possible that both protonation and electrocyclization are more entropically favored in the catalyzed reaction than in the uncatalyzed reaction.
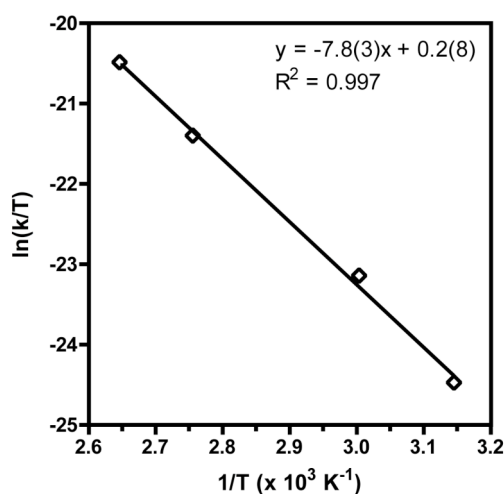
Figure 5.18. Eyring plot used to determine activation parameters for the uncatalyzed reaction of **2b**.
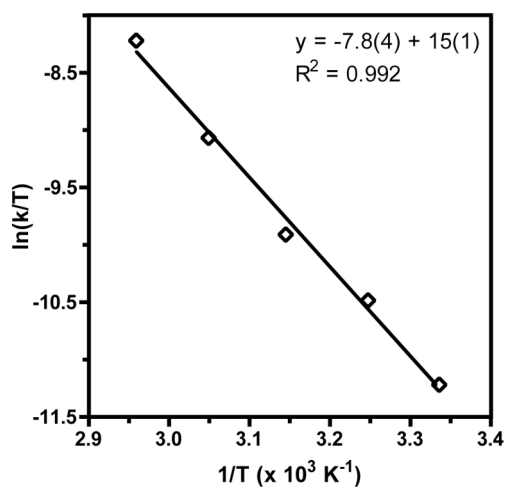
Figure 5.19. Eyring plot used to determine activation parameters for the **1**-catalyzed reaction of **2b**.

Conclusion

Mechanistic studies of the **1**-catalyzed Nazarov cyclization of 1,4-pentadien-3-ols were conducted, and comparisons were made to the uncatalyzed reaction to understand the role of encapsulation in this catalysis. Kinetic analysis of the reaction, [18]O exchange experiments, and computational studies implicate a mechanism in which encapsulation, protonation and water loss from substrate are reversible, followed by irreversible electrocyclization. While electrocyclization is rate-determining in the uncatalyzed reaction, the barrier for water loss and for electrocyclization are nearly equal in the **1**-catalyzed reaction. Analysis of the proposed energetics of the catalyzed and uncatalyzed reaction revealed that transition state stabilization contributes significantly to the catalytic rate acceleration. This, in addition to the enhanced basicity caused by encapsulation in **1**, is responsible for the dramatic million-fold rate enhancement over the uncatalyzed reaction. Comparison of the activation parameters for the catalyzed and uncatalyzed reaction seems to support the proposed origin of the rate acceleration.

Experimental Section

General Experimental Procedures. Unless otherwise noted, all reactions and manipulations were performed using standard Schlenk and high-vacuum techniques at room temperature. All glassware was dried in an oven at 150 °C for at least 12 h or flame-dried under vacuum prior to use.

Instrumentation. NMR spectra were obtained on Bruker Avance AVQ 400 (400 MHz), AV 400 (400 MHz), AV 500 (500 MHz), or AV 600 (600 MHz) spectrometers as indicated. Chemical shifts are reported as δ in parts per million (ppm) relative to residual protonated solvent resonances. In the case of D_2O samples, ^{13}C shifts were referenced to an internal standard of CH_3OH.[34] Chemical shifts for ^{19}F NMR data were referenced to an internal standard of trifluoroethanol.[35] NMR data are reported in the following format: (s = singlet, d = doublet, t = triplet, q = quartet, m = multiplet, b = broad; integration; coupling constant). The temperatures of the kinetics experiments carried out in a circulating oil bath were measured using a calibrated mercury thermometer and varied ±0.1 ºC. The temperatures of the kinetics experiments carried out in an NMR probe were determined from the ^1H NMR chemical shifts of ethylene glycol and CH_3OH samples, and varied ±0.1 ºC. Mass spectral data were obtained at the QB3 Mass Spectrometry Facility operated by the College of Chemistry, University of California, Berkeley. Fast atom bombardment (FAB) mass spectra were recorded on a Micromass ZAB2-EQ magnetic sector instrument. Electron impact (EI) and chemical ionization (CI) mass spectra were recorded on a Micromass ProSpec magnetic sector instrument equipped with an EI and a CI source.

Materials. Unless otherwise noted, reagents were obtained from commercial suppliers and used without further purification. Ethyl ether (Et_2O) and tetrahydrofuran (THF) were dried by passing through columns of activated alumina under nitrogen pressure and were sparged with nitrogen before use.[36] $K_{12}Ga_4L_6$ (K_{12}**1**) was prepared according to literature procedure.[37] (*Z*)-2-bromo-2-butene is occasionally available commercially from Sigma-Aldrich, and can be separated from the *E* isomer by preparative gas chromatography (see Chapter 3 or reference 1).

Synthesis of 4-Trifluoromethyl-3,5-Dimethylhepta-2-*trans*-5-*trans*-dien-4-one (2-CF₃). This procedure was adapted for a small scale from a published procedure for the large-scale preparation of **2**.[38] A 2-necked round-bottomed flask equipped with a magnetic stir bar and a reflux condenser was charged with lithium wire (155.5 mg, cut into 4 mm lengths, 22.4 mmol) and 1 mL dry Et_2O. (*Z*)-2-bromo-2-butene was purified and dried immediately before use by passage through a pipette column of basic alumina. The first 0.7 mL of (*Z*)-2-bromo-2-butene (total of 2.0 mL, 11.2 mmol) was added dropwise to the stirred solution via syringe over the course of several minutes. At this point, the reaction initiated, as indicated by the evolution of heat and bubbling of the reaction mixture. An additional 10 mL of fresh Et_2O was added, and the remainder of the bromide was added slowly to keep the reaction at reflux. After the addition of the bromide was complete, 5 mL of fresh Et_2O was added and stirring was continued for one additional hour. The reaction mixture was then cooled to 0 °C in an ice bath and quenched by the slow addition of ethyl trifluoroacetate (0.7 mL, 5.9 mmol) diluted to 50% with Et_2O. The reaction mixture was poured into saturated aqueous NH_4Cl and extracted five times with 20 mL Et_2O. The combined organic layers were washed with brine and dried over $MgSO_4$, and the

solvent was removed by rotary evaporation to obtain the title compound (0.65 g, 3.1 mol) as a yellow liquid in 56% yield and 85% purity. The contaminant is the *E,Z* stereoisomer. **¹H NMR** (400 MHz, CDCl₃): δ 5.52 (q, 2H, ^3J = 7.3 Hz), 1.87 (s, 6H), 1.60 (d, 6H, ^3J = 7.2 Hz) ppm; **¹³C{¹H} NMR** (100.6 MHz, CDCl₃): δ 134.1, 128.7, 126.5 (q, 1C, $^2J_{FC}$ = 150 Hz) 78.8 (q, 1C, $^3J_{FC}$ = 28 Hz), 22.3 (q, 2C, $^4J_{FC}$ = 2.7 Hz), 18.3 ppm; **¹⁹F NMR** (376.5 MHz, CDCl₃): δ -77.58 ppm (*E,Z* stereoisomer at -76.12 ppm); **HRMS (EI)**: Exact mass calcd for $C_{10}H_{14}F_3O$ [M-H]⁺: 207.0997, found 207.0998. Exact mass calcd for $C_{10}H_{15}F_3O$ [M]⁺: 208.1075, found 208.1067 (50% intensity with respect to [M-H]⁺).

K₁₂[2-CF₃ ⊂ 1]. The potassium salt of **1** (15.0 mg, 4.0 μmol) was dissolved in 0.6 mL D₂O (buffered to pD 8.0 with 0.1 M KH₂PO₄), and the resulting solution was then mixed thoroughly with **2-CF₃** (2.5 mg, 12.0 μmol). The solution was transferred to an NMR tube, and the spectrum of the host-guest complex was recorded within 20 minutes. No reaction was observed after the sample was heated at 50 °C for 5 hours. Quantitative guest binding was not observed; the binding efficiency is 77%, which represents the relative ¹H-NMR integrations of the guest to host peaks. The unencapsulated guest is sparingly soluble in D₂O, and only broad resonances were observed. **¹H NMR** (400 MHz, D₂O): δ 7.94 (d, 12H, ^3J = 7.7, Ar-*H*), 7.78 (d, 12H, ^3J = 8.5 Hz, Ar-*H*), 7.34 (d, 12H, ^3J = 8.2 Hz, Ar-*H*), 7.01 (t, 12H, ^3J = 8.1 Hz, Ar-*H*), 6.73 (d, 12H, ^3J = 7.2 Hz, Ar-*H*), 6.58 (t, 12H, ^3J = 7.8 Hz, Ar-*H*), -0.90 (d, 3H, ^3J = 7.0, encaps.), -1.07 (d, 3H, ^3J = 7.0, encaps.), -1.20 (s, 3H, encaps.), -1.29 (s, 3H, encaps.) ppm. **¹⁹F NMR** (376.5 MHz, D₂O): δ -80.83 ppm.

Kinetic Analysis of 1-Catalyzed Reactions. Representative procedure for kinetic runs: 2.0 mg substrate (13.0 μmol), 3.5 mg K₁₂**1** (0.9 μmol), 2.0 mg maleimide (20.6 μmol), and 3.0 mg sodium *p*-toluenesulfonate (15.4 μmol, added as an integration standard) were dissolved in 0.3 mL DMSO-*d₆* and 0.3 mL D₂O (buffered with 100 mM phosphate buffer, adjusted to the desired pD). The solution was transferred to an NMR tube and inserted into the NMR probe preheated to 45 °C. After allowing the sample temperature to equilibrate for two minutes, ¹H-NMR spectra were acquired every 20 seconds until >95% of the starting material was consumed. Variable [D⁺] kinetic runs were conducted using both 100 mM phosphate buffer and 100 mM tris(hydroxymethyl)aminomethane (TRIS) buffer. The **1**-catalyzed reactions run in TRIS buffer proceeded at a rate one order of magnitude greater than that of the analogous reaction run in phosphate buffer. The variable-pD kinetics of reactions run in TRIS display an apparent order of 0.6 in [D⁺] (Figure 5.20), similar to the results from the reactions run in phosphate buffer. Standard errors for all reported values are given in parentheses.

Substrate	[**1**] (mM)	Temp. (°C)	pD	Buffer	Rate (mM/s)
2b	0.29	45	8.0	Phosphate	$1.4(2) \times 10^{-3}$
2b	0.65	45	8.0	Phosphate	$2.8(2) \times 10^{-3}$
2b	1.29	45	8.0	Phosphate	$5.6(2) \times 10^{-3}$
2b	1.53	45	8.0	Phosphate	$6.2(3) \times 10^{-3}$

Table 5.2. Rate data for variable-[**1**] kinetics of the **1**-catalyzed Nazarov cyclization of **2b**. The reported initial rates are for the appearance of product during the first 15% of conversion.

Substrate	[1] (mM)	Temp. (°C)	pD	Buffer	Rate (mM/s)
2b	1.53	45	7.24	Phosphate	$1.36(3) \times 10^{-2}$
2b	1.53	45	7.47	Phosphate	$8.8(2) \times 10^{-3}$
2b	1.53	45	7.95	Phosphate	$3.7(3) \times 10^{-3}$
2b	1.53	45	8.55	Phosphate	$2.9(1) \times 10^{-3}$

Table 5.3. Rate data for variable-[D^+] kinetics of the **1**-catalyzed Nazarov cyclization of **2b** in phosphate-buffered solution. The reported initial rates are for the appearance of product during the first 15% of conversion.

Substrate	[1] (mM)	Temp. (°C)	pD	Buffer	Rate (mM/s)
2b	1.53	27	7.5	TRIS	$3.5(1) \times 10^{-2}$
2b	1.53	27	8.0	TRIS	$2.50(7) \times 10^{-2}$
2b	1.53	27	8.5	TRIS	$1.49(6) \times 10^{-2}$
2b	1.53	27	9.0	TRIS	$5.1(2) \times 10^{-3}$

Table 5.4. Rate data for variable-[D^+] kinetics of the **1**-catalyzed Nazarov cyclization of **2b** in TRIS-buffered solution. The reported initial rates are for the appearance of product during the first 15% of conversion.
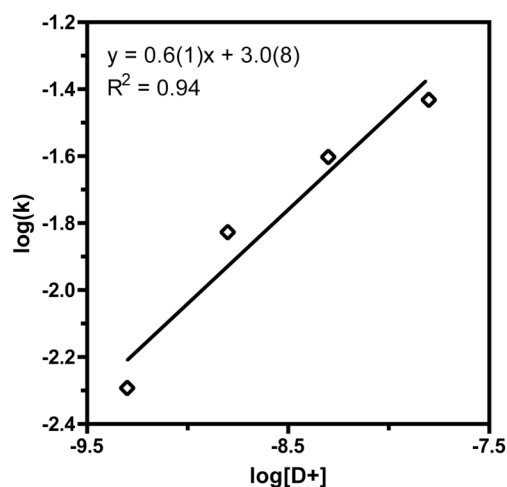

Figure 5.20. Rate dependence on [D^+] for the **1**-catalyzed Nazarov cyclization of **2b** in 1:1 D_2O/DMSO-d_6 at 45 °C (aqueous portion buffered with 100 mM TRIS).

114

Substrate	[1] (mM)	Temp. (°C)	pD	Buffer	k_{cat} (s^{-1})
2b	1.53	25	8.0	Phosphate	4.0(2) x 10^{-3}
2b	1.53	35	8.0	Phosphate	1.04 x 10^{-2}
2b	1.53	35	8.0	Phosphate	6.81(6) x 10^{-3}
2b	1.53	45	8.0	Phosphate	1.58(4) x 10^{-2}
2b	1.53	55	8.0	Phosphate	3.78(6) x 10^{-2}
2b	1.53	65	8.0	Phosphate	9.1(1) x 10^{-2}

Table 5.5. Rate data for variable-temperature kinetics of the **1**-catalyzed Nazarov cyclization of **2b**. The reported rate constants were calculated from the Michaelis-Menten equation using observed dissociation constant of $1 \subset 2b$.

       Kinetic Analysis of Uncatalyzed Reactions. The procedure for sample preparation was analogous to that used for the catalyzed reaction, except that **1** and maleimide were omitted and silylated glassware was used. For experiments conducted at lower pD values (between 3.0 and 4.0) the aqueous portion of solvent was buffered with 100 mM potassium hydrogen phthalate. The sample was sealed under vacuum in a thin-walled NMR tube and heated at 45 °C in a circulating oil bath. Partially silylated tubes, in which only the portion of the NMR tube that contacts the reaction mixture was silylated and the remainder was unmodified, were prepared in the following fashion:

Hexamethyldisilazane (0.7 mL, purified by distillation) was transferred by syringe into a thin-walled NMR tube, with care being taken so that the reagent did not contact any part of the tube except the bottom portion. The NMR tube was capped and heated at 70 °C in a circulating oil bath for twelve hours. The hexamethyldisilazane was then pipetted out of the NMR tube and discarded, and the tube was heated in an oven for at least 24 hours at 150 °C.

       This procedure yielded consistent results, and over the course of eight weeks at 45 °C low but reproducible levels of conversion were observed. Conversion was substantially faster when the reaction was conducted at higher temperature, and up to 50% conversion was observed after 16 days. When low conversion was observed (<10%), the initial reaction rate was treated as the derivative of a first-order process, the rate constant was calculated from the equation d[SM]/dt = - k_{uncat} [SM]. When >10% conversion is observed, the rate constant is determined by fitting exponential decay of [**2b**]. Kinetics data measured at lower pD were monitored by in-probe NMR spectroscopy as described above.

Substrate	Temp. (°C)	pD	k_{uncat} (s^{-1})	Half-life (h)
2b	45	8.0	8(2) x 10^{-9}	9(2) x 10^7
2b	45	8.0	7(1) x 10^{-9}	1.0(1) x 10^8
2b	60	8.0	2.2(7) x 10^{-8}	3(1) x 10^7
2b	60	8.0	2.5(7) x 10^{-8}	2.8(8) x 10^7
2b	60	8.0	2.9(5) x 10^{-8}	2.4(4) x 10^7
2b	60	8.0	3.8(7) x 10^{-8}	1.8(3) x 10^7
2b	60	8.0	2.2(7) x 10^{-8}	3(1) x 10^7
2b	60	8.0	4.2(5) x 10^{-8}	1.6(2) x 10^7
2b	90	8.0	1.8(2) x 10^{-7}	3.9(2) x 10^6
2b	90	8.0	1.9(1) x 10^{-7}	3.6(2) x 10^6
2b	105	8.0	4.8(3) x 10^{-7}	1.44(9) x 10^6
2b	105	8.0	5.0(3) x 10^{-7}	1.39(8) x 10^6
2b	105	8.0	4.6(2) x 10^{-7}	1.51(7) x 10^6

Table 5.6. Rate data for variable-temperature kinetics of the uncatalyzed Nazarov cyclization of **2b**.

Substrate	Temp. (°C)	pD	k_{uncat} (s^{-1})	Half-life (h)
2b	45	8.0	8(2) x 10^{-9}	9(2) x 10^7
2b	45	8.0	7(1) x 10^{-9}	1.0(1) x 10^8
2b	45	3.0	6.95(9) x 10^{-4}	9.9(1) x 10^2
2b	45	3.4	3.19(5) x 10^{-4}	2.17(3) x 10^3
2b	45	3.7	2.12(3) x 10^{-4}	3.27(5) x 10^3
2b	45	4.0	1.14(2) x 10^{-4}	6.1(1) x 10^3

Table 5.7. Rate data for variable-[D$^+$] kinetics of the uncatalyzed Nazarov cyclization of **2b**.

^{18}O Labeling Studies. The procedure for sample preparation was analogous to that used for the kinetic studies: 5.2 mg **2b** (33.7 μmol), 3.5 mg K$_{12}$**1** (0.9 μmol), and 2.4 mg maleimide (24.7 μmol) were dissolved in 0.3 mL DMSO and 0.3 mL [^{18}O]-water (buffered with 100 mM phosphate adjusted to pH 8.0). The solution was transferred to an NMR tube and heated at 45 °C for one hour in a circulating oil bath. A model reaction using the same quantity of reagents in deuterated solvents was monitored by ^{1}H-NMR, and 50% conversion of starting material was observed after one hour. After heating, the reaction mixture was extracted three times with 0.5 mL portions of ethyl acetate. The combined organics were washed three times with brine, dried over MgSO$_4$ and filtered. The resulting solution was analyzed by mass spectrometry (CI) to determine the extent of ^{18}O incorporation. The parent ion of **2** was not observed by other methods of mass spectrometry, such as gas chromatography-mass spectrometry (GC-MS), EI, and FAB. In these experiments only dehydrated species were observed, and ^{18}O incorporation could not be determined. In preparing buffer solutions of [^{18}O]-water, unlabelled water was unavoidably introduced into the solution, affecting the maximum extent of ^{18}O-incorporation in

the experiment. The concentration of [^{18}O]-water in the buffer solutions were determined in the following fashion:

An oven-dried GC-MS vial was charged with 1.5 mL dry THF, and 0.1 mL of the buffer solution was immediately added by syringe. The vial was capped and the solution was mixed thoroughly by inverting the vial ten times. The sample was analyzed by GC-MS without the usual solvent delay, allowing for the analysis of volatile species. The [^{18}O]-water content was approximately 90% for both buffer solutions used. Samples prepared with unlabeled water added contained no [^{18}O]-water. Samples prepared without any added water did not contain significant quantities of water, confirming that these samples were not contaminated with unlabeled, adventitious water.

The ^{18}O content measured by mass spectrometry was adjusted by dividing by 0.9, which is the maximum extent of incorporation possible. For the acid-catalyzed and the uncatalyzed reactions, the above procedure was followed except that **1** and maleimide were omitted. [^{18}O]-Water was buffered with 100 mM potassium hydrogen phthalate for the acid-catalyzed reaction. A model reaction using the same quantity of reagents in deuterated solvent (aqueous portion buffered to pD 3.4) was monitored by ^{1}H-NMR, and 10% conversion of starting material was observed after fifteen minutes, while 50% conversion of starting material was observed after one hour.

DFT Calculations. All calculations were performed using the Gaussian 03 software package with the GaussView graphical user interface.[39] Energies were calculated by performing geometry optimizations, minimizations, and frequency calculations at the B3LYP/6-31G(d) level of theory. Transition states were confirmed by performing intrinsic reaction coordinate searches. For acyclic pentadienyl cations **8a** and **8b**, the starting conformation of the molecule determined the stereochemistry of the minimized structure; regardless of the starting geometry, the minimized structure always corresponded to one of the minimized structures reported below.
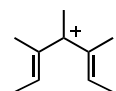
E_{SCF} = -390.819943 Hartrees
Zero-point correction = 0.243950 Hartrees
No Imaginary Frequencies

C	2.42095900	0.48496800	0.15552600
C	1.23557600	-0.13032000	-0.17021800
H	2.39020200	1.49782600	0.54985800
C	0.00962200	0.60306200	0.02196800
C	-1.25102500	-0.07957700	0.20085000
C	-2.39400900	0.49486200	-0.29913700
H	-2.31768200	1.44131600	-0.82792300
C	0.04211700	2.10510200	0.09060400
H	0.30975400	2.40127600	1.11604700
H	0.76773000	2.54849900	-0.59301800
H	-0.93717900	2.55151700	-0.08418200

C	-1.31107500	-1.42116900	0.91501800
H	-1.56576400	-2.25005500	0.24688400
H	-0.37090600	-1.65945600	1.41344500
H	-2.08148400	-1.37642000	1.69170700
C	1.22922800	-1.53929900	-0.73935200
H	1.45386800	-2.30286100	0.01269000
H	0.27188100	-1.78592700	-1.19957500
H	1.98822300	-1.61870700	-1.52337600
C	3.77841200	-0.10787200	0.08952800
H	4.41486100	0.51546900	-0.55681600
H	4.24824900	-0.06525400	1.08261600
H	3.80289500	-1.13577200	-0.27196500
C	-3.75619700	-0.09467900	-0.28886800
H	-4.45125900	0.61190900	0.18875600
H	-4.12043900	-0.20726500	-1.31989200
H	-3.82459200	-1.05656000	0.21923700
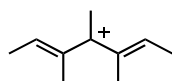
E_{SCF} = -390.827970 Hartrees
Zero-point correction = 0.243548 Hartrees
No Imaginary Frequencies

C	-1.40514200	-0.95051700	-0.54654100
C	-1.24605500	0.23929000	0.13084800
H	-0.58108000	-1.28893800	-1.16863100
C	0.01095700	0.92434700	0.00429600
C	1.26059300	0.22205400	-0.10900600
C	1.37522700	-1.00131700	0.51727600
H	0.52887400	-1.33624800	1.11060600
C	0.03249000	2.42077300	-0.04120200
H	0.42493100	2.74157500	-1.01646800
H	-0.95068700	2.86925500	0.09100700
H	0.72204600	2.83121600	0.70796700
C	2.43645600	0.91924900	-0.76142400
H	2.16094500	1.34231000	-1.73298900
H	2.80150800	1.74352500	-0.13699200
H	3.27324000	0.23939600	-0.92100400
C	-2.39664500	0.90336500	0.86549700
H	-3.02296100	0.15235400	1.35279300
H	-2.04235400	1.58360700	1.64315000
H	-3.04069700	1.47266600	0.18461900
C	-2.63820900	-1.77331400	-0.63647100
H	-3.02494700	-1.73947000	-1.66600800

H	-2.39148200	-2.82822100	-0.45377200
H	-3.43385800	-1.47036900	0.04447300
C	2.56656200	-1.88528800	0.58551800
H	2.97032900	-1.87375000	1.60944700
H	2.26116800	-2.92470100	0.40590100
H	3.36762900	-1.62605000	-0.10684600
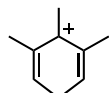
E_{SCF} = -390.804428 Hartrees
Zero-point correction = 0.243970 Hartrees
No Imaginary Frequencies

| C | -2.45013200 | 0.10890900 | -0.28662600 |
C	-1.13405500	0.52213400	-0.34306100
C	-0.02150200	-0.25006300	0.13506800
C	1.25114300	0.38577300	0.41279200
C	2.45769600	-0.14374000	0.03921800
C	-0.13528700	-1.71461900	0.41849300
H	-0.53820900	-1.82964500	1.43748700
H	-0.80184500	-2.24561300	-0.26378300
H	0.84075100	-2.19757500	0.44677000
C	1.25550400	1.71710300	1.16502100
H	1.39313500	2.57602500	0.50166600
H	0.33808700	1.86960000	1.73831400
H	2.08895000	1.71171100	1.87467000
C	-0.86865600	1.86359000	-1.01921600
H	-0.89043900	2.69530400	-0.30822300
H	0.09847800	1.87732400	-1.52742700
H	-1.63932600	2.05785200	-1.77021200
H	-3.14766000	0.78506500	-0.78199100
H	3.32810700	0.42986700	0.36087000
C	2.79835600	-1.27726600	-0.86886600
H	3.44839100	-0.89685200	-1.66838100
H	3.40235800	-2.02281300	-0.33254900
H	1.94556900	-1.77215100	-1.33451600
C	-3.12769500	-1.04297000	0.36485800
H	-4.10952900	-0.72274000	0.72994500
H	-3.33202600	-1.82032400	-0.39020500
H	-2.57702100	-1.50813500	1.18148300
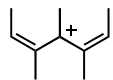
E_{SCF} = -390.810440 Hartrees
Zero-point correction = 0.243755 Hartrees
No Imaginary Frequencies

C	-1.49569600	-1.03239200	-0.65229200
C	-1.28254200	0.13982100	0.03814700
C	-0.04025600	0.86257900	-0.01011400
C	1.26404000	0.25899000	-0.06319200
C	1.59873100	-0.85420100	0.67291700
C	-0.12742000	2.35874900	0.02258900
H	0.82834100	2.85121900	-0.14325700
H	-0.86107600	2.73270800	-0.70228200
H	-0.50106900	2.66519100	1.01108600
C	2.38144200	0.99002000	-0.80040000
H	2.03023600	1.43792200	-1.73419500
H	2.82517500	1.78563000	-0.19117200
H	3.18143600	0.28735100	-1.04859500
C	-2.47970400	0.80864900	0.69896200
H	-2.23953300	1.16506700	1.70628200
H	-2.83477700	1.67021100	0.12188300
H	-3.31200500	0.10604300	0.78233600
H	-2.52269300	-1.39703800	-0.60271200
H	2.65427200	-1.12514100	0.61576700
C	0.83587500	-1.69500500	1.63356000
H	0.78241600	-2.72525400	1.25063000
H	1.40227700	-1.76452300	2.57131500
H	-0.17679200	-1.35285900	1.84425800
C	-0.64032600	-1.84576200	-1.55628400
H	-0.49462600	-2.84399600	-1.11622500
H	-1.18464200	-2.02080200	-2.49330300
H	0.33819300	-1.42041200	-1.77517200
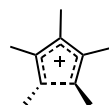
TS1
(from **8a**)

E_{SCF} = -390.820707 Hartrees
Zero-point correction = 0.242894 Hartrees
Single Imaginary Frequency = -172.74 cm^{-1}

C	0.30156300	0.61370500	0.56287900
C	0.62733000	1.90590600	0.09897300
C	-0.45692400	2.76606900	-0.19223600
C	-1.68214000	2.09411900	-0.40220500
C	-1.59295100	0.72509100	-0.74174000
H	-0.52250300	0.53054300	1.26506700
H	-0.80562300	0.43723600	-1.43179400
C	-3.01444200	2.78589100	-0.25701500
H	-3.26804600	3.30424900	-1.19170200
H	-3.81941500	2.07405900	-0.06323200
H	-3.00794800	3.52986000	0.54361700
C	-0.29295900	4.25464300	-0.28804300
H	-1.23941400	4.76532000	-0.46978700
H	0.16234800	4.67121200	0.61781700
H	0.37888600	4.50106400	-1.12132300
C	2.05310300	2.35207600	-0.09414500
H	2.77132000	1.55677500	0.10840100
H	2.22536800	2.73377700	-1.10703100
H	2.27228800	3.17631900	0.59742100
C	1.21315800	-0.57000700	0.52664100
H	1.79946400	-0.60891700	1.45715700
H	0.63190000	-1.49783400	0.49939700
H	1.90772800	-0.55916600	-0.31651200
C	-2.69485000	-0.27510600	-0.60442700
H	-3.32036700	-0.25508800	-1.50990200
H	-2.28563600	-1.28861100	-0.54209500
H	-3.34135400	-0.09656200	0.25822700
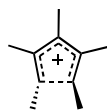
TS2
(from **8b**)

E_{SCF} = -390.761190 Hartrees
Zero-point correction = 0.242853 Hartrees
Single Imaginary Frequency = -270.15cm^{-1}

C	1.11420700	-0.89415800	-0.45893500
C	1.24226500	0.39922300	0.07926700
C	0.13694000	1.27836300	-0.01352400
C	-1.09979900	0.59807000	-0.09684500
C	-1.18331000	-0.69345700	0.45920100
H	1.79225400	-1.63947600	-0.03364000
H	-1.96868800	-1.32816300	0.03918100

C	-2.30971400	1.19528000	-0.78052900
H	-2.97722200	0.40717800	-1.14230400
H	-2.89095700	1.79605600	-0.06861000
H	-2.03961800	1.83986200	-1.62097200
C	0.28171000	2.76894200	0.00526200
H	-0.65687100	3.27740500	-0.22185000
H	0.59261800	3.09247500	1.00942300
H	1.05426400	3.11425600	-0.69013300
C	2.53242200	0.81663700	0.74510000
H	3.15432400	-0.04949500	0.98619500
H	3.11579700	1.44783700	0.06081200
H	2.36120200	1.39710300	1.65726300
C	0.59592800	-1.29896600	-1.81138700
H	1.47670000	-1.42823600	-2.45864100
H	0.09781400	-2.27340300	-1.78500400
H	-0.06237700	-0.56052400	-2.27054500
C	-0.74544200	-1.15155200	1.82229300
H	-1.63868400	-1.12384100	2.46501400
H	-0.41199900	-2.19415300	1.81729100
H	0.02174200	-0.52120000	2.27360300
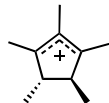
E_{SCF} = -390.859658 Hartrees
Zero-point correction = 0.245162 Hartrees
No Imaginary Frequencies

C	0.64937000	-1.16715900	0.14908200
C	1.13796500	0.24331900	0.20529600
C	0.10677900	1.16872100	-0.00750000
C	-1.08039200	0.45317300	-0.21123600
C	-0.85919300	-1.02599200	-0.14658800
H	0.79488200	-1.59633500	1.15417000
H	-1.08112800	-1.42588600	-1.14961400
C	-2.42189300	1.03779800	-0.44407800
H	-3.05359800	0.37579300	-1.04359700
H	-2.92630600	1.15985900	0.52851900
H	-2.37896400	2.02676300	-0.90663900
C	0.27753500	2.66266900	0.00120700
H	-0.62591700	3.18002300	-0.32706400
H	0.51384000	3.02363000	1.00940400
H	1.09588300	2.97070400	-0.65780200
C	2.55731200	0.59496400	0.44153500

H	3.09284800	-0.18963300	0.98263800
H	3.05786200	0.71079500	-0.53429600
H	2.66509300	1.55014000	0.96372200
C	1.42695300	-2.05904900	-0.84751700
H	2.48618300	-2.12261000	-0.58380200
H	1.01682800	-3.07263100	-0.82845400
H	1.34458700	-1.67386000	-1.86906000
C	-1.78708800	-1.75485600	0.85320600
H	-2.83950400	-1.63245700	0.58309300
H	-1.56391500	-2.82545800	0.84643100
H	-1.64276800	-1.38036100	1.87192100

References

(1)   Hastings, C. J.; Pluth, M. D.; Bergman, R. G.; Raymond, K. N. *J. Am. Chem. Soc.* **2010**, *132*, 6938.

(2)   Bondi, A. *J. Phys. Chem.* **1964**, *68*, 441.

(3)   Charton, M. *J. Am. Chem. Soc.* **1969**, *91*, 615.

(4)   Uneyama, K. *Organofluorine Chemistry*; Blackwell Publishing: Ames, Iowa, 2006.

(5)   Chiu, N. W. K.; Sorensen, T. S. *Can. J. Chem.* **1973**, *51*, 2776.

(6)   Deno, N. C.; Pittman, C. U. *J. Am. Chem. Soc.* **1964**, *86*, 1871.

(7)   Schleyer, P. v. R.; Dine, G. W. V.; Scholkopf, U.; Paust, J. *J. Am. Chem. Soc.* **1966**, *88*, 2868.

(8)   Schleyer, P. v. R.; Slinwinski, W. F.; Dine, G. W. v.; Schollkopf, U.; Paust, J.; Fellenberger, K. *J. Am. Chem. Soc.* **1972**, *94*, 125.

(9)   Brumaghim, J.; Michels, M.; Pagliero, D.; Raymond, K. *Eur. J. Org. Chem.* **2004**, 5115.

(10)   Oda, M.; Okawa, K.; Tsuri, H.; Kuroda, S. *Tetrahedron* **2003**, *59*, 795.

(11)   Bartlett, P. D.; McCollum, J. D. *J. Am. Chem. Soc.* **1956**, *78*, 1441.

(12)   Deno, N. C.; Edwards, T.; Perizzolo, C. *J. Am. Chem. Soc* **1957**, *79*, 2108.

(13)   Hall, H. K. *J. Am. Chem. Soc* **1957**, *79*, 5441.

(14)   Pluth, M. D.; Bergman, R. G.; Raymond, K. N. *Science* **2007**, *316*, 85.

(15)   Pluth, M. D.; Bergman, R. G.; Raymond, K. N. *J. Am. Chem. Soc.* **2007**, *129*, 11459.

(16)   Pluth, M. D.; Bergman, R. G.; Raymond, K. N. *J. Am. Chem. Soc.* **2008**, *130*, 11423.

(17)   Pluth, M. D.; Bergman, R. G.; Raymond, K. N. *Acc. Chem. Res.* **2009**, *42*, 1650.

(18)   Caulder, D.; Powers, R.; Parac, T.; Raymond, K. *Angew Chem Int Edit* **1998**, *37*, 1840.

(19)   Parac, T.; Scherer, M.; Raymond, K. *Angew Chem Int Edit* **2000**, *39*, 1239.

(20)   Davis, A. V.; Fiedler, D.; Seeber, G.; Zahl, A.; van Eldik, R.; Raymond, K. N. *J Am Chem Soc* **2006**, *128*, 1324.

(21)   Sgarlata, C.; Mugridge, J. S.; Pluth, M. D.; Tiedemann, B. E. F.; Zito, V.; Arena, G.; Raymond, K. N. *J Am Chem Soc* **2010**, *132*, 1005.

(22)   Houk, K. N.; Leach, A. G.; Kim, S. P.; Zhang, X. Y. *Angew. Chem. Int. Ed.* **2003**, *42*, 4872.

(23)   Hirst, S. C.; Hamilton, A. D. *J. Am. Chem. Soc.* **1991**, *113*, 382.

(24)   Scarso, A.; Trembleau, L.; Rebek *Angew. Chem. Int. Edit.* **2003**, *42*, 5499.

(25)   Ajami, D.; Rebek, J. *J. Am. Chem. Soc.* **2006**, *128*, 15038.

(26)   Purse, B.; Rebek *Proc. Natl. Acad. Sci. USA* **2006**, *103*, 2530.

(27)   Biros, S. M.; Bergman, R. G.; Raymond, K. N. *J. Am. Chem. Soc.* **2007**, *129*, 12094.

(28)   Rebek, J. *Chem. Commun.* **2007**, 2777.

(29)   Ajami, D.; Rebek, J. *Nat. Chem.* **2009**, *1*, 87.

(30)   Fiedler, D.; Bergman, R. G.; Raymond, K. N. *Angew. Chem. Int. Ed.* **2004**, *43*, 6748.

(31) Fiedler, D.; Van Halbeek, H.; Bergman, R. G.; Raymond, K. N. *J. Am. Chem. Soc.* **2006**, *128*, 10240.

(32) Hastings, C. J.; Fiedler, D.; Bergman, R. G.; Raymond, K. N. *J. Am. Chem. Soc.* **2008**, *130*, 10977.

(33) Parac, T.; Caulder, D.; Raymond, K. N. *J. Am. Chem. Soc* **1998**, *120*, 8003.

(34) Gottlieb, H.; Kotlyar, V.; Nudelman, A. *J. Org. Chem.* **1997**, *62*, 7512.

(35) Ribeiro, A. A.; Glen, M. J. *J. Magn. Reson., Ser. A* **1994**, *107*, 158.

(36) Alaimo, P.; Peters, D.; Arnold, J.; Bergman, R. *J. Chem. Educ.* **2001**, *78*, 64.

(37) Caulder, D.; Powers, R.; Parac, T.; Raymond, K. *Angew. Chem. Int. Ed.* **1998**, *37*, 1840.

(38) Threlkel, R. S.; Bercaw, J. E.; Seidler, P. F.; Stryker, J. M.; Bergman, R. G. In *Organic Syntheses*; Wiley: New York, 1993; Vol. VIII, p 505.

(39) Frisch, M. J. T., G. W.; Schlegel, H. B.; Scuseria, G. E.; Robb, M. A.; Cheeseman, ; J. R.; Montgomery, J., J. A.; Vreven, T.; Kudin, K. N.; Burant, J. C.; Millam, J. M.; ; Iyengar, S. S. T., J.; Barone, V.; Mennucci, B.; Cossi, M.; Scalmani, G.; Rega, N.; ; Petersson, G. A. N., H.; Hada, M.; Ehara, M.; Toyota, K.; Fukuda, R.; Hasegawa, ; J.; Ishida, M. N., T.; Honda, Y.; Kitao, O.; Nakai, H.; Klene, M.; Li, X.; Knox, J. ; E.; Hratchian, H. P. C., J. B.; Bakken, V.; Adamo, C.; Jaramillo, J.; Gomperts, R.; ; Stratmann, R. E. Y., O.; Austin, A. J.; Cammi, R.; Pomelli, C.; Ochterski, J. W.; ; Ayala, P. Y. M., K.; Voth, G. A.; Salvador, P.; Dannenberg, J. J.; Zakrzewski, ; V. G.; Dapprich, S. D., A. D.; Strain, M. C.; Farkas, O.; Malick, D. K.; Rabuck, A. ; D.; Raghavachari, K. F., J. B.; Ortiz, J. V.; Cui, Q.; Baboul, A. G.; Clifford, S.; ; Cioslowski, J. S., B. B.; Liu, G.; Liashenko, A.; Piskorz, P.; Komaromi, I.; ; Martin, R. L. F., D. J.; Keith, T.; Al-Laham, M. A.; Peng, C. Y.; Nanayakkara, A.; ; Challacombe, M. G., P. M. W.; Johnson, B.; Chen, W.; Wong, M. W.; Gonzalez, C.; ; and Pople, J. A. *Gaussian 03, Revision C0.2*; Gaussiasn, Inc.: Wallingford CT, 2004.